THE BEHAVIOUR OF SANDS

UNDER THREE DIMENSIONAL STRESS SYSTEMS

Thesis submitted for the
Degree of Doctor of Philosophy in Engineering
of the University of Glasgow

by

WILLIAM MARIUS KIRKPATRICK, B.Sc., A.R.T.C.

October 1954.

ProQuest LLC.
789 East Eisenhower Parkway
P.O. Box 1346
Ann Arbor, MI 48106 – 1346

ACKNOWLEDGEMENTS

The work was carried out in the Department of Civil and Mechanical Engineering at the Royal Technical College, Glasgow. The author wishes to thank Professor A.S.T. Thomson, D.Sc., Ph.D., A.R.T.C., M.I.Mech.E. for support of the research and provision of facilities within the Department. Thanks are also due to William Hunter, B.Sc., Ph.D., A.R.T.C., A.M.I.C.E., M.I.Struct.E. for the freedom of the Civil Engineering laboratory, and to William Frazer, B.Sc., A.R.T.C., A.M.I.C.E., A.M.I.Mech.E. for constant advice and guidance throughout the work.

Part of the work was carried out while receiving a Henry Bell Senior Scholarship and a grant from the Cross Trust. The author is grateful for this financial assistance.

C O N T E N T S

Page

A P P E N D I C E S

§§§§§§§§§§

PRINCIPAL NOTATION

General

σ	effective normal stress (total minus hydrostatic).
$\sigma_1, \sigma_2, \sigma_3$	principal stresses (refer to yield in Part I).
T	shearing stress
$\lambda = \frac{\sigma_3}{\sigma_1}$	ratio of minor to major principal stress at yield
$U = \frac{2\ \sigma_2 - \sigma_3 - \sigma_1}{\sigma_3 - \sigma_1}$	Lode's parameter (where $\sigma_1 \geqslant \sigma_2 \geqslant \sigma_3$).
θ	angle defining position of stress vector on right section of yield surface.
f	a function of.

Soil Properties

ϕ	true angle of internal friction.
C	true cohesion.

Thick Cylinder Tests

r	any radius.
a,b	bore and outside radius.
P_i, P_o	bore and outside pressure (refer to conditions at yield in Part I)
σ_r, σ_t, σ_a	radial, tangential, and axial principal stresses at yield, subscript av. refers to average stresses.

Other infrequently used symbols are defined where they occur in the text.

INTRODUCTION AND SUMMARY

Most problems of soil mechanics may be divided into two principal groups namely; problems of stability, and problems of deformation. Stability problems deal with the equilibrium of soils immediately preceding yield and into this category come the problems of earth pressure, of bearing capacity and of stability of slopes.

Deformation problems deal with the deformation of the soil due to its own weight or due to superimposed loads. Settlement problems fall into this category. To solve these problems the relationship between stress and strain must be known but the stress conditions for yield need not be considered.

The French engineer Coulomb[9](*) (1773) was the first to present a hypothesis explaining the criteria for yield of soils under stress. Coulomb's equation can be expressed by

$$T = C_a + \sigma' \tan \phi_a$$

where T denotes shearing strength
C_a denotes apparent cohesion
σ' denotes total normal compressive stress on the planes of slip
ϕ_a denotes the apparent angle of internal friction.

(*) The number refers to Bibliography in Appendix VI.

The values of C_a and ϕ_a in this equation can be determined from laboratory tests.

In saturated soils a state of stress is always associated with a change of water content. If the stresses which ultimately cause failure are applied more rapidly than the water content can change, a part of the applied normal stress will be carried by a stress set up in the water. This stress is normally referred to in Soil Mechanics as the excess hydrostatic pressure. In Coulomb's equation C_a and ϕ_a should be regarded as empirical coefficients which define a straight line. They are not absolute constants but depend on the consolidation and conditions of drainage of the soil.

A more basic form of the Coulomb equation was suggested by Hvorslev[13] in 1937. In this equation allowance is made for the excess hydrostatic pressure in order to calculate the effective normal stress. The equation is

$$T = C + (\sigma' - u)\tan\phi$$

where C denotes true cohesion

ϕ denotes true angle of internal friction

u denotes excess hydrostatic pressure.

C and ϕ are absolute constants for a soil.

In Britain the tendency at present is to use the total stress method in stability problems. Conditions of consoli-

dation and drainage met with in the field are simulated in laboratory tests and the values of C_a and ϕ_a associated with these conditions are found. In the United States the use of the Hvorslev equation is more popular. The hydrostatic excess pressure is either measured directly in the field or estimated from seepage force calculations.

The Coulomb equation in its various forms is a special case of the Mohr theory of strength. This theory assumes that yield is independent of the intermediate principal stress. Existing information on the behaviour of soils under stress comes mainly from the results of the triaxial compression test in which the intermediate principal stress has a value equal to the minor principal stress. The results of these tests show a linear increase in strength with increase in compressive stress as predicted by the Mohr-Coulomb theory and it is practice to assume this theory in their interpretation and application to problems of stability. The stress systems in many problems of stability are compatible with that existing in the triaxial compression test. In the solution of these problems it is admissible to use the Mohr-Coulomb theory with the soil constants found from the tests without enquiry into the assumptions on which the theory is based. In other problems, including those involving the states of stress around drill holes, shafts and in deep bins, the intermediate principal stress varies in magnitude between the values of the minor and

the major principal stresses. A solution to these problems can be obtained assuming the Mohr-Coulomb theory but a rigorous analysis cannot be made until the effect of the intermediate principal stress on the condition of yield is investigated.

In Part I of the thesis an investigation into the condition of yield for drained tests on a sand is reported. The investigation is conducted from the aspect of determining the shape of the experimental surface of yield for the material in a principal stress system of coordinates. The application and adaption to sands of several existing theories of strength is considered, and the surfaces of yield which these theories represent are compared to form the basis of the experimental investigation. Yield is taken as the peak point on the stress strain curve and the shape of the experimental surface of yield is determined from the results of three different types of test. These tests and the stress systems they produce are:

1) The Triaxial Compression Test in which the intermediate principal stress has a value equal to the minor principal stress.
2) The Triaxial Extension Test in which the intermediate principal stress has a value equal to the major principal stress.
3) The Thick Cylinder Test in which the intermediate

principal stress has a value approximately equal to the mean of the values of the major and minor principal stresses.

The triaxial compression test consists of subjecting a cylindrical sample of soil to a hydrostatic pressure and increasing the axial stress until failure is induced. This test is the standard method for investigating the stress-strain relationships for soils.

The triaxial extension test is performed in a similar manner but in this case the axial stress is decreased until failure is induced. This test was carried out in the same apparatus as that used for the triaxial compression test.

A stress system in which the intermediate principal stress has a value approximately equal to the mean of the values of the major and the minor principal stresses can be produced by forming a sample of soil into a thick walled cylinder and subjecting it to an external and an internal pressure, failure being induced by increasing the internal pressure. An apparatus to carry out such a test was developed and its design, construction, and operation are described.

The results of these three tests performed on the sand at a low porosity are used to illustrate the shape of the experimental surface of yield. The results are presented in a two dimensional form by a method derived in Appendix III. It is

found that the Mohr-Coulomb theory accurately predicts yield for stress systems where the intermediate principal stress has a value either equal to the major or the minor principal stress, but for stress systems where the intermediate principal stress has a value approximately equal to the mean of the values of the major and minor principal stresses the theory slightly underestimates the strength.

Due to the controversial nature of the results of triaxial compression and extension tests reported by other investigators additional triaxial compression and extension tests were carried out at porosities ranging throughout the limits for the sand. From these tests it is concluded that the Mohr-Coulomb theory is applicable throughout the range of porosity for the sand.

In general it is concluded in Part I that the Mohr-Coulomb theory provides a reliable means of estimating the strength of sands under conditions of full drainage.

The observation of the volume changes associated with deformation forms an essential part of the testing of sands. The volume changes have an important significance in problems of stability and provide a valuable aid in understanding the strength and failure characteristics of the material. In Part II of the thesis the volume change and other relevant data, for the tests performed for the purposes of Part I, are presented. These results are discussed with reference to the

strength and deformation of sands and it is tentatively concluded that in the failure of sands the complete mass under stress does not deform but that failure is due to the deformation of a number of wedges or zones of material within the mass. The limitations of standard shear testing apparatuses for measuring the dilatancy properties of sands are also pointed out.

PART I

THE CONDITION OF YIELD FOR SANDS

SECTION 1.

Review of Previous Experimental Work.

As far as is known the only comprehensive investigation into the yield condition of soils was performed by Habib[3][4] in Paris. This investigation was conducted simultaneously with that of the author. Incidental with other investigations the effect of the intermediate principal stress was studied from the results of triaxial compression and extension tests. In these tests the intermediate principal stress is equal to the minor principal stress and the major principal stress respectively.

As part of the investigation carried out by Habib, drained triaxial compression and extension tests were performed on several sands. The sands were tested near their critical porosity. The results showed that the angle of internal friction calculated from the Mohr-Coulomb theory was considerably lower in the extension tests than in the compression tests. Taylor[14] also reported a lower angle of internal friction for sands in the extension test than in the compression test.

Results published by Bishop and Eldin[1] (a report of results obtained by Eldin[2]) showed agreement between the angle of internal friction in compression and extension tests.

This agreement was obtained throughout the range of porosity of the sand.

The inconsistencies of these results led the author to carry out a comprehensive series of triaxial compression and extension tests in the investigation reported in this thesis. These tests were performed to allow the results to be studied at porosities covering the range for the sand.

Habib continued his investigations into the yield of sands by subjecting specimens to a series of torsion tests. These tests were performed on cylindrical samples with the sand confined by rubber membranes in the usual way. The intermediate principal stress was varied between the limits of the minor and the major principal stresses by applying axial loads to the sample. The results varied widely from the Mohr-Coulomb theory of strength.

The results of these investigations are discussed in the light of the author's findings in Section 7.

SECTION 2.

Existing Theories of Strength.

The different behaviour of various materials under similar conditions of stress has led to the development of several criteria to predict yield. Only the theories which are applicable or can be adapted to provide a possible explanation of the behaviour of soils are presented.

Reference is made in this and in subsequent sections to surfaces of yield. An explanation of the surface of yield and the terms used in referring to it are given here.

A state of stress can be described by its three principal stresses σ_1, σ_2, and σ_3 and can be represented as a point in a system of three dimensional coordinates $(\sigma_1, \sigma_2, \sigma_3)$. The locus of all the points representing states of stress which are sufficient to cause yield trace out a surface in space which will be known as the surface of yield. The equation representing the yield condition of the various theories of strength define theoretical surfaces of yield in this system of coordinates.

The shape of the surface of yield can be illustrated by sections taken through it. Those sections which are perpendicular to the axis of the surface are referred to as right sections. For an isotropic material the axis of the surface coincides with the space diagonal, the line in space whose equation is $\sigma_1 = \sigma_2 = \sigma_3$.

2 a) The Theory of Von Mises.

Von Mises in 1913[6] suggested that yield in a material takes place when the stresses are such that

$$(\sigma_1 - \sigma_2)^2 + (\sigma_2 - \sigma_3)^2 + (\sigma_3 - \sigma_1)^2 = \text{constant} \quad \ldots\ldots(1)$$

Hencky[6], later, gave the law a physical meaning by stating that yield takes place when the elastic energy of distortion reaches a critical value. A further physical interpretation was given to the law by Nadai[9] by stating that at the point of yield the octahedral shearing stress, T_o, is a constant. T_o can be proved to have the value

$$T_o = \frac{1}{3}\sqrt{(\sigma_1 - \sigma_2)^2 + (\sigma_2 - \sigma_3)^2 + (\sigma_3 - \sigma_1)^2} \quad \ldots\ldots\ldots(2)$$

The condition at yield is therefore described by the equation

$$T_o = \text{constant} \quad \ldots\ldots\ldots\ldots\ldots\ldots\ldots\ldots\ldots(3)$$

Equations (1) and (3) define the limiting surface of yielding. The surface is a straight circular prism with its axis coinciding with the space diagonal.

The Von Mises condition assumes that the limiting strength

does not depend on the mean normal stress $\frac{\sigma_1 + \sigma_2 + \sigma_3}{3}$ and infers that right sections of the yield surface are similar at any distance along the space diagonal. In materials where it has been established that the strength varies with the mean normal stress equation (1) can be modified to (4) as suggested by Schleicher[12]

$$(\sigma_1 - \sigma_2)^2 + (\sigma_2 - \sigma_3)^2 + (\sigma_3 - \sigma_1)^2 = [f(\sigma_1 + \sigma_2 + \sigma_3)]^2 \quad \ldots(4)$$

as a possible means of explaining their behaviour. The surface of yield defined by (4) is a solid of revolution with its axis along the space diagonal. Right sections of the surface are circles which vary in diameter with distance along the axis.

2 b) <u>The Maximum Shearing Stress Theory of Tresca</u>.

Observations made in the course of extrusion tests on soft metals led Tresca in 1864[6] to the assumption that the plastic state in such metals is created when the maximum shearing stress reaches a limiting value which is a constant for the material. Further support was lent to this assumption by the appearance of slip layers in deformed metals which approximately coincided with the directions of maximum shearing stress. The condition for yielding in this theory is

expressed by

$$\tau_{max} = \frac{\sigma_1 - \sigma_3}{2} = \text{constant} \quad \ldots\ldots\ldots\ldots\ldots\ldots\ldots\ldots (5)$$

where $\sigma_1 \geq \sigma_2 \geq \sigma_3$.

This condition can be expressed in its most general form by the equation

$$\left[(\sigma_1 - \sigma_2)^2 - \sigma_o^2\right]\left[(\sigma_2 - \sigma_3)^2 - \sigma_o^2\right]\left[(\sigma_3 - \sigma_1)^2 - \sigma_o^2\right] = 0 \quad \ldots (6)$$

where σ_o = constant

representing six conditions of yield from which the intermediate principal stress is always absent.

The surface of yield for the Tresca theory is a straight hexagonal prism whose axis coincides with the space diagonal. The hexagonal prism can be inscribed in the circular cylinder representing the theory of Von Mises by suitably choosing the constant in (1) and (6).

The Tresca theory assumes that yield is independent of the mean normal stress. For materials whose behaviour does depend on the mean normal stress the theory can be adapted, in a manner similar to that described for the Von Mises theory (eqn.(4)), by assuming that at the point of yield the maximum shearing stress becomes equal to a function of the mean normal

stress. The general condition of yield is then defined by

$$\left\{(\sigma_1-\sigma_2)^2-\left[f(\sigma_1+\sigma_2+\sigma_3)\right]^2\right\}\left\{(\sigma_2-\sigma_3)^2-\left[f(\sigma_1+\sigma_2+\sigma_3)\right]^2\right\}$$
$$\left\{(\sigma_3-\sigma_1)^2-\left[f(\sigma_1+\sigma_2+\sigma_3)\right]^2\right\} = 0 \quad \ldots\ldots\ldots\ldots\ldots\ldots (8)$$

The yield surface defined by (8) is a solid with its axis along the space diagonal. Right sections of the surface are regular hexagons varying in dimension at different distances along the axis.

2 c) <u>The Mohr Theory of Strength</u>.

According to Mohr (1900)[9] a material may yield when either the shearing stress T in the planes of slip has reached a value which will depend on the normal stress acting across these planes or when the largest tensile normal stress has reached a limiting value.

In certain ductile metals and natural rocks which have been deformed, slip lines can be detected. These lines form two systems of isogonal planes of slip which are inclined to the directions of the major (σ_1) and minor (σ_3) principal stresses and intersect each other along the direction of the intermediate principal stress (σ_2).

Consider a point P in the Mohr diagram (Fig.1) to represent a plane in the stressed material along which slip is imminent.

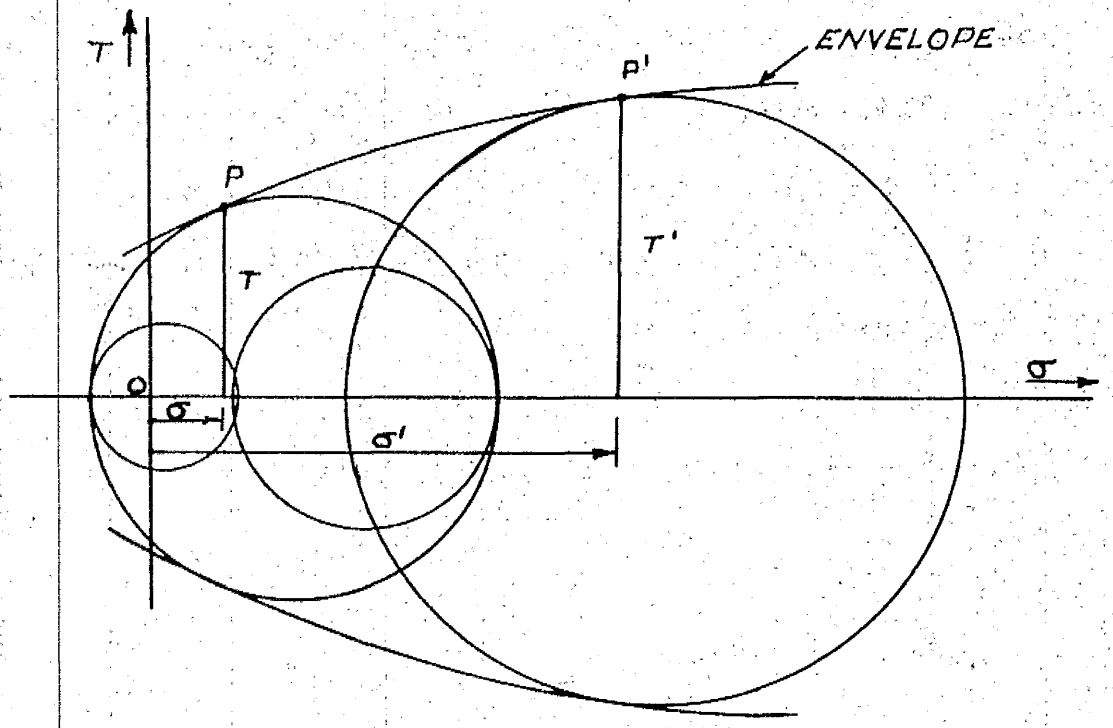

THE MOHR DIAGRAM

FIG. 1

The coordinates of P are σ and T. Since, according to the Mohr theory, the limiting shearing stress is dependent only on the normal stress in the plane of slip, T must be a function of σ. The curve $T = f(\sigma)$ therefore represents the locus of all points P, P', etc., which have the limiting values of the component stresses in the planes of slip. $T = f(\sigma)$ therefore represents the common tangent of all major stress circles which define stresses sufficient to cause yield. This curve is generally referred to as the Mohr envelope. The equation of the Mohr envelope can be expressed analytically in terms of the principal stresses by

$$\left(\frac{\sigma_1 - \sigma_3}{2}\right) = \pm f\left(\frac{\sigma_1 + \sigma_3}{2}\right) \quad \ldots\ldots\ldots\ldots\ldots \quad (9)$$

where $\sigma_1 \geq \sigma_2 \geq \sigma_3$

$\frac{(\sigma_1 - \sigma_3)}{2}$ represents the radii of the largest principal stress circles and $\frac{(\sigma_1 + \sigma_3)}{2}$ represents the distances of the centres of these circles from the origin of the Mohr diagram.

The Mohr condition of yield in its most general form is expressed by

$$\left\{(\sigma_1-\sigma_2)^2 - \left[f(\sigma_1+\sigma_2)\right]^2\right\}\left\{(\sigma_2-\sigma_3)^2 - \left[f(\sigma_2+\sigma_3)\right]^2\right\}$$
$$\left\{(\sigma_3-\sigma_1)^2 - \left[f(\sigma_3+\sigma_1)\right]^2\right\} = 0 \quad \ldots\ldots\ldots\ldots\ldots\ldots (10)$$

representing six conditions of flow from which the intermediate principal stress is always absent. The surface of yield defined by (10) is complex and is deduced later in Section 3 b for the special Coulomb case.

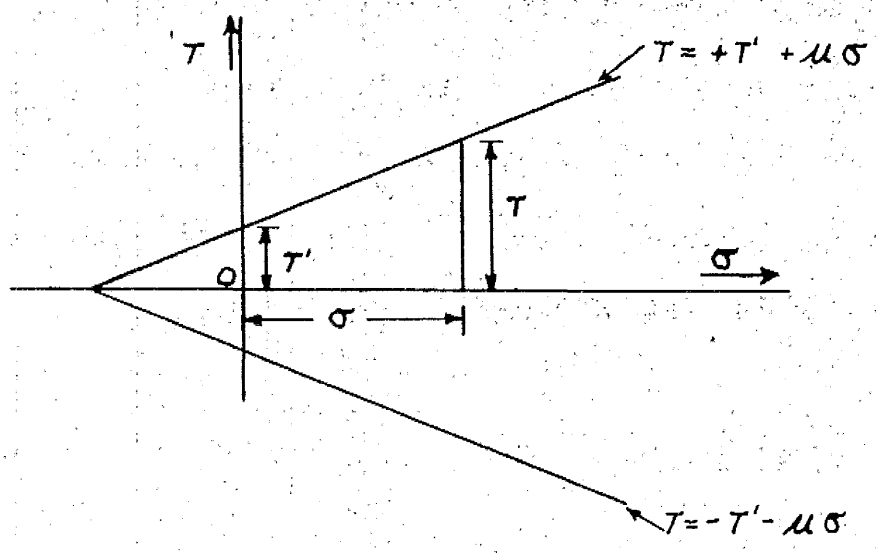

MOHR DIAGRAM FOR COULOMB EQUATION

FIG. 2

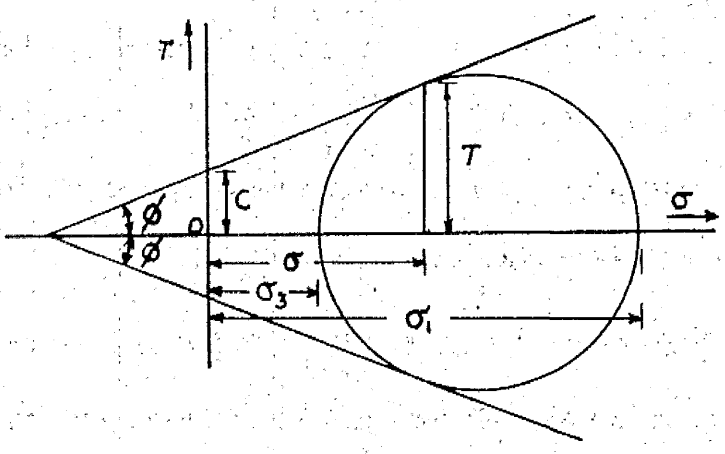

MOHR DIAGRAM FOR SOILS

FIG. 3

2 d) The Mohr-Coulomb Theory of Strength as Applied to Soils.

It has been assumed for a long time that the criterion for yield in a mass of soil under compressive stress is given by the equation of Coulomb (1773)[9]. The Coulomb equation, in its classical form, is given by

$$T = \pm T' \pm \mu\sigma \quad \ldots\ldots\ldots\ldots\ldots\ldots\ldots\ldots (11)$$

where T = shearing stress on planes of slip,

σ = effective normal stress (compressive) on planes of slip,

T' and μ are given positive material constants.

Equation (11) can be viewed as being a special case of the Mohr theory of strength where the enveloping curve consists of two straight lines inclined at the same angle with the σ axis (Fig.2). The use of equation (11) to represent the Mohr Strength envelope on the Mohr diagram gives the "Mohr-Coulomb Theory" as it is used in Soil Mechanics today.

According to equation (11) yield will occur when the shearing stress in the planes of slip reaches a critical value T, which depends on a certain shearing stress T_1, but is proportional to the normal compressive stress on these planes. The strength, therefore, will increase at greater distances

along the compressive σ axis of the Mohr diagram. The quantity $\mu\sigma$ in equation (11) can be termed as a frictional force, μ being interpreted as the coefficient of internal friction. μ can therefore be replaced by the quantity tan ϕ where ϕ is the angle of internal friction of the soil. If we substitute the cohesion C, for the constant shearing stress T_1, and tan ϕ for μ in equation (11) the more familiar form of the equation is obtained.

$$T = \pm (C + \sigma \tan \phi) \quad \ldots\ldots\ldots\ldots\ldots\ldots (12)$$

The angle ϕ is the angle made by the enveloping lines with the σ axis of the Mohr diagram as shown in Fig. 3.

In the Mohr diagram Fig.3 the principal stress circle which is tangential to the enveloping lines represents a state of stress at incipient yield of the soil. The condition of yield expressed in terms of the principal stresses can be derived from the geometry of Fig.3. Equation (12) then becomes

$$(\sigma_1 - \sigma_3) = \pm (2C \cos \phi + (\sigma_1 + \sigma_3) \sin \phi) \quad \ldots\ldots\ldots (13)$$

where $\sigma_1 \geq \sigma_2 \geq \sigma_3$.

Two special cases of the Mohr Coulomb theory are commonly met with in soil testing. For a purely cohesive material,

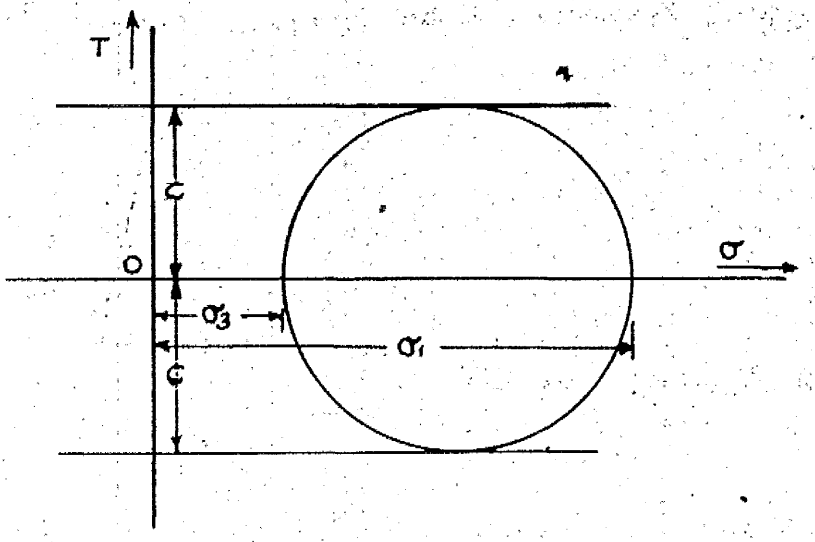

MOHR DIAGRAM FOR A PURELY COHESIVE SOIL

FIG. 4

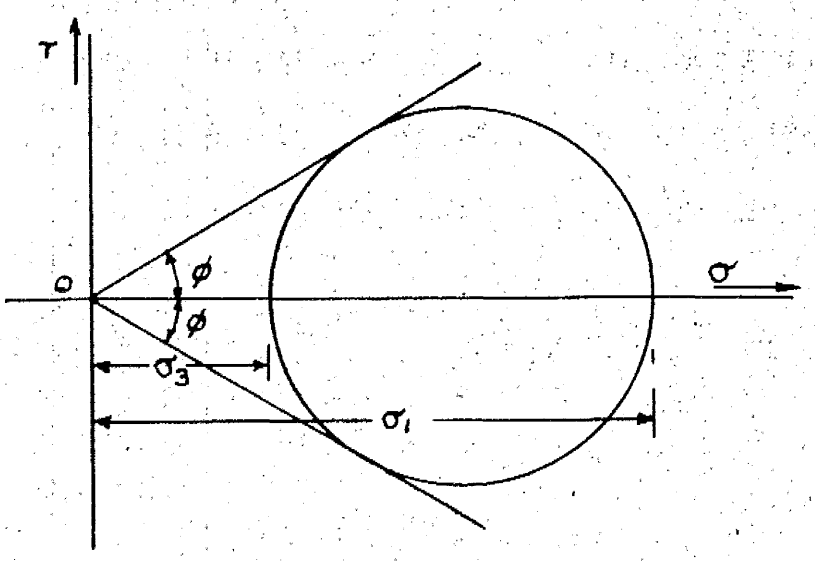

MOHR DIAGRAM FOR SANDS

FIG. 5

the angle of internal friction ϕ is zero, equation (12) becomes

$$T = \pm C \quad \text{.................................} (14)$$

and equation (13) degenerates to

$$\sigma_1 - \sigma_3 = \pm 2C \quad \text{.................................} (15)$$

The envelope Fig.4 becomes two straight lines parallel to the σ axis and at a distance C from it. For this case the Mohr theory becomes coincident with the Tresca theory of maximum shearing stress.

The second special case concerns a granular material possessing no cohesion. The envelope consists of two straight lines which are inclined equally to the σ axis and which pass through the origin of the Mohr diagram (Fig.5). From an analysis of Fig.5 equation (12) becomes

$$T = \pm \sigma \tan \phi \quad \text{.........................} (16)$$

and (13) becomes

$$(\sigma_1 - \sigma_3) = \pm (\sigma_1 + \sigma_3) \sin \phi \quad \text{..................} (17a)$$

From equation (17a) the principal stress ratio at yield is

computed to be

$$\frac{\sigma_3}{\sigma_1} = \frac{1 - \sin \phi}{1 + \sin \phi} \qquad \text{.....(17b)}$$

at yield. The ratio $\frac{\sigma_3}{\sigma_1}$ is generally known as λ.

The investigation in this thesis is concerned only with sands in which C = 0 and later reference will only be made to the case covered by equations (16), (17a), and (17b).

The Mohr-Coulomb theory of strength represents the existing theoretical basis used in the calculation of the strength of soils. The theory assumes that yield is dependent solely on the values of the major and minor principal stresses, σ_1 and σ_3. The third principal stress may have any value as indicated by $\sigma_1 \geq \sigma_2 \geq \sigma_3$ without having an effect on the yield of the soil.

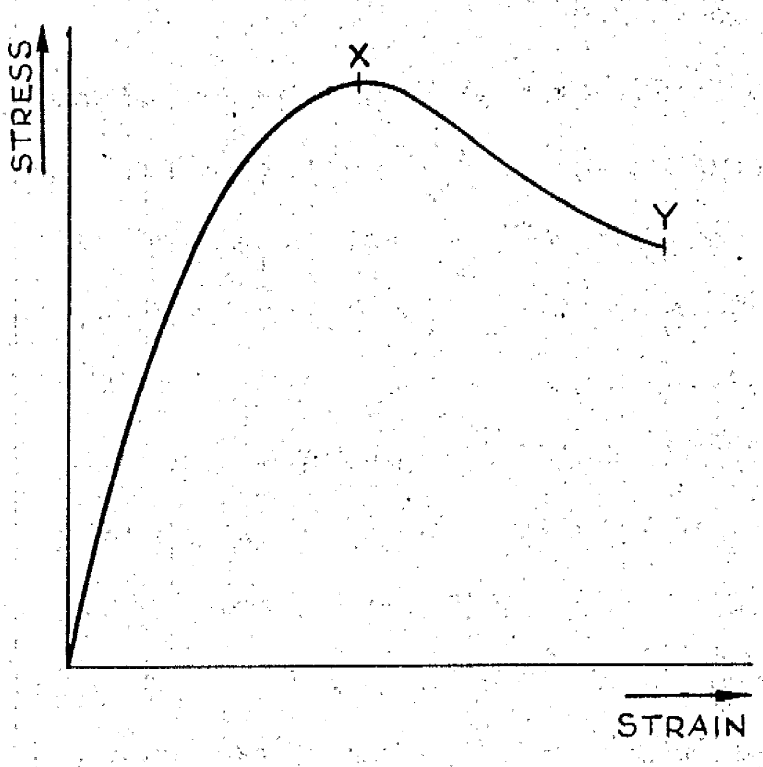

TYPICAL STRESS STRAIN CURVE
FOR SHEAR TEST ON SAND

FIG. 6.

SECTION 3.

Discussion Forming the Basis of Experimental Investigation of the Surface of Yield.

3 a) Definition of Yield.

In materials such as sands which undergo deformations which are not recoverable it is not possible to relate the point of yielding in a stress strain curve to the limit of elasticity of the material. A typical stress strain curve for a shear test on a sand is shown in Fig.6. Two points on the curve are fairly well defined and these are represented by X giving the peak stress and Y giving the ultimate stress at a value lower than X. Yielding is conventionally assumed to occur at point X and the strength is calculated from the stresses at this peak value. The peak stresses will be referred to hereinafter as the stresses defining the yield of the material.

3 b) The Mohr-Coulomb Surface of Yield.

The surface of yield representing the Mohr-Coulomb theory of strength has not been described before as far as is known and is therefore deduced below.

The Mohr-Coulomb condition of yield for sands in the

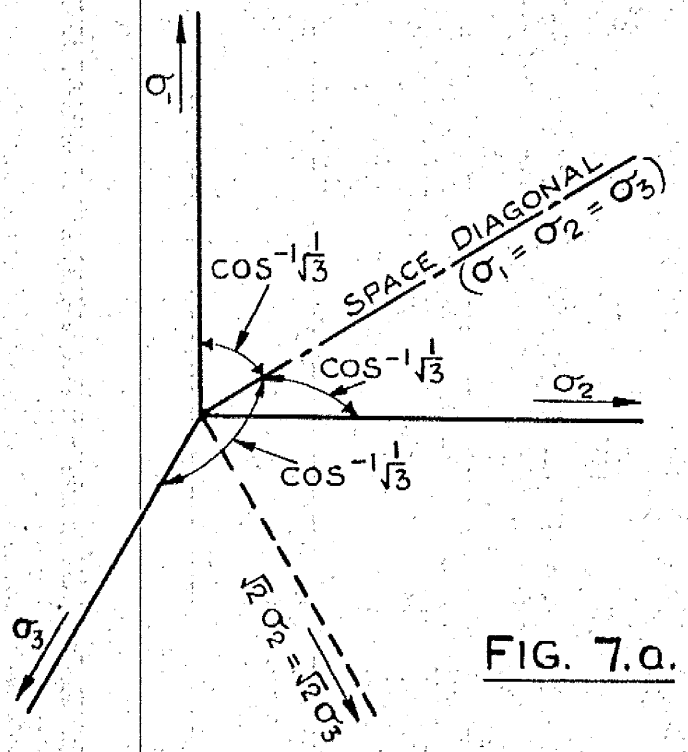

FIG. 7.a.

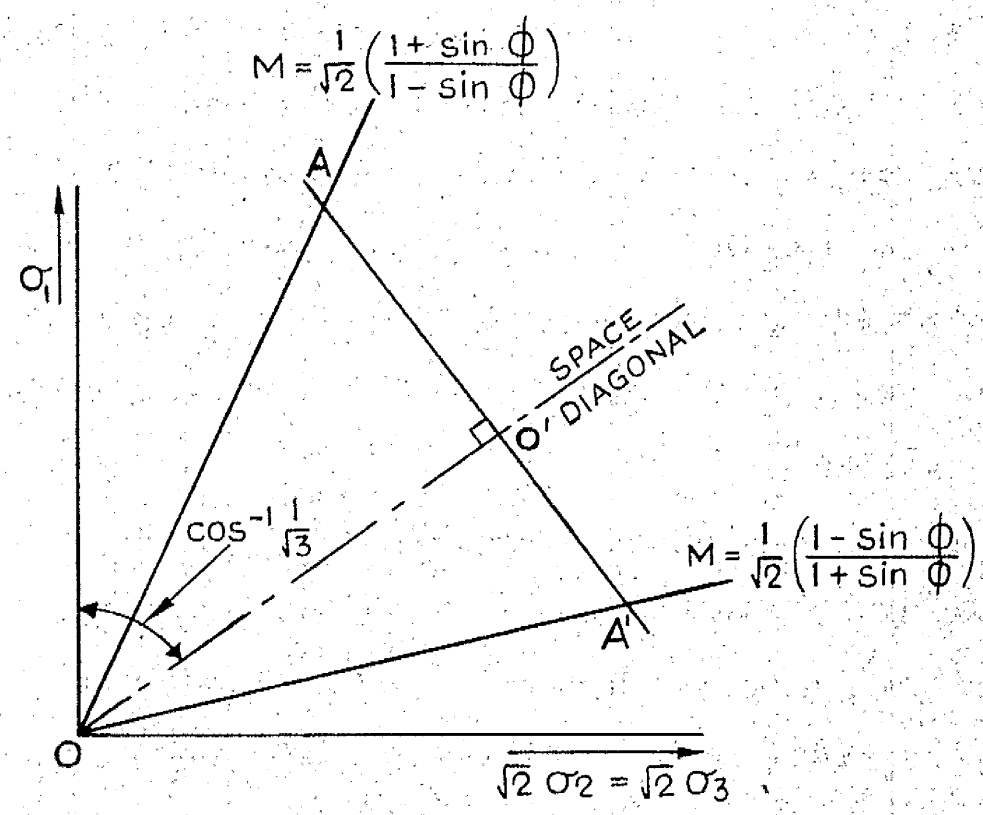

FIG. 7.b.

FIG. 7.

isotropic state can be expressed in its most general form by

$$\left\{(\sigma_1-\sigma_2)^2-\left[\sin\phi(\sigma_1+\sigma_2)\right]^2\right\}\left\{(\sigma_2-\sigma_3)^2-\left[\sin\phi(\sigma_2+\sigma_3)\right]^2\right\}$$

$$\left\{(\sigma_3-\sigma_1)^2-\left[\sin\phi(\sigma_3+\sigma_1)\right]^2\right\} = 0 \quad \ldots\ldots\ldots (18)$$

where ϕ is the angle of internal friction of the material.

Equation (18) represents six conditions of flow from which the intermediate principal stress is always absent.

Sands cannot transmit tensile stresses therefore the surface can only exist along the compressive directions of the system of three dimensional coordinates denoted by σ_1 , σ_2 and σ_3 . By equating $\sigma_1 = \sigma_2 = \sigma_3 = 0$ in (18) the surface at the origin of the system of coordinates is found to be a point. Sections of the surface must increase in dimension at greater distances from the origin along the compressive directions of the coordinates.

In Fig.7a the compressive directions of the axes of reference are shown. In a section bisecting the plane of σ_2 σ_3 and along σ_1 the Mohr-Coulomb surface will be as shown in Fig.7b. This section passes through the space diagonal and its axis of reference become σ_1 and $\sqrt{2}\ \sigma_2 = \sqrt{2}\ \sigma_3$. The angle made by the space diagonal and the σ_1 axis is

$$\cos^{-1}\frac{1}{\sqrt{3}} = 54^\circ\ 44'.$$

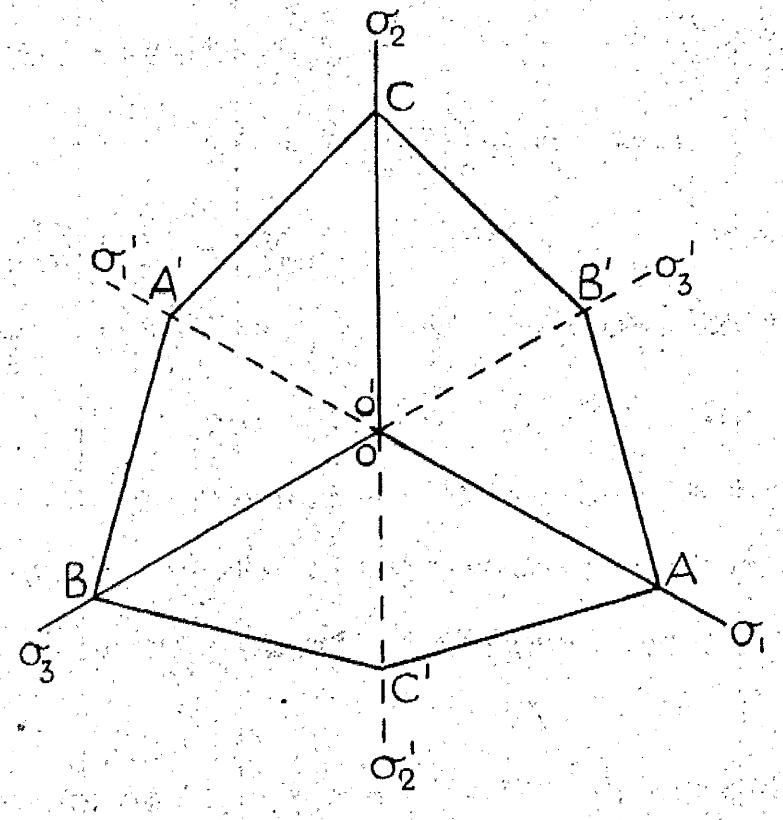

RIGHT SECTION OF MOHR COULOMB SURFACE OF YIELD

FIG. 8.

The lines bounding the section of the surface in Fig.7b are straight and their slopes with reference to the axis $\sqrt{2}\,\sigma_2 = \sqrt{2}\,\sigma_3$ are given by $M = \frac{1}{\sqrt{2}}\left(\frac{1 + \sin\phi}{1 - \sin\phi}\right)$ and $M = \frac{1}{\sqrt{2}}\left(\frac{1 - \sin\phi}{1 + \sin\phi}\right)$ (see eqn.17b). In a section perpendicular to the space diagonal A O'A' in Fig.7b the intercept A O' made by line $M = \frac{1}{\sqrt{2}}\left(\frac{1 + \sin\phi}{1 - \sin\phi}\right)$ and the space diagonal $\left(= 00' \tan\left(\tan^{-1}\frac{1}{\sqrt{2}}\left(\frac{1 + \sin\phi}{1 - \sin\phi}\right) - 35^\circ\ 16'\right)\right)$ is greater than the intercept made by line $M = \frac{1}{\sqrt{2}}\left(\frac{1 - \sin\phi}{1 + \sin\phi}\right)$ and the space diagonal $\left(= 00' \tan\left(35^\circ\ 16' - \tan^{-1}\frac{1}{\sqrt{2}}\ \frac{1 - \sin\phi}{1 + \sin\phi}\right)\right)$. The values are 00' tan 29° 30', and 00' tan 22° for $\phi = 30^\circ$. Sections of the surface of yield perpendicular to the space diagonal are therefore not symmetrical about the space diagonal. The amount of eccentricity is dependent on the angle of internal friction ϕ.

Taking a view looking down the space diagonal in Fig.7b two points on the yield surface A and A' are obtained. For similar constructions points B and B', and C and C' can be obtained. These points are the corner points of a right section of the yield surface. The right section of the surface found in this way is shown in Fig.8 and it is seen to be a hexagon with equal sides but opposite sides not being parallel.

The shape of the Mohr-Coulomb surface of yield for sands is therefore a hexagonal pyramid with its apex at the origin

and existing along the compressive directions of the system of coordinates (σ_1, σ_2, σ_3). The slopes of the sides of the surface are determined by ϕ and are constant. Right sections of the surface increase in size at increasing distances from the origin along the axis (the space diagonal). The shape of the right sections are similar at any distance along the axis and are in general as shown in Fig.8. The shape of the right section is dependent on ϕ and reduces towards a triangle as ϕ tends to 90°. The right section tends towards a regular hexagon as ϕ tends to 0.

3 c) Application of Other Possible Theories.

Existing information on the behaviour of sands under stress comes mainly from the triaxial compression test and it is usual to assume the Mohr-Coulomb theory in the interpretation of the results. It is possible however, to suggest other yield criteria which in the light of existing knowledge would be just as satisfactory. In this respect the Tresca and Von Mises theories of strength can be used for sands by extending the condition of yield to include dependency on the mean normal stress.

The extended Tresca condition then becomes (from eqn.6)

$$\left\{(\sigma_1-\sigma_2)^2-\left[K_1\frac{1}{3}(\sigma_1+\sigma_2+\sigma_3)\right]^2\right\}\left\{(\sigma_2-\sigma_3)^2-\left[K_1\frac{1}{3}(\sigma_1+\sigma_2+\sigma_3)\right]^2\right\}$$
$$\left\{(\sigma_3-\sigma_1)^2-\left[K_1\frac{1}{3}(\sigma_1+\sigma_2+\sigma_3)\right]^2\right\}=0 \quad \ldots\ldots\ldots \quad (19)$$

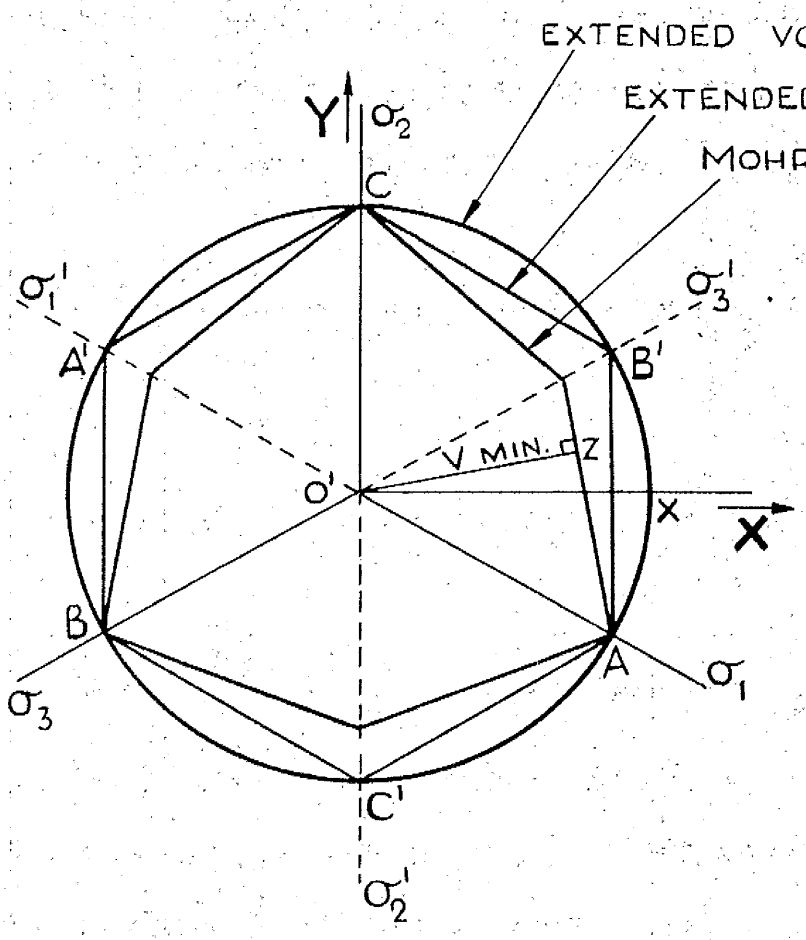

RIGHT SECTION OF
THEORETICAL YIELD SURFACES

FIG. 9.

where K_1 is a constant related to f(sin ϕ).

The extended Tresca surface of yield represented by eqn.19 is a regular hexagonal pyramid with its apex at the origin of the system of three dimensional coordinates. Right sections of this surface coincide with right sections of the Mohr Coulomb surface along the major principal stress directions at points A, B and C in Fig.9.

The extended Von Mises condition of yield (from eqn.1) is expressed by

$$(\sigma_1-\sigma_2)^2+ (\sigma_2-\sigma_3)^2+ (\sigma_3-\sigma_1)^2 = \left[K_2 \frac{1}{3} (\sigma_1+\sigma_2+\sigma_3)\right]^2 \quad \ldots\ldots(20)$$

where K_2 is a constant also related to f(sin ϕ).

The extended Von Mises surface represented by eqn.20 is a cone with its apex at the origin of the system of three dimensional coordinates. Right sections of this surface are circular and coincide with right sections of the Mohr-Coulomb surface and the extended Tresca surface along the major principal stress directions, at points A, B and C in Fig.9.

3 d) <u>General Properties of The Surface of Yield</u>.

In materials such as sands where yield depends on the mean normal stress the sections of the surface will vary with the distance along the space diagonal. In the investigation

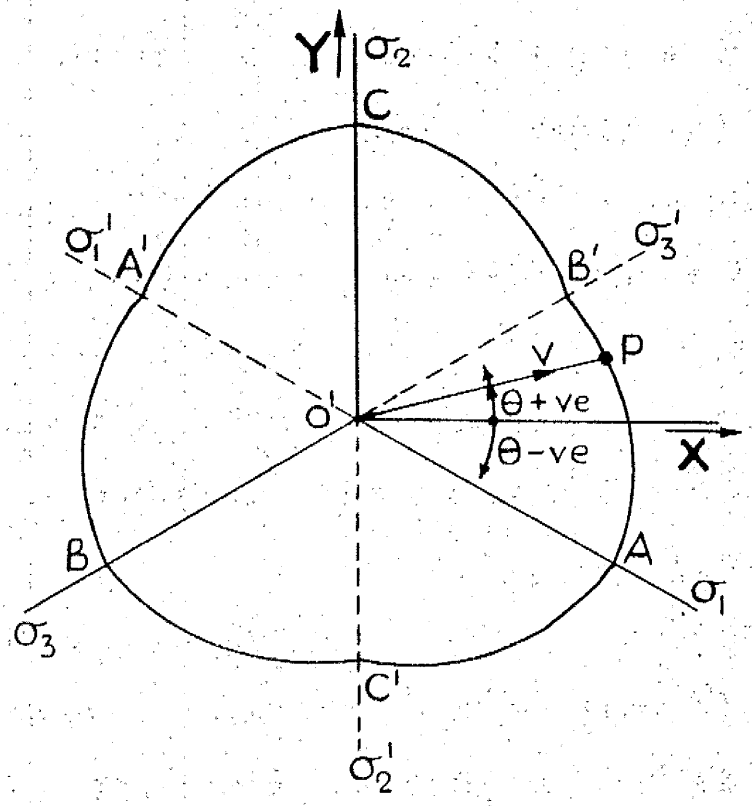

A RIGHT SECTION OF A YIELD SURFACE FOR AN ISOTROPIC MATERIAL

FIG. 10.

of right sections of the surface of yield for such materials the precaution must be taken that the points on the surface, defined by their principal stresses, exist on the same right section. The points will exist on the same right section if the stresses defining them obey the condition that $\sigma_1 + \sigma_2 + \sigma_3 = C$ where C is a constant.

Fig.10 shows a right section of a surface of yield in a system of three dimensional coordinates σ_1, σ_2, σ_3. This section is in the plane of the paper and it exists at some distance along the space diagonal, the axis, such that $\sigma_1 + \sigma_2 + \sigma_3 = C$, a constant. It is sufficient for the purposes here to consider that a new origin is situated at O' (in the plane of the paper) and that the extended major stress directions are negative.

The right section of the yield surface may be concave or convex in any 120° segment but not so that a radius cuts it twice. For an isotropic material if the stresses $(\sigma_1, \sigma_2, \sigma_3)$ represent yield so also do the stresses $(\sigma_2, \sigma_1, \sigma_3)$ etc. The right section of the surface is therefore symmetrical about AA', BB' and CC' Fig.10. In other words the shape of the right section of the yield surface marked off by the three coordinate directions is the same apart from reflections. In the experimental determination of the yield surface it is sufficient to apply only these stress systems whose vectors lie in a selected 60° segment. This may otherwise be expressed

in terms of the parameter U introduced by Lodé[8].

$$U = \frac{2\sigma_2 - \sigma_3 - \sigma_1}{\sigma_3 - \sigma_1}$$

where $\sigma_1 \geq \sigma_2 \geq \sigma_3$ (i.e. for segment B'O'A Fig.10)

It can be shown that $U = -\sqrt{3} \tan \theta$ where θ is the angle made by the stress vector O'P' with direction O'X in Fig. 10. θ is negative or positive in the directions shown in Fig.10. (This is deduced in Appendix II, see also Hill[6]). The right section of the experimental surface of yield can be completely determined by applying stress systems such that θ covers the range from 0° to $+30^\circ$ and 0° to -30° in Fig.10 with U varying from -1 to 0 to +1.

3 e) <u>The Stress Systems Required for an Experimental Investigation of the Surface of Yield</u>.

The three theories which have a possible application in the prediction of yield in sands are the Mohr-Coulomb theory, the extended Tresca theory and the extended Von Mises theory. The extensions made to the Tresca and Von Mises theories are described in Section 3 c). The right sections of the yield surface which these theories represent are shown in Fig.9. In Fig.9 the right sections for all three theories have been

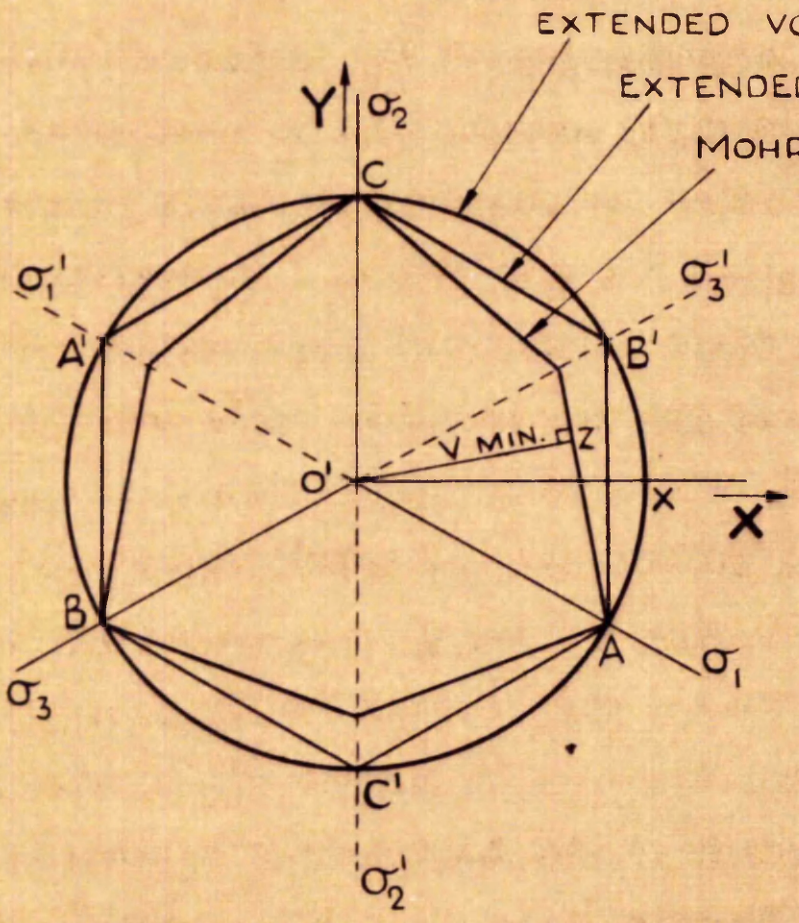

RIGHT SECTION OF
THEORETICAL YIELD SURFACES

FIG. 9.

made to coincide along the major principal stress directions, at points A, B and C. The right sections of the surfaces represented by the extended Tresca and Von Mises surfaces in addition coincide at points A', B' and C'.

In the investigation of the surface of yield only a 60^{o} segment of the right section need be considered. For simplicity further reference is only made to one of these segments, segment B'O'A in Fig.9. In segment B'O'A a large deviation is found between the right sections of the Mohr-Coulomb surface and the extended Tresca and Von Mises surfaces along the direction O'B'. The deviation between the Mohr-Coulomb right section and the Tresca right section is greatest along this direction. The greatest deviation between the extended Tresca and the extended Von Mises right sections is found along the bisector of segment B'O'A, that is along O'X. The right section of the Mohr-Coulomb surface deviates most from the Von Mises surface alone O'Z. O'Z is the smallest stress vector ($V_{min.}$) from the centre to the Mohr-Coulomb surface. The position of Z for O'Z to be a minimum varies with the value of ϕ in the equation (18).

The right sections of the theoretical surfaces are based on the values of the constants ϕ, K_1 and K_2, in equations (18) (19) and (20), which are obtained from a system of stress which provides a point on the right section of the surface of yield at position A. A stress system which provides experimental

points on the right section of the surface of yield along direction O'B' will indicate whether the Mohr-Coulomb theory or the extended Tresca and Von Mises theories are applicable. If the Mohr-Coulomb theory is proved wrong and the point on the experimental right section along O'B' coincides with that of the extended Tresca and Von Mises theories a stress system which provides points along the direction O'X will prove to the best advantage which of these theories is applicable. Furthermore if the stress system which provides experimental points along O'B' shows that none of the theories is applicable the best further indication of the true shape of the experimental purface of yield will be given by a stress system which provides points along the direction O'X which is intermediate between the positions of the points already found along O'A and O'B'.

A complete and rigorous experimental investigation of the right section of the surface of yield would require points to be obtained on the surface at close intervals between B' and A. An investigation as comprehensive as this would not be justified if the right section proved to be close to that of one of the theories. The stress systems which give points on the right section of the surface of yield along the directions O'A, O'B' and O'X will provide the best first approximation to the true shape of the right section of the experimental surface of yield. If the experimental right section is found to vary

widely from the theoretical right sections additional points will have to be obtained between X and B' and X and A.

The stress systems which are desired for the experimental investigation of the right section of the surface of yield are:

1) To provide points along direction O'A (Fig.9)

$$\sigma_1 > \sigma_2 = \sigma_3$$

which in terms of Lode's parameter

$$U = \frac{\sigma_3 - \sigma_1}{\sigma_3 - \sigma_1} = +1$$

and $$\theta = -\tan^{-1}\frac{1}{\sqrt{3}} = -30^\circ$$

2) To provide points along direction O'B' (Fig.9)

$$\sigma_1 = \sigma_2 > \sigma_3$$

$$U = -\frac{\sigma_3 + \sigma_1}{\sigma_3 - \sigma_1} = -1$$

and $$\theta = \tan^{-1}\frac{1}{\sqrt{3}} = +30^\circ$$

3) To provide points along O'X (Fig.9)

$$\sigma_1 > \sigma_2 > \sigma_3$$

$$\text{where} \quad \sigma_2 = \frac{\sigma_1 + \sigma_3}{2}$$

$$U = \frac{0}{\sigma_3 - \sigma_1} = 0$$

$$\text{and} \quad \theta = 0$$

In addition to the investigation of the right sections of the surface of yield it is also necessary to establish the shape of the surface in space. The surfaces of yield for the Mohr Coulomb and the extended Tresca theories are hexagonal pyramids and that of the extended Von Mises theory is a cone. The apex of all three surfaces is at the origin of the system of three dimensional coordinates and the right sections are similar in shape but increase in dimension in the compressive directions at greater distances from the origin along the space diagonal. In order to establish the shape of the experimental surface in space it is therefore necessary that the stress systems 1), 2) and 3) should provide a sufficient range of stress to allow the shape of the surface to be investigated at sections at different distances along the space diagonal.

3 f) <u>The Apparatus Required for the Experimental Investigation of the Surface of Yield</u>.

The standard apparatuses used in the strength testing of

soils are the direct shear apparatus, and the triaxial apparatus. In the direct shear apparatus the normal and shearing stresses on the plane of slip are measured and by assuming a condition of yield the value of the major and minor principal stresses can be found. The value of the intermediate principal stress is indeterminate.

In the triaxial compression test a cylindrical sample is subjected to a fluid pressure and yield can be induced by increasing the axial stress. The principal stresses are known throughout the test. The minor principal stress is equal to the intermediate principal stress and is the value of the fluid pressure. The major principal stress is the sum of the fluid pressure and the increase in axial stress caused by the axial load.

Of the stress systems required for the investigation into the yield conditions (Section 3 e) 1) and 2) can be obtained in the triaxial apparatus.

Stress system 1) $\sigma_1 > \sigma_2 = \sigma_3$ represents the stress conditions in an ordinary triaxial compression test as described above.

Stress system 2) $\sigma_1 = \sigma_2 > \sigma_3$ can also be obtained in the triaxial apparatus by adapting it to produce yield by relieving the axial stress so that the major and intermediate principal stresses are equal to the fluid pressure. The axial stress is the minor principal stress. This test is generally known as

the triaxial extension test.

In the triaxial apparatus the fluid pressure can be altered to allow the surface of yield to be investigated at sections at different distances from the origin of the system of coordinates.

For the remaining stress system 3) where $\sigma_2 = \frac{\sigma_1 + \sigma_3}{2}$ a new apparatus must be devised since no standard soil testing apparatus can produce such a system of stress.

SECTION 4.

The Design and Description of the New Apparatus (The Thick Cylinder Apparatus.

4 a) Analysis of Conditions at Point of Yield.

A suitable method of obtaining the desired stress distributions is by testing the material in the form of a thick walled cylinder. The thick cylinder sample can be constrained by an inside and outside pressure, the inside pressure can then be increased until yield is induced. An element of material is therefore subjected to radial, tangential and axial compressive stresses.

As was stated in Section 3 e) it was decided to apply a system of stress which will provide points along O'X, intermediate between O'B' and O'A in the right section of the surface of yield Fig.9, and if the results required a fuller enquiry to apply other stress systems which will provide additional points on the surface between X and B', and X and A as a supplementary part of the investigation. Using the thick cylinder method of testing the first stress system can be approximately obtained by arranging the dimensions of the sample such that the axial stress (intermediate) has a value

$$\sigma_2 \doteq \frac{\sigma_1 + \sigma_3}{2} \quad \text{(where } \sigma_1 \geqslant \sigma_2 \geqslant \sigma_3\text{)},$$

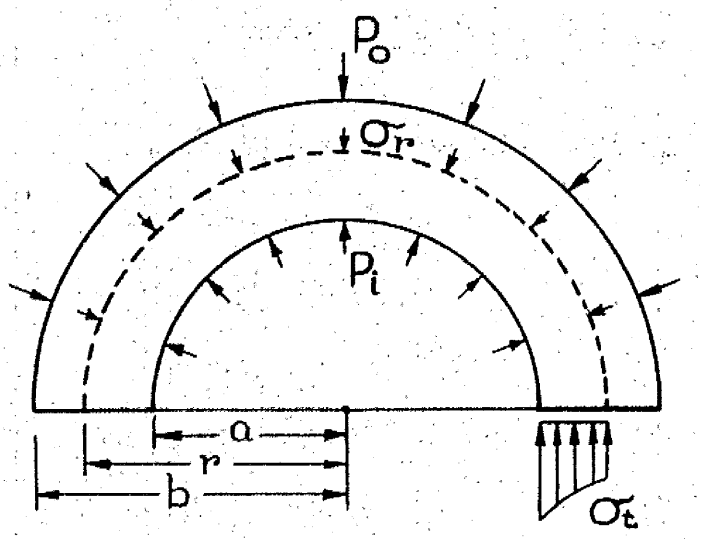

STRESSES IN WALL OF THICK CYLINDER SAMPLE

FIG. 11.

the axial stress being produced by load differences on the sealed cap of the sample. Other stress systems, if they are required, can be obtained in the thick cylinder apparatus by adapting it to produce relief or increase of the axial stress.

For guidance in the design of the apparatus it was assumed that the Mohr-Coulomb theory of strength holds.

The stresses in a vertical section of the thick cylinder sample will be as shown in Fig.11 where

b denotes the outside radius
a " " bore radius
P_o " " outside pressure
P_i " " bore pressure
σ_r " " radial stress at any radius r
σ_t " " tangential " " " " " r

The forces must be in equilibrium

∴ at any radius r

$$P_i a - \sigma_r r + \int_a^r \sigma_t \, dr = 0 \quad \ldots\ldots\ldots\ldots (21a)$$

On differentiation (21a) becomes

$$- \sigma_r - \frac{r \, d\sigma_r}{dr} + \sigma_t = 0 \quad \ldots\ldots\ldots\ldots (21b)$$

σ_r is the major principal stress and σ_t is the minor principal

stress. Assuming the Mohr-Coulomb condition of yield $\sigma_t = \lambda \sigma_r$ (eqn.17b). Substituting for σ_t in (21b) at yield

$$\frac{dr}{r} = \frac{d\sigma_r}{\sigma_r (\lambda - 1)} \quad \ldots\ldots\ldots\ldots\ldots\ldots\ldots\ldots (21c)$$

On integrating (21c) becomes

$$\log r = \frac{1}{(\lambda - 1)} (\log \sigma_r - \log A)$$

$$\text{or} \quad \sigma_r = A\, r^{(\lambda - 1)} \quad \ldots\ldots\ldots\ldots\ldots\ldots\ldots\ldots (21d)$$

where A is a constant of integration

giving σ_r and hence σ_t at any radius at the point of yield. During the test the outside pressure will be kept constant and the inside pressure will be increased until failure occurs.

At outside radius b , $\sigma_r = P_o$. Substituting for σ_r in (21d)

$$A = \frac{P_o}{b^{(\lambda - 1)}}$$

The radial stress at yield at any radius r is therefore given by

$$\sigma_r = P_o \left(\frac{r}{b} \right)^{(\lambda - 1)} \quad \ldots\ldots\ldots\ldots\ldots\ldots\ldots\ldots (22)$$

The pressure at the bore (r = a) which will just cause yield

is given by

$$\sigma_{r_a} = P_i = P_o\left(\frac{a}{b}\right)^{(\lambda - 1)} \quad \ldots\ldots\ldots\ldots(23)$$

and the tangential stress at yield at the bore by

$$\sigma_{t_a} = \lambda P_o\left(\frac{a}{b}\right)^{(\lambda - 1)} \quad \ldots\ldots\ldots\ldots\ldots\ldots(24)$$

The average radial stress in the wall of the sample can be obtained from (22).

At any radius r the radial stress $\sigma_r = P_o\left(\frac{r}{b}\right)^{(\lambda - 1)}$

The average radial stress $= \dfrac{P_o}{b^{(\lambda - 1)}} \displaystyle\int_a^b \frac{r^{(\lambda - 1)}\,dr}{b - a}$

$$\therefore \quad \sigma_{r_{av.}} = \frac{1}{\lambda} \frac{P_o}{b^{(\lambda - 1)}(b - a)} (b^{\lambda} - a^{\lambda}) \quad \ldots\ldots(25)$$

The average tangential stress is obtained from conditions of equilibrium of the sample

$$\sigma_{t_{av.}} = \frac{P_o\, b - P_i\, a}{b - a} \quad \ldots\ldots\ldots\ldots\ldots\ldots(26)$$

The axial stress is constant over the horizontal sections of

the wall and is given by

$$\sigma_a = \frac{P_o \pi b^2 - P_i \pi a^2}{\pi b^2 - \pi a^2} \quad \text{.....(27)}$$

and

from (23) $$\sigma_a = P_o \left[\frac{b^2/a^2 - (b/a)^{(1-\lambda)}}{b^2/a^2 - 1} \right] \quad \text{.....(28)}$$

The axial stress, the intermediate principal stress, varies in magnitude between the values of the radial stress, the major principal stress, and the tangential stress, the minor principal stress, depending on the value of λ and the ratio of the sample dimensions b/a. A minimum wall thickness of $3/4$" was decided upon for the medium sand to be used and the sample dimensions were chosen for convenience. The outside radius was fixed at 2" and maintaining a wall thickness of $3/4$" the bore radius becomes $1\frac{1}{4}$" making the ratio $b/a = 1.6$.

The values of the average major, minor and intermediate principal stresses at yield for the chosen sample dimensions are shown in Table 1. The stresses are computed from eqns. (25), (26) and (27) for $\lambda = 0.3$ (angle of internal friction $\phi = 32^\circ\ 36'$) and $\lambda = 0.2$ ($\phi = 42^\circ\ 12'$).

A comparison of the last two columns of Table I shows that the axial stress is very nearly equal to half the sum of

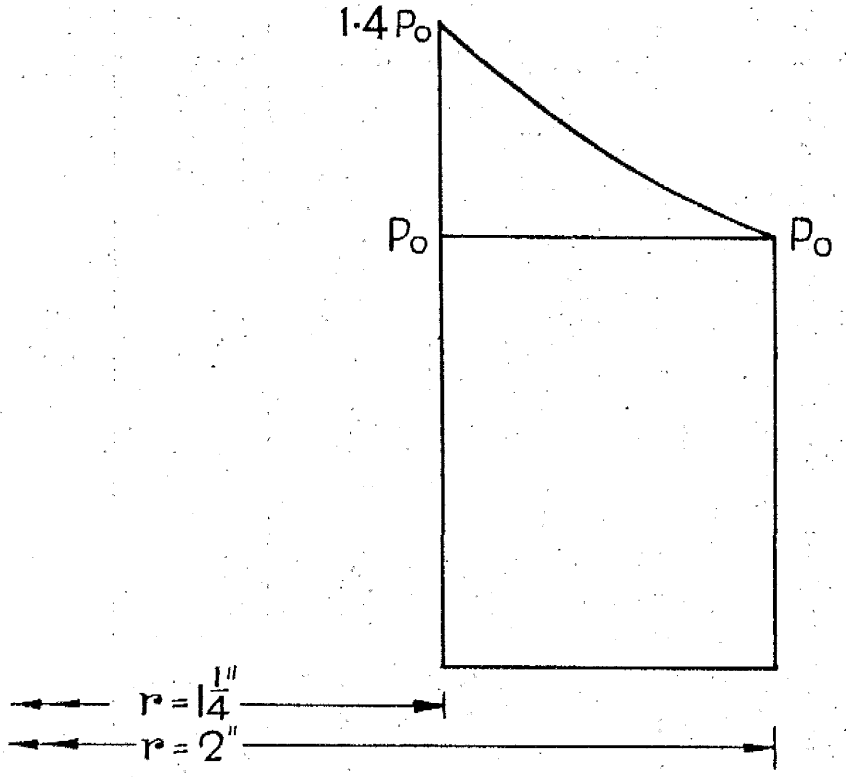

THICK CYLINDER SAMPLE

DISTRIBUTION OF RADIAL STRESS ACCORDING TO MOHR COULOMB THEORY ($\lambda = 0.3$)

FIG. 12.

the major and minor principal stresses for λ values representing a range of angles of internal friction of at least from 32^{o} to 42^{o}.

Table I

λ	σ_1 ($\sigma_{r_{av.}}$)	σ_3 ($\sigma_{t_{av.}}$)	σ_2 (σ_a)	$\frac{\sigma_1 + \sigma_3}{2}$
0.3	1.155 P_o	0.347 P_o	0.750 P_o	0.751 P_o
0.2	1.200 P_o	0.240 P_o	0.705 P_o	0.720 P_o

The distribution of radial stress across the wall of the sample also varies with the value of λ . The radial stress at any radius is given by equation (22)

$$\sigma_r = P_o \left(\frac{r}{b} \right)^{(\lambda - 1)}$$

The distribution of radial stress for $\lambda = 0.3$ is shown in Fig.12. The curve is slightly convex but very nearly linear within the sample dimensions. The tangential stress at any radius is equal to λ times the radial stress.

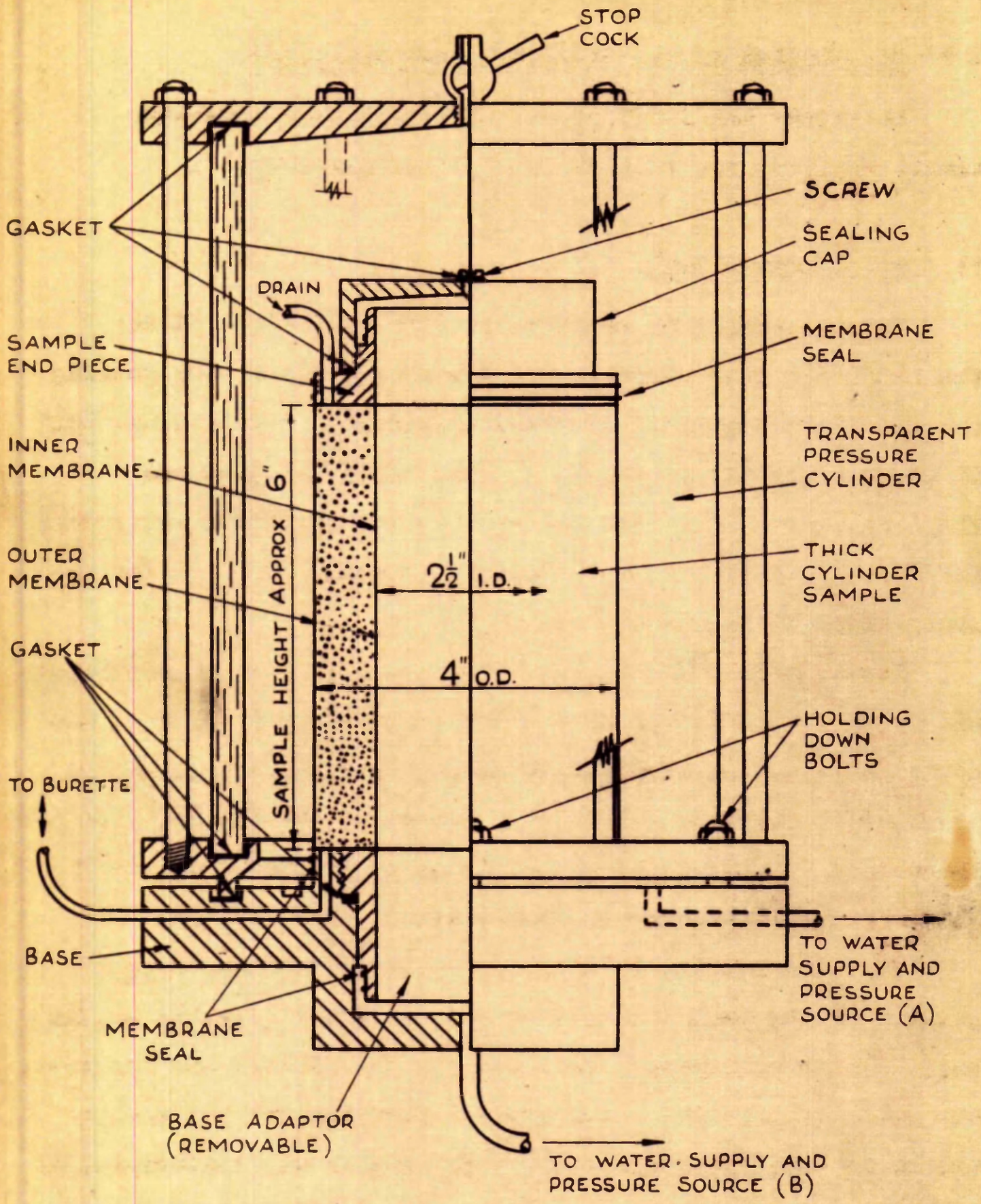

THICK CYLINDER APPARATUS

HALF SECTION OF PRESSURE CELL

FIG. 13.

4 b) Description of the Thick Cylinder Apparatus.

There are two parts to the thick cylinder apparatus namely the pressure cell and the pressurising system.

1) The Pressure Cell.

The pressure cell consists of five individual parts: the base, the base adaptor, the sample end piece, the sealing cap and the transparent pressure cylinder. The pressure cell is shown assembled in Fig.13 . The base, the base adaptor, the sample end piece, and the sealing cap are shown separately in Figs.14 and 15. The transparent pressure cylinder is shown in photo Fig.16 .

The base is a steel plate with a raised ring on its upper side. The ring forms the pedestal for the sample and is the position of the outer membrane seal. Entries for water are provided to the bore and to the outside of the sample. An entry to the base of the sample is also provided to allow volume change measurements to be made.

The base adaptor is a hollow cylinder with the upper portion of the wall threaded to mate with the pedestal on the base. A gasket forms a seal between the adaptor and the base. The recessed portion on the adaptor provides the position of the lower inner membrane seal. The sum of the thicknesses of the adaptor and the base pedestal make up the wall of the sample.

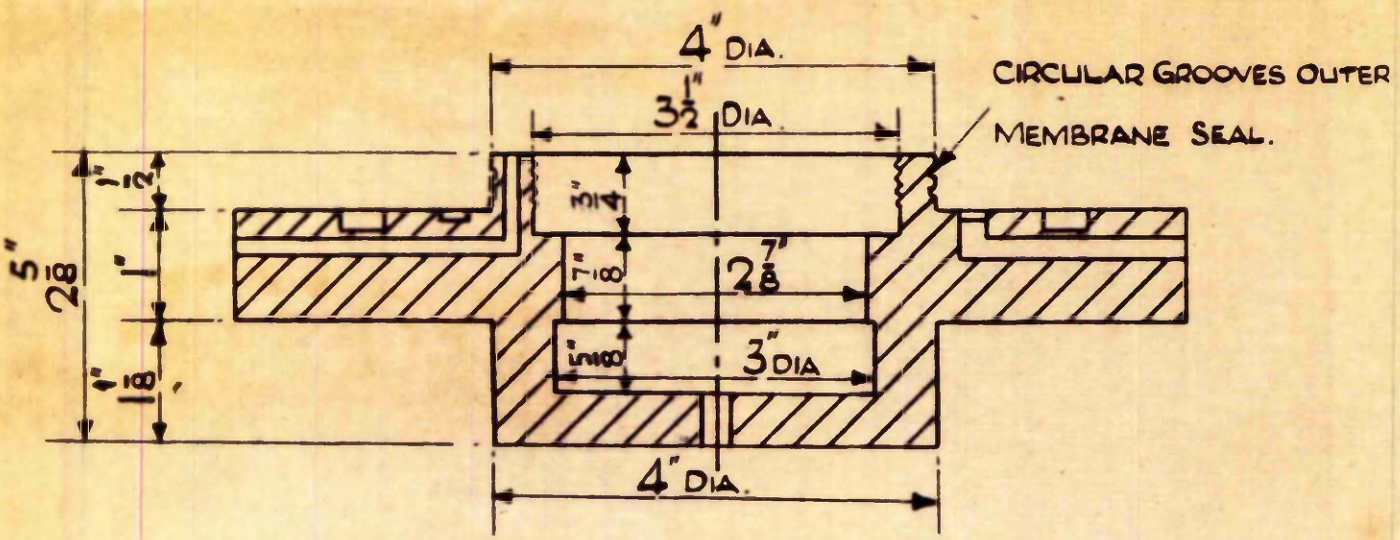

SECTION

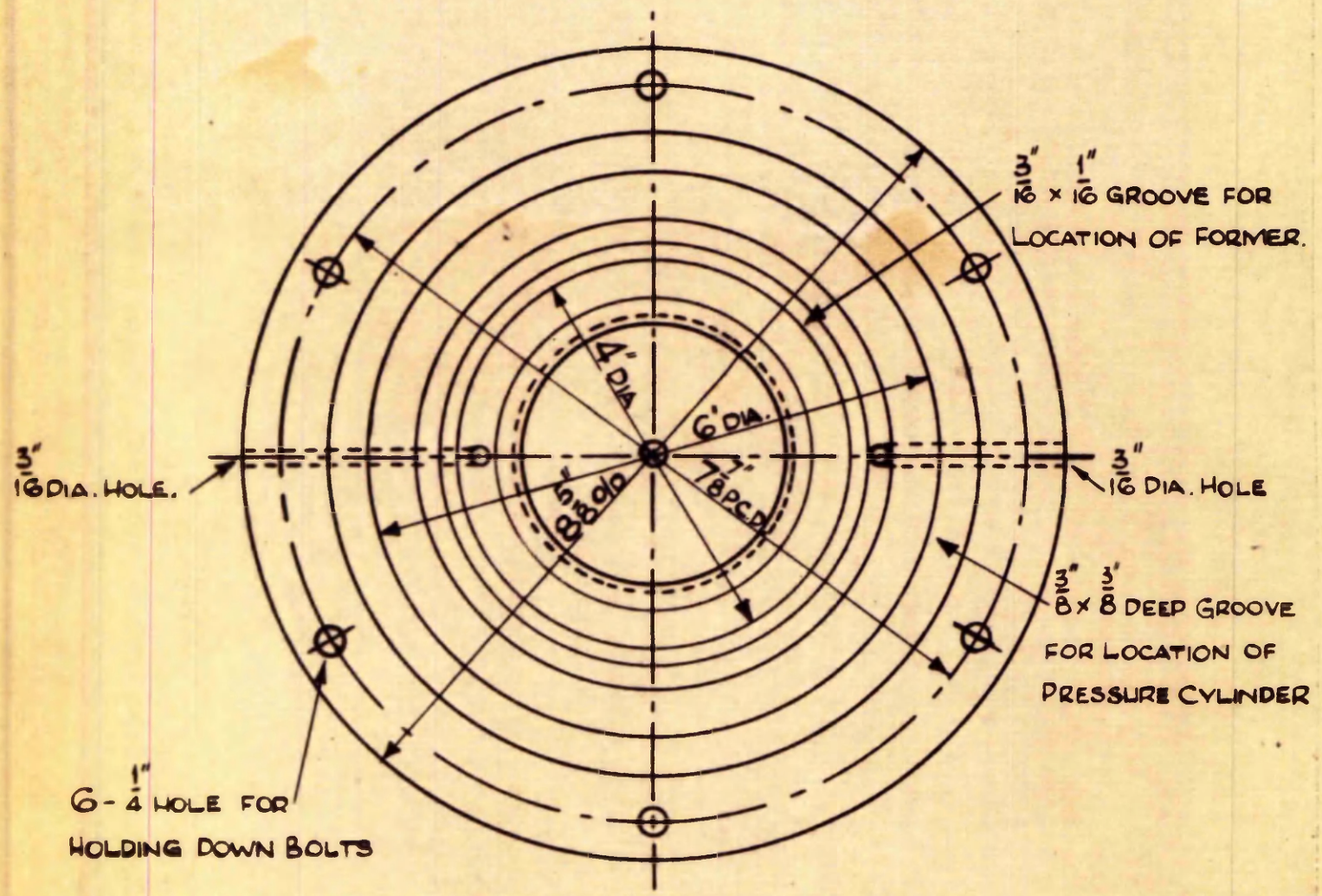

PLAN

THICK CYLINDER TESTING APPARATUS

CELL BASE

FIG. 14

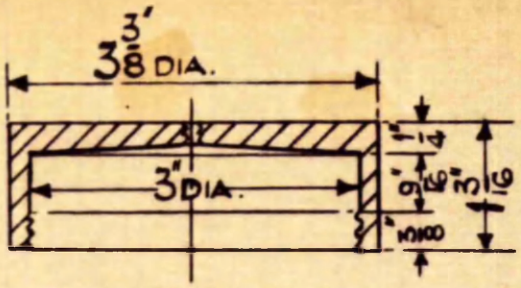

SECTION

CIRCULAR SEALING CAP

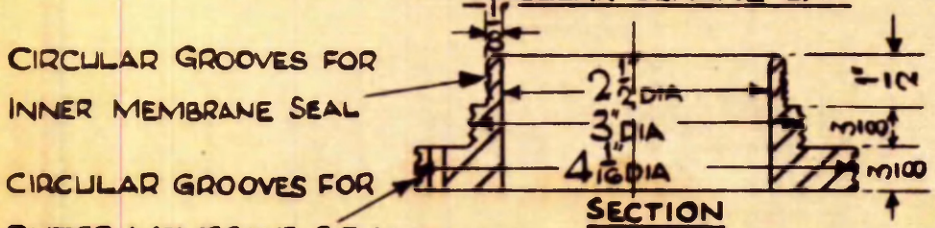

SECTION

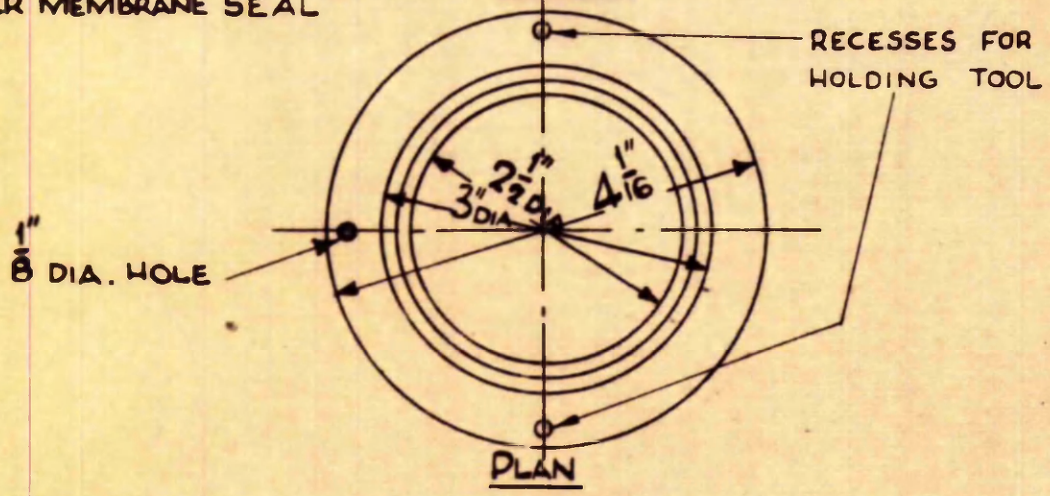

PLAN

SAMPLE ENDPIECE

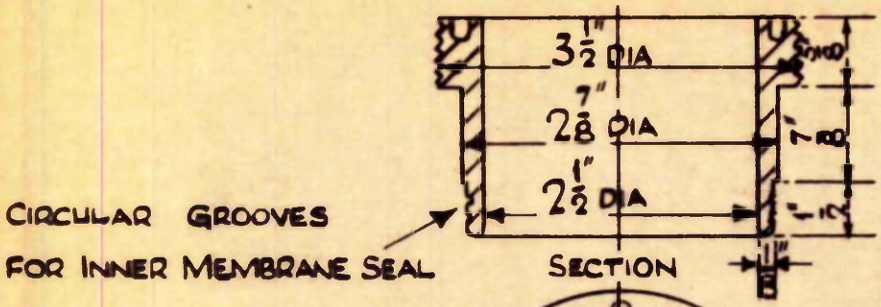

SECTION

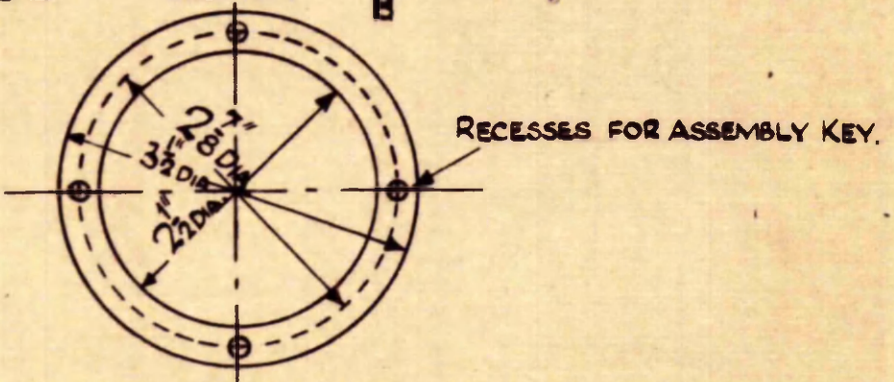

PLAN

BASE ADAPTOR

THICK CYLINDER TESTING APPARATUS

PRESSURE CELL PARTS

FIG. 15

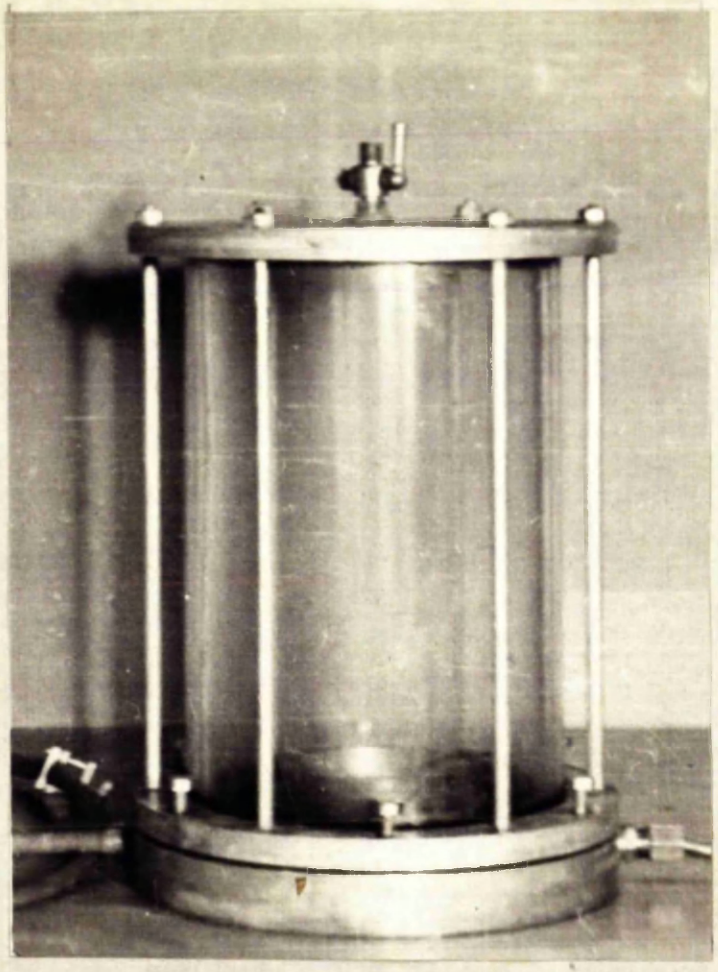

FIG. 16. TRANSPARENT PRESSURE CYLINDER.

FIG. 17. OUTSIDE AND INSIDE FORMERS.

The provision made in designing the base adaptor so that it is removable from the base allows the apparatus to be simply adapted for testing other soils in which different wall thicknesses are required.

The sample end piece forms the position of the upper seal for the inner and outer membranes. An entry is allowed to the wall so that the sample can be completely saturated with water. The sealing cap screws down over the sample end piece. A holding tool which fits into two recesses on the end piece allows the cap to be sealed without applying a torque to the sample.

The roof of the sealing cap is coned to allow the evacuation of air from the bore of the sample when it is filled with water. The final seal, isolating the bore from the outside of the sample, is effected by a screw and gasket in the cap.

The pressure cylinder is located on a groove on the base plate and is held down by six bolts.

The outside and inside formers required to prepare the sample are shown in Photo Fig.17. The outer former is a split hollow cylinder with an inside diameter of 4 in. This former fits into a groove on the base plate and locates the sample on the pedestal. The inside former is a solid wooden cylinder. The thick cylinder samples have bore diameter of $2\frac{1}{2}$ in. an outside diameter of 4 in. and a height of 6 in. The rubber membranes used to confine the samples have a wall thickness of 0.008 in.

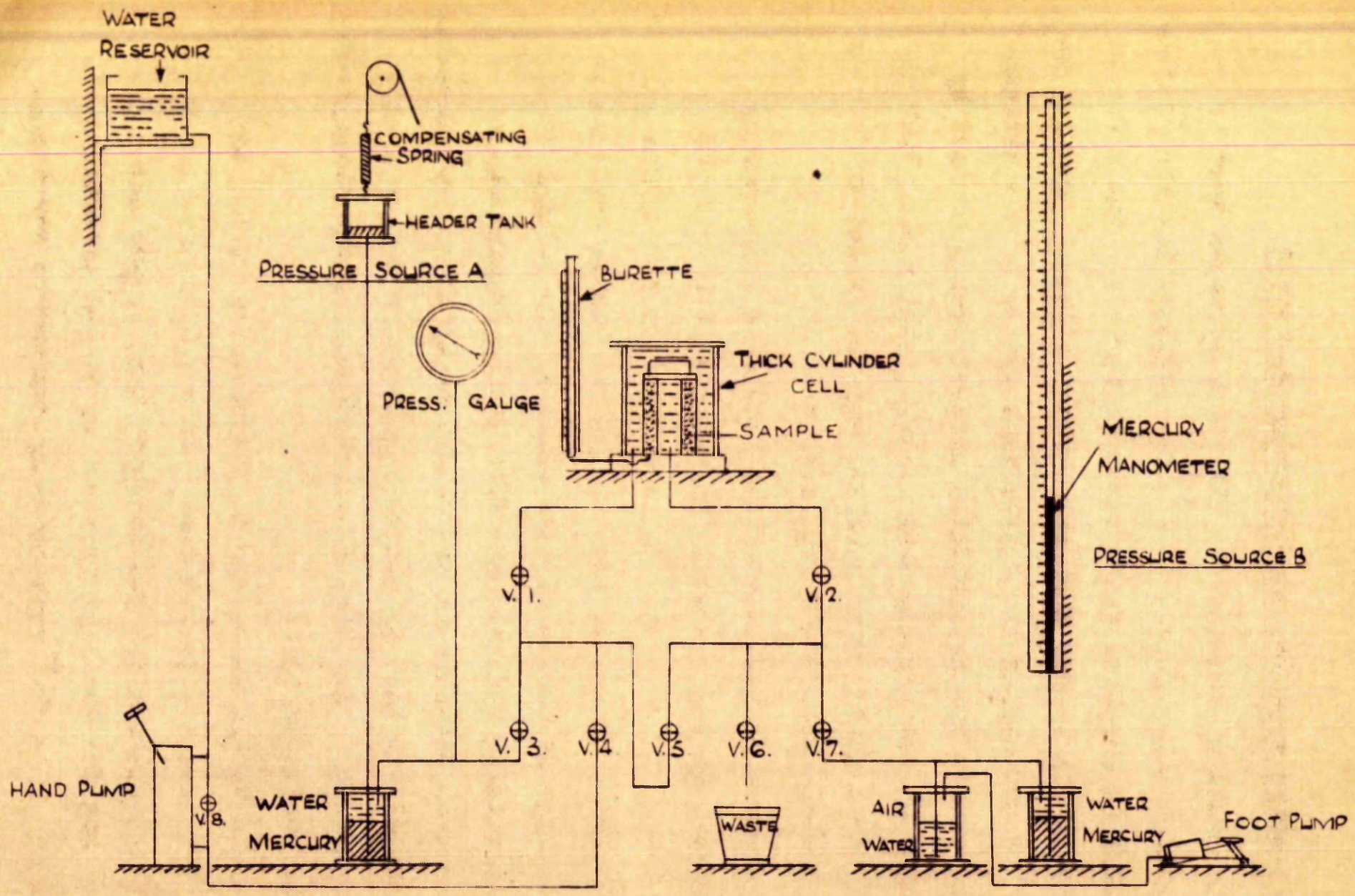

DIAGRAMATIC PICTURE OF PRESSURISING SYSTEM.

FIG. 18.

2) The Pressure Applying and Measuring Equipment.

The pressure system used in the thick cylinder test is shown diagramatically in Fig.18 . The pressure for the outside of the sample is supplied from pressure source A. The pressure is produced by the header tank and mercury column. Changes in the amount of mercury in the header tank caused by the deformation of the sample are accommodated without change of head by the extension of the compensating spring. The header tank is suspended from a string over a pulley and can be set to produce pressures ranging from 0 - 70 lb./in^2.

The pressure at the bore of the sample is increased by pumping mercury up the manometer by means of the foot pump. (Pressure source B, Fig.18). Narrow (3/16" I.D.) tubing was chosen for the manometer so that the volume change would cause relatively large decreases in head allowing equilibrium conditions to be quickly obtained and thus giving strain control.

The outside pressure is accurately measured on the monometer at the start of the test by connecting pressure source A with pressure source B. The bore pressures are measured throughout the test on the manometer.

The scale on the manometer is graduated in inches and tenths. The pressure is obtained from a calibration curve which makes allowances for the changing head in the air-water change-over and for the head of water up to the pressure cell. A pressure of 1 lb./in^2 represents approximately two inches

on the manometer. Readings on the scale can be made with an accuracy of at least $1/20^{th}$ inch giving a possible error of $\pm$ $1/40^{th}$ inch representing an accuracy of $\pm$ .063% at a pressure of 20 lb./in^2. This is within the desired accuracy as shown in Appendix IV.

3) Measurement of Sample Dimensions.

The importance of the diameter measurements of the specimen is illustrated in Appendix IV. The diameters are measured before the test and after failure of the specimen. The outside diameter is measured by ordinary outside callipers. For the measurement of the bore diameter, special callipers for inside measurement had to be made. Estimations of $1/100^{th}$ inch could be made with these. The accuracy of measuring the diameters is $\pm$ $\frac{1}{200}$ th. inch representing a possible error of $\pm$ $\frac{1}{400}$ th. or $\pm$ 0.2% on an inside radius of 1.25 inches and $\pm$ 0.125% on an outside radius of 2 inches.

SECTION 5.

Description of Experimental Work.

5 a) The Sand Used.

Loch Aline sand was used in all tests reported in this thesis. The sand is fully described in Appendix I.

5 b) The Tests Performed.

A summary of the tests performed is shown in Table II.

Table II.

Summary of Tests Performed

Type of Test	Series	Average Initial Porosity
Triaxial Compression Triaxial Extension	1	43.0%
Triaxial Compression Triaxial Extension	2	38.5%
Triaxial Compression Triaxial Extension	3	36.6%
Triaxial Compression Triaxial Extension	4	35.1%
Thick Cylinder	5	35.6%

Four series of tests at different porosities were carried out in the triaxial apparatus, each series consisting of a range of compression and extension tests. One series of tests was performed at a low porosity in the thick cylinder apparatus.

The results of triaxial compression and extension tests reported by Taylor[14] and Habib[3][4] (Section 1) disagreed with the results of an early series of tests performed by the author. In view of this disagreement three additional series of triaxial compression and extension tests were performed by the author in order to confirm that the early results were representative of the conditions at porosities ranging throughout the limits for the sand. The results for the additional series confirmed the results of the early series and showed close agreement with the Mohr-Coulomb theory. The thick cylinder tests were performed on samples at one porosity as the time taken to perform the tests was lengthy and the results indicated further confirmation of the Mohr-Coulomb theory.

It was found that by adopting the same procedure in placing the sand in the samples of each series, the porosity within the series could be kept approximately constant. This was desired to allow the results of the individual series to be compared and the Mohr envelopes for the triaxial tests to be drawn. The porosity reported in Table II is the average initial porosity for the series, the initial porosity being

the porosity after consolidation under the confining pressure. The initial porosity of the thick cylinder tests is close to that for the triaxial tests of series of 4 and the results of these tests are compared later.

The methods used in placing the samples were as follows:-

Triaxial Samples

Series 1:- Samples were formed by allowing the sand to settle under a static head of water.

Series 2:- Samples were formed by placing the sand in three layers, each layer being tamped 25 times with $\frac{1}{2}$" diameter wooden rod.

Series 3:- Samples were formed by placing the sand in three layers, each layer being vibrated internally by a hand vibrator.

Series 4:- Samples were formed by placing the sand in fifteen layers, each layer being tamped lightly 100 times with a $\frac{1}{2}$" diameter wooden rod.

Thick Cylinder Samples.

Thick cylinder samples were formed by placing the sand in three layers, each layer being vibrated by the application of a hand vibrator to the inside and outside formers.

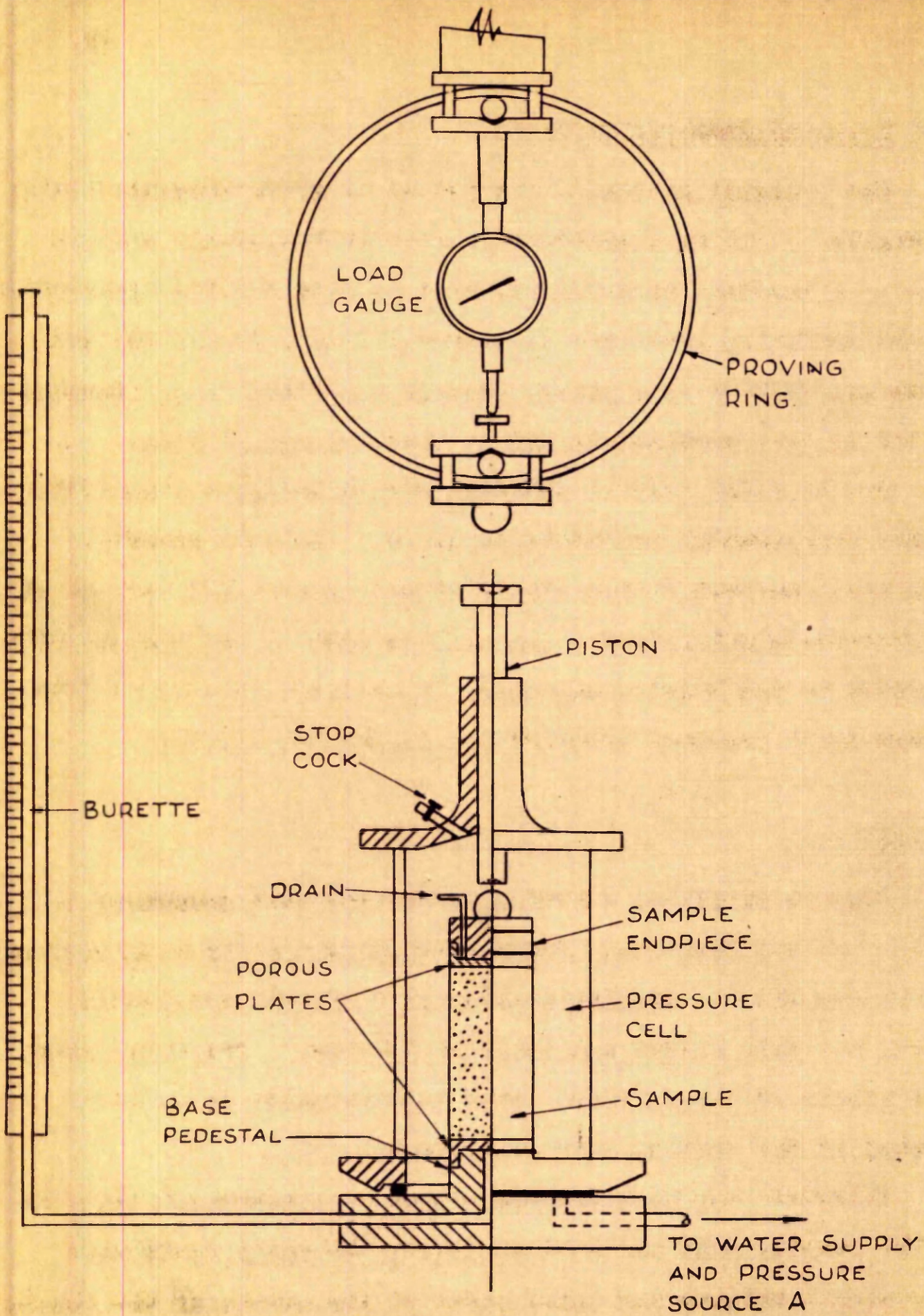

TRIAXIAL APPARATUS

LAYOUT FOR COMPRESSION TESTS

FIG. 19

5 c) Triaxial Compression Tests.

The triaxial apparatus and set up is shown diagramatically in Fig.19 . It is a standard machine of the strain control type. A constant head mercury tank is used for the application of the confining pressures (Pressure Source A in Fig.18) and loads are applied by a piston through a proving ring. Samples tested on this machine are 1⅜" in diameter and 3" long.

The triaxial test is standard and no detailed description of the experimental procedure is given. Lateral pressures were kept constant during the tests and failure was induced by an increasing axial load. During the test volume changes were observed in the burette and axial deflections were noted from strain gauge readings taken at the top of the piston.

Corrections.

A study of piston friction at various cell pressures was made. It was found that the variation in the friction between the piston and the sealing chamber at different extents of travel was only slight and could be ignored. The total error as a result of the friction could be eliminated by careful zeroing of the proving ring extensometer.

Allowance was made for the change of cross-sectional area of the sample. It was noticed during the early tests that appreciable bulging had taken place at the centre of the sample before the peak stresses were reached. The central cross-

sectional area of the sample was calculated using Simpson's Rule assuming that the area of the sample increased parabolically from the ends to the centre. The end areas were assumed to remain constant throughout the test and the central area was obtained from

$$A_c = \frac{4 \cdot \frac{V_o \pm dv}{L_o - dl} - (A_t + A_b)}{6}$$

where A_c denotes the central area of the sample
A_t " " area at the top of the sample
A_b " " " " " bottom of the sample
V_o " " original volume " " "
L_o " " " length " " "
dv " " measured volume change of the sample
dl " " " change in length

dv and dl were obtained from the test data.

The correction was only applied after bulging of the sample was noted; previous to this the area used in stress calculations was obtained from

$$A = \frac{V_o \pm dv}{L_o - dl}$$

(with the above notation).

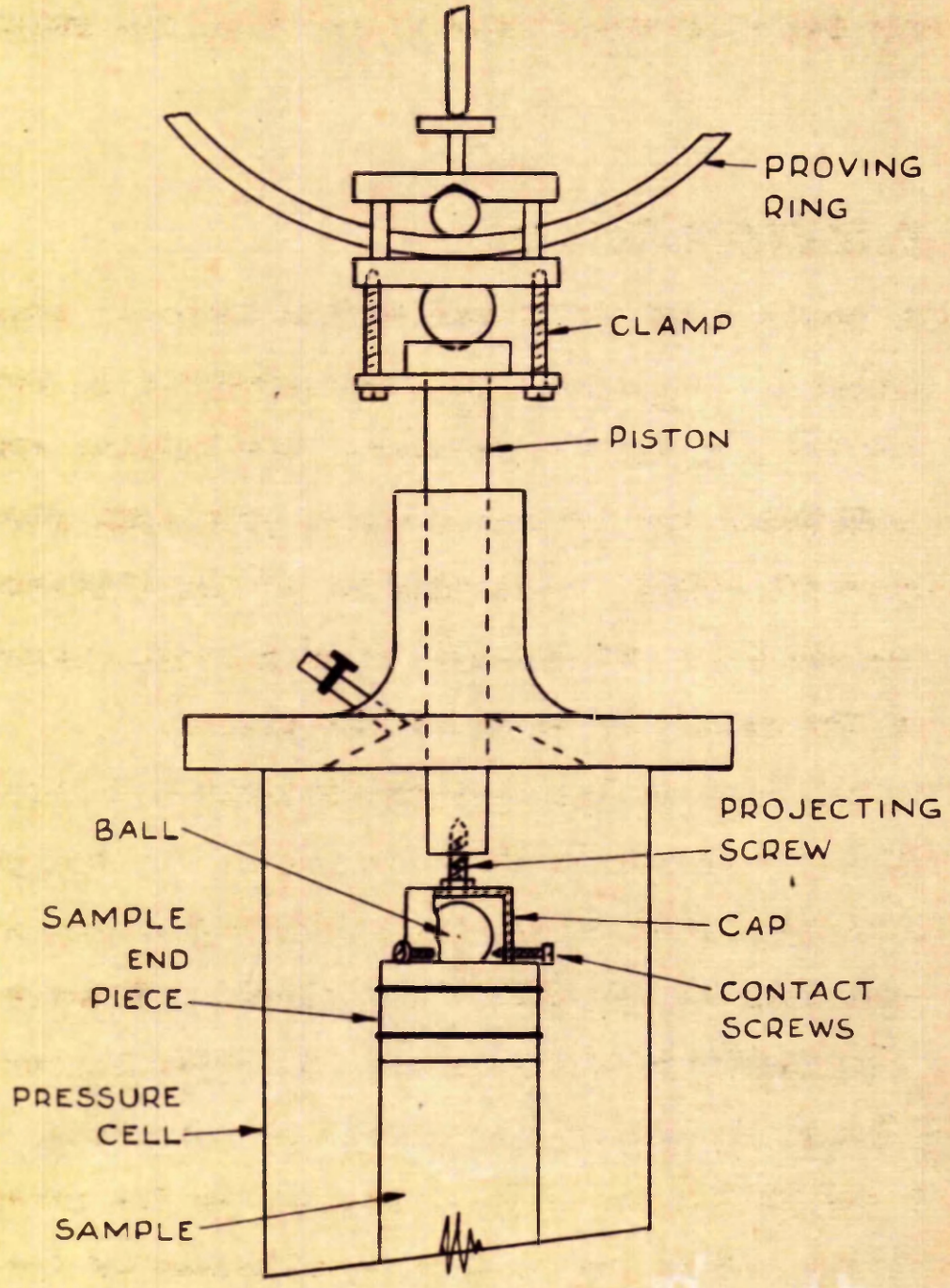

TRIAXIAL APPARATUS

ADAPTION FOR EXTENSION TESTS

FIG. 20

In the samples tested at low porosity (series 4) only the stresses after the peak point were affected by the bulging correction.

5 d) Triaxial Extension Tests.

In these tests, also performed on the triaxial apparatus the stress system $\sigma_1 = \sigma_2 > \sigma_3$ was obtained by reducing the axial load until yield was reached. The lateral confining pressures constituted the two major equal principal stresses, the minor principal stress being made up of the difference of this confining pressure and the relief of stress transmitted to the end of the sample by means of the piston.

The adaption made to the triaxial apparatus to produce the axial relief of stress is shown in Fig.20 . The relief of stress was transmitted to the sample through a cap which fitted over the ball on the sample end piece. Three contact screws made connection with the ball. A projecting screw on the cap was picked up by a mating thread in the piston and the other end of the piston was clamped rigidly to the proving ring. The axial stress was reduced by withdrawing the piston from the pressure chamber. The tension in the piston was measured by the proving ring.

A movement of about ¾ mm. was allowed before the contact screws on the cap made connection with the ball on the sample end piece. This movement was necessary to make the allowance

for friction and for the zeroing of the proving ring extensometer.

In the extension tests the range of major principal stress is limited by the capacity of the constant head pressurising system. The maximum pressure obtainable from the system as described in Section 4 b) 2) is 70 lb./in^2. In the tests of series 4, where the λ values were low it was necessary to increase the capacity of the system to reduce the effect of errors in the estimation of the minor principal stress. A closed circuit pressurising system was temporarily used where the pressures were produced and controlled by a foot pump. Pressures up to 150 lb./in^2 were obtained by this system.

Corrections.

Extension test samples retained their cylindrical shape till after the peak stresses were reached. The cross-sectional area, used in stress computations, was calculated on the assumption that the sample deformed as a right cylinder having a volume and height as those indicated by the test data.

An allowance was made for the tension in the rubber membrane caused by the extension of the sample. This correction was measured after the completion of each test; the confining pressure was taken off; the piston was lowered until zero deflection was registered on the strain measuring extensometer; the piston was then raised and the loads were measured at strains

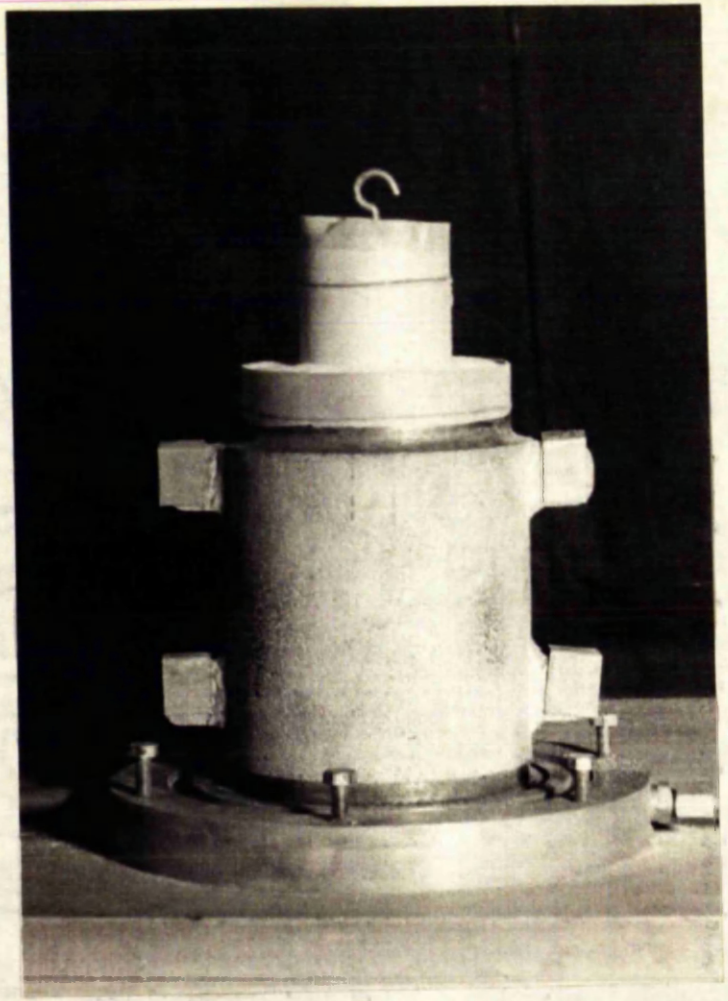

FIG. 21. THICK CYLINDER SAMPLE UNDER PREPARATION.

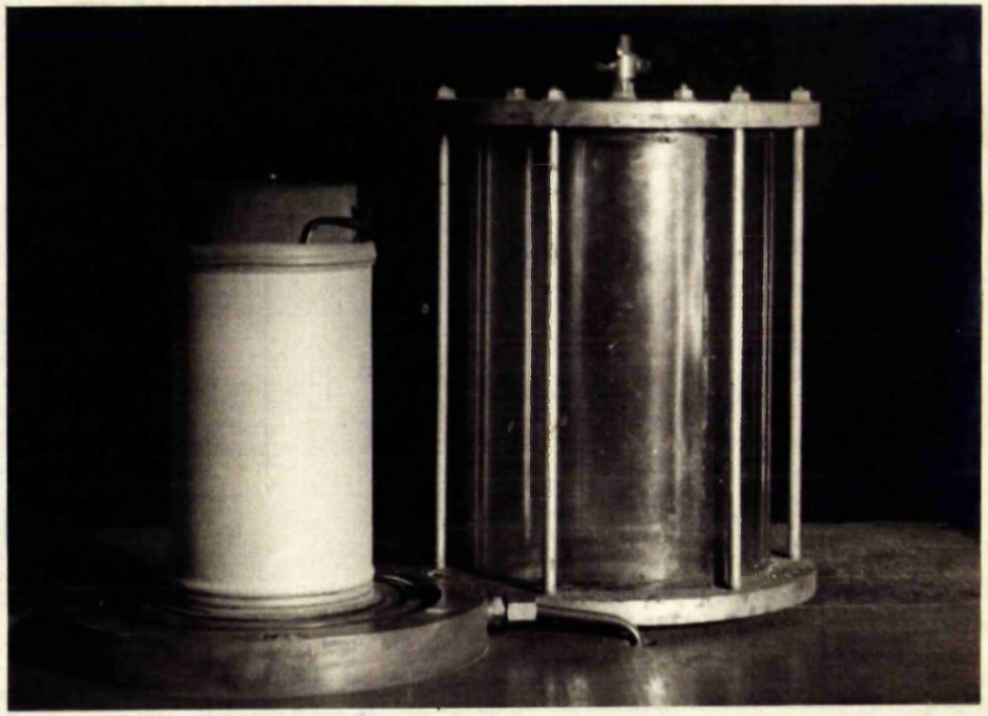

FIG. 22. THICK CYLINDER SAMPLE READY FOR TEST.

corresponding to those of the test. The assumption was made that the membrane tension was independent of the cell pressure and these piston loads were subtracted from those measured in the test.

5 e) Thick Cylinder Tests.

The thick cylinder apparatus and pressurising system is described in Section 4 b.

1) Preparation of the Sample.

The method adopted in preparing thick cylinder samples is described with reference to Figs.13 to 16. The base adaptor was removed from the base and the inner rubber membrane was fitted and sealed. The membrane was turned inside the collar of the adaptor and the whole screwed into the base, making a seal on the gasket. The inside former was then fitted inside the membrane and adaptor, and after the outer membrane was fitted to the base the outside former was placed in the locating groove. The outer membrane was stretched and folded over the top of the outside former. The sand was filled between the outside and bore formers in the manner described previously in Section 5 b. Care was taken during filling to keep the inside former centred. When the sand was level with the top of the outside former the sample end piece was placed and the bore and outside membranes sealed. The sample was then saturated

by allowing water to flow into the base from the burette and when saturation was complete, the drain on the sample end piece was closed. A slight vacuum was applied to the sample through the burette and the formers were removed and the sample was measured. The sealing cap was then carefully placed on the end piece using a holding tool which fitted into the recesses on the sample end piece to prevent any torque being applied to the sample while the cap was being screwed down. The bore of the sample was filled by allowing water to flow from the reservoir through valves 4, 5 and 2 (Fig.18). When the bore was full valve 5 was closed and the final seal, isolating the bore from the outside, was made by the screw and gasket on the top of the cap. The transparent pressure cylinder was then fitted and the space between the outside of the sample and the cylinder was filled with water by opening valve 1. When the pressure cylinder was full valve 1 and the stop cock on the pressure cylinder were closed. Photographs of a sample under preparation and ready for test are shown in Figs.21 and 22.

2) Test Procedure.

The header tank of Pressure Source A in Fig.18 was set to the required level using the pressure gauge as a guide. The bore and the outside of the sample were then pressurised simultaneously by opening valves 1, 2 and 5 and then valve 3.

This pressure at which the outside of the sample remains throughout the test was measured accurately from the reading on the mercury manometer after valve 7 had been opened. The test was ready to start when valve 5 was closed isolating the bore from the outside of the sample.

The bore pressure was increased by pumping mercury up the manometer using the foot pump (Pressure Source B). Increments of approximately 1 lb./in^2 were applied initially. After each pressure increment sufficient time was allowed for the sample to drain and to allow the volume changes to be read on the burette.

As the yield point was approached the pressure increments were reduced to approximately 0.2 lb./in^2. As yield took place the volume of the bore of the sample increased and the inside pressure fell until it came into equilibrium with the reduced strength of the sample. Further pumping resulted in a further increase in the bore volume and the resulting equilibrium was reached at a lower inside pressure. The reserve of mercury in the small bore tube of the mercury manometer was sufficiently small to prevent runaway failures from taking place. The peak stresses were easily picked out since they were followed by a marked reduction of the inside pressure.

Several tests were conducted beyond the yield point to study the failure of the sample. Most tests however were stopped as soon as yield was noticed.

After completion of the test the inside and outside pressures were equalised by opening valve 5 (Fig.18). After a slight vacuum had been applied to the sample the pressure was released and the water from the cell drained to waste through valve 6. The pressure cylinder was then removed and the bore and outside dimensions measured.

3) Factors Affecting the Determination of the Yield Stresses in Thick Cylinder Test.

a) Sample Dimensions.

The calculation of the stresses in the thick cylinder test requires the knowledge of the bore and outside pressures and diameters of the sample.

Yield in the thick cylinder was manifested by a crack in the centre of the sample after a slight uniform bulging had occurred (Section 9 a Part II). The test in the majority of cases was stopped immediately the yield stresses had been recorded and the sample was measured up. These dimensions were used in the calculation of the yield stresses. In a few of the samples tested beyond yield, observations showed that strains after the yield point were caused by the outward rotation of part of the wall on one side of the crack while the remainder of the sample did not alter. It was thus possible to obtain the sample dimensions at yield, in these tests, from measurements

taken on the failed sample.

b) Rubber Membranes.

The effect of the bulging of the thick cylinder sample induces stresses in the rubber membranes confining the sample. The stresses in the outside membrane would cause a radial stress which increases the outside radial stress while the stresses in the bore membrane will reduce the inside radial stress. The outside radial stress will thus be slightly greater and the bore radial stress slightly less than those measured.

An estimation of the error induced by the influence of the rubber membrane can be obtained knowing the sample dimensions and the extension properties of the membranes. A hoop tension is induced into the membrane by the bulging. The tension t per unit length of membrane can be calculated from

$$t = M e_c$$

The change in radial stress caused by this tension

$$d\sigma_r = t/r \quad \text{i.e.} \quad d\sigma_r = \frac{M e_c}{r}$$

where M denotes the extension modulus of the membrane ($\doteq$ 1.5 lb./in for the 0.008" thick membranes used (Henkel and Gilbert[5]).

e_c denotes the circumferential strain

r denotes the sample radius considered.

To obtain the true radial stress $d\sigma_{r=b}$ must be added to the measured outside pressure and $d\sigma_{r=a}$ must be subtracted from the measured bore pressure. These corrections are small at the yield point (in the order of 0.025 lb./in^2 at the outside) and have a slight effect only at low pressures. After the yield point the membrane extends locally in the region of the crack and the above correction cannot be applied.

SECTION 6.

Experimental Results.

6 a) Method of Presentation of Results.

Difficulty arises in representing the experimental results to illustrate the shape of the right section of the surface of yield. The right sections vary in dimension along the space diagonal and different results define points on different right sections. (This is discussed in Appendix III). The experimental surface in space however proves to be bounded by straight lines which pass through the origin of the system of coordinates (e.g. PO in Fig.AP.III.2, Appendix III) and the difficulty in illustrating the shape of the right section was overcome by plotting the tangent of the angle made by the line joining the experimental point on the surface to the origin and the space diagonal. In this way the experimental results can be reduced so that they can be considered to represent points on an equivalent right section. This equivalent right section is referred to as the reduced right section. The coordinates of the points representing the experimental results on the reduced right section are derived in Appendix III.

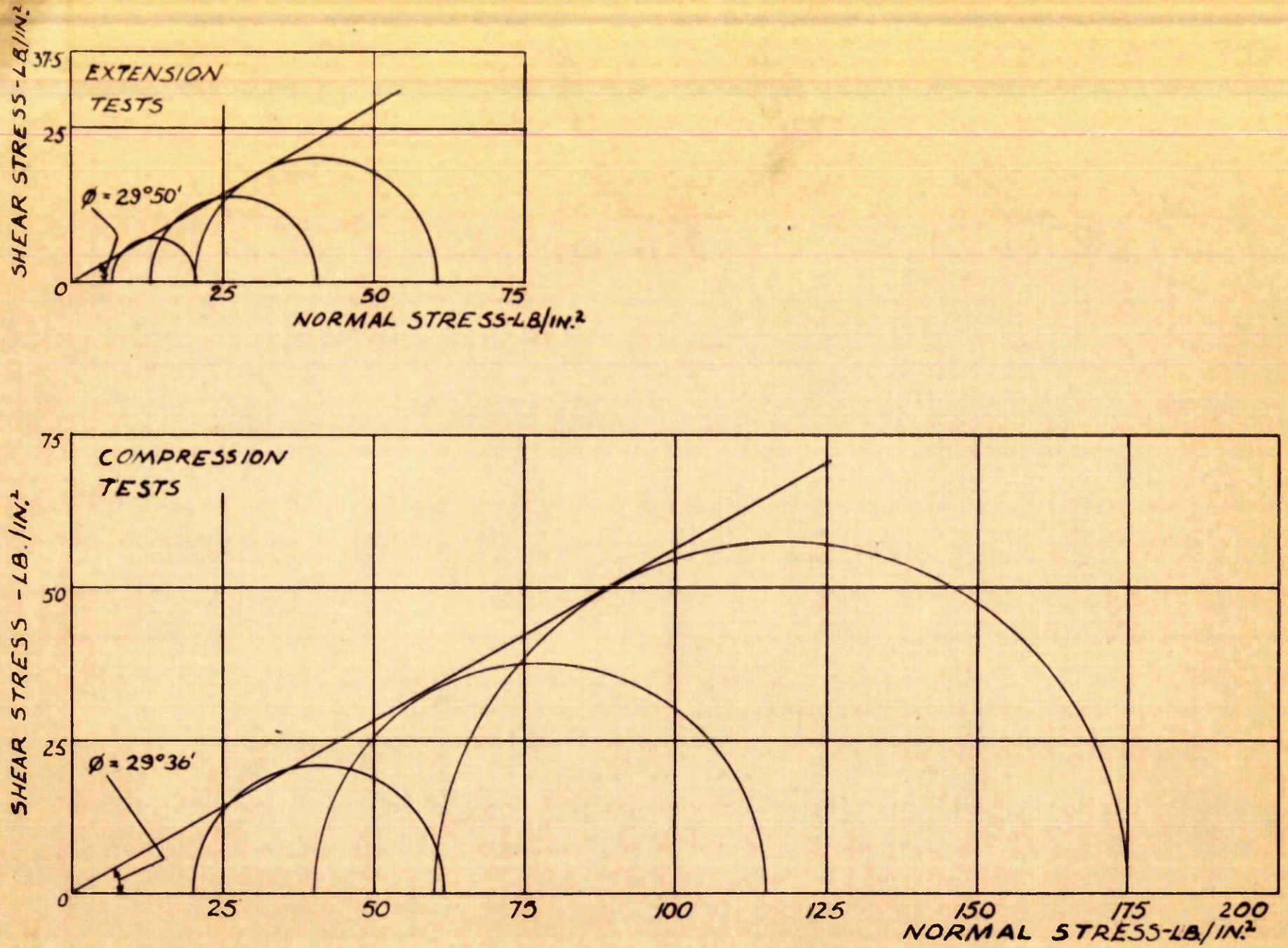

MOHR DIAGRAMS-TRIAXIAL TESTS SERIES I

FIG. 23

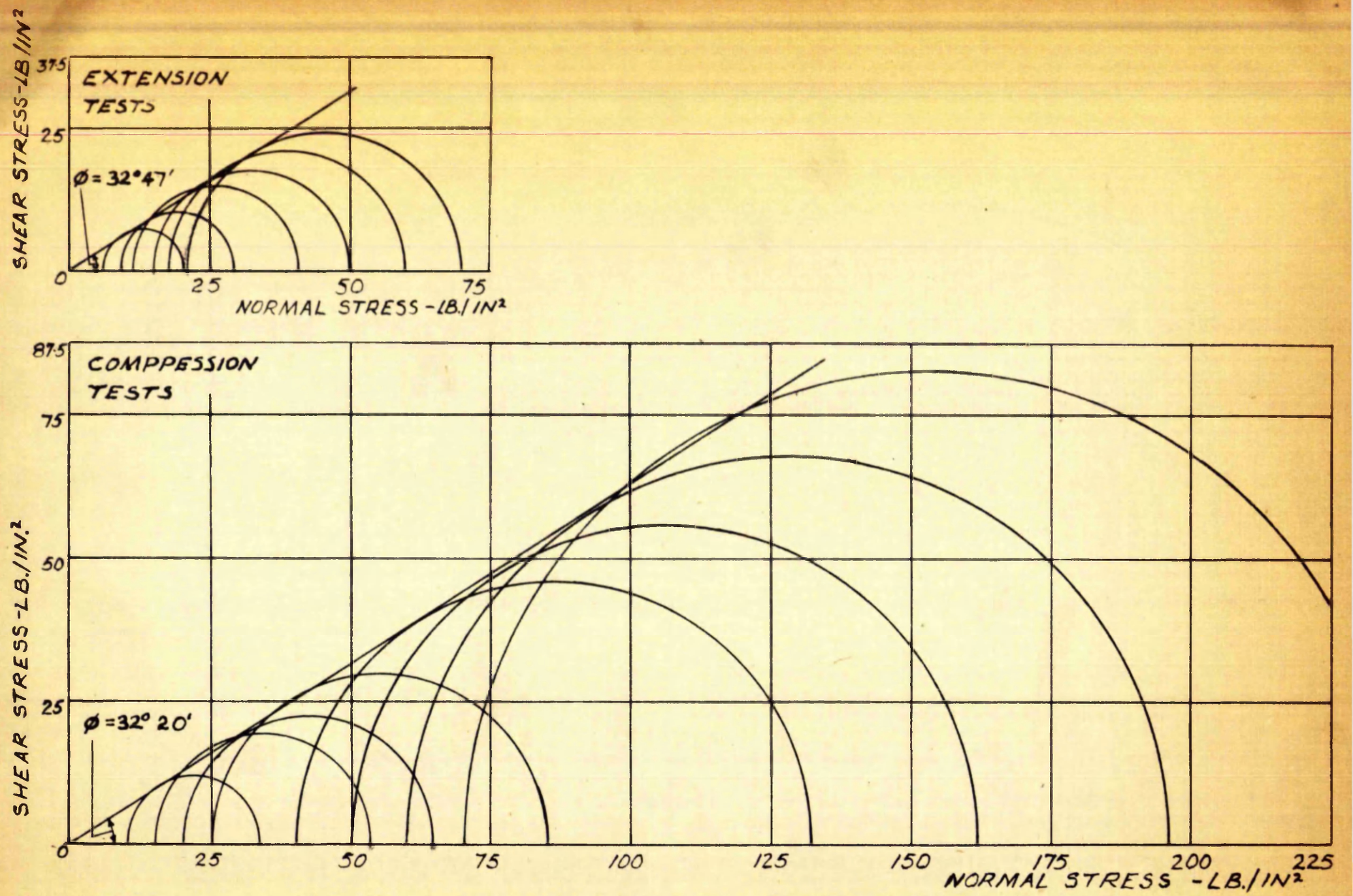

MOHR DIAGRAMS - TRIAXIAL TESTS SERIES 2

FIG. 24

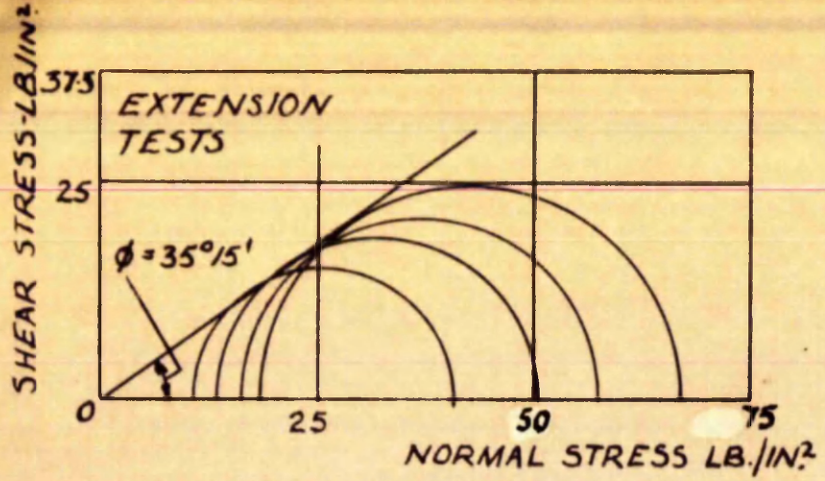

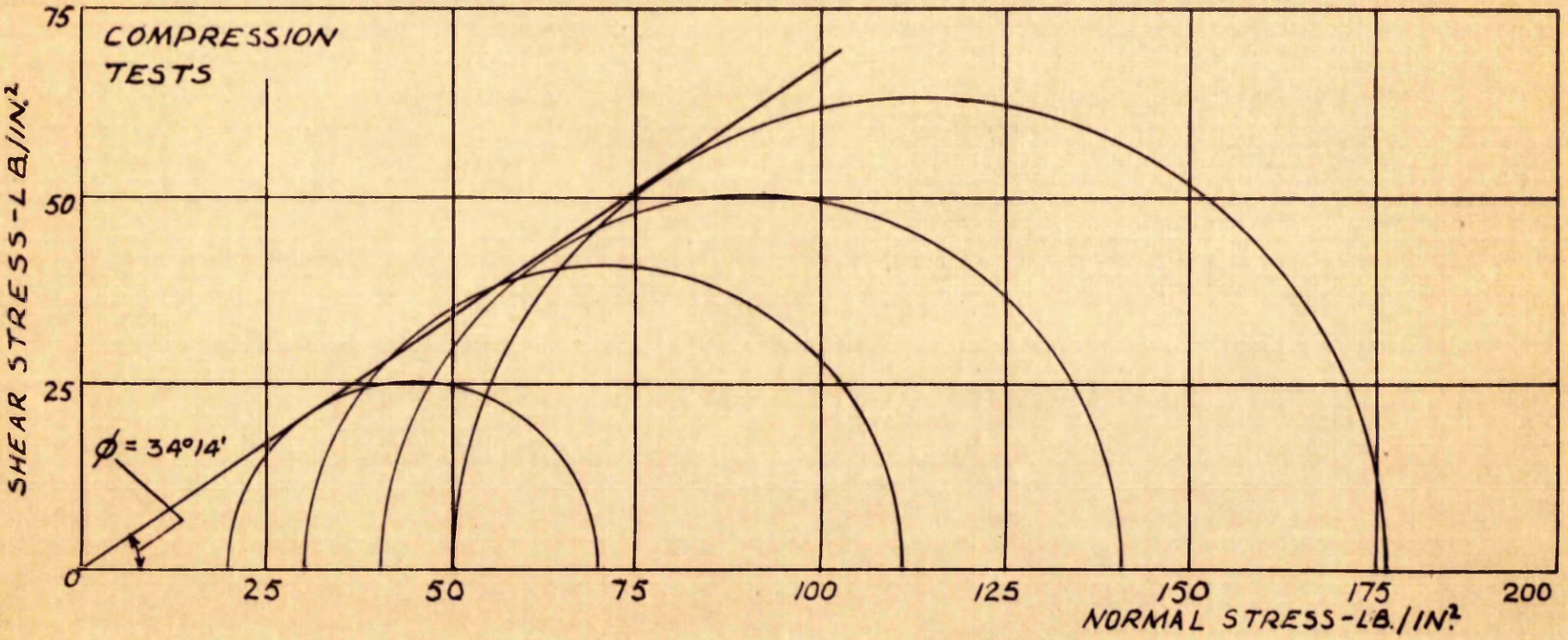

MOHR DIAGRAMS-TRIAXIAL TESTS SERIES 3

FIG. 25

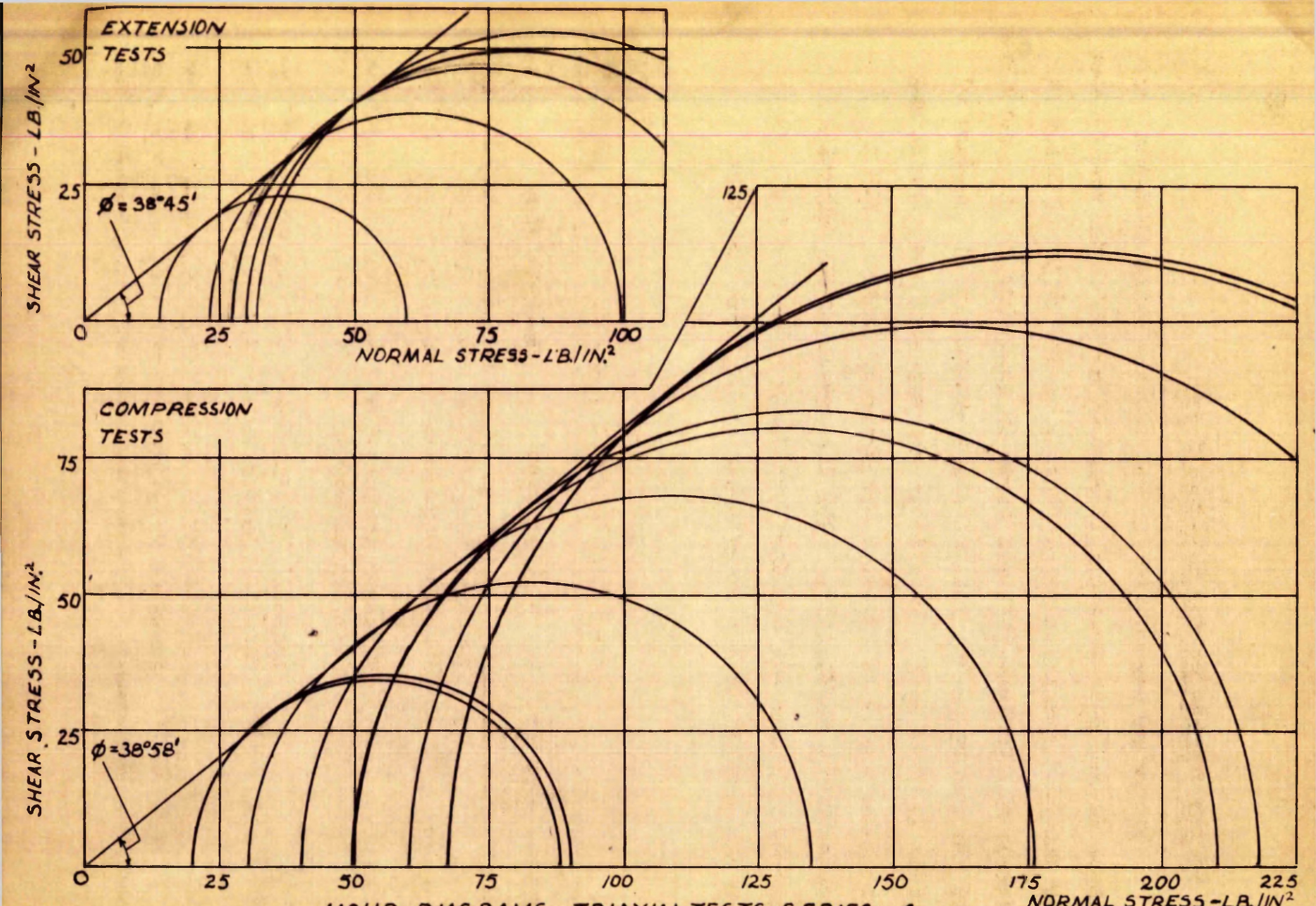

MOHR DIAGRAMS - TRIAXIAL TESTS SERIES 4

FIG. 26

6 b) The Results of the Triaxial Tests.

The major stress circles for all the triaxial tests are shown in the Mohr diagrams of Figs.23 to 26. The inclination of the Mohr envelopes corresponding to the angle of internal friction ϕ in eqns.(17) are shown in Table III. The positions of the points on the reduced right section of the surface of yield defined by the results of the triaxial compression and extension tests of series 4 are shown by points 1 and 2 respectively in Fig.27 . The theoretical Mohr-Coulomb and extended Tresca and Von Mises surfaces (see Sect.3 c), based on the results of the compression tests, are also shown.

Table III

Summary of Triaxial Results.

Series	Average Initial Porosity	Type of Test	Stress Distribution	ϕ
1	43.0%	Triaxial Compression	$\sigma_1 > \sigma_2 = \sigma_3$	29° 36′
		Triaxial Extension	$\sigma_1 = \sigma_2 > \sigma_3$	29° 50′
2	38.5%	Triaxial Compression	$\sigma_1 > \sigma_2 = \sigma_3$	32° 20′
		Triaxial Extension	$\sigma_1 = \sigma_2 > \sigma_3$	32° 47′
3	36.6%	Triaxial Compression	$\sigma_1 > \sigma_2 = \sigma_3$	34° 14′
		Triaxial Extension	$\sigma_1 = \sigma_2 > \sigma_3$	35° 15′
4	35.1%	Triaxial Compression	$\sigma_1 > \sigma_2 = \sigma_3$	38° 58′
		Triaxial Extension	$\sigma_1 = \sigma_2 > \sigma_3$	38° 45′

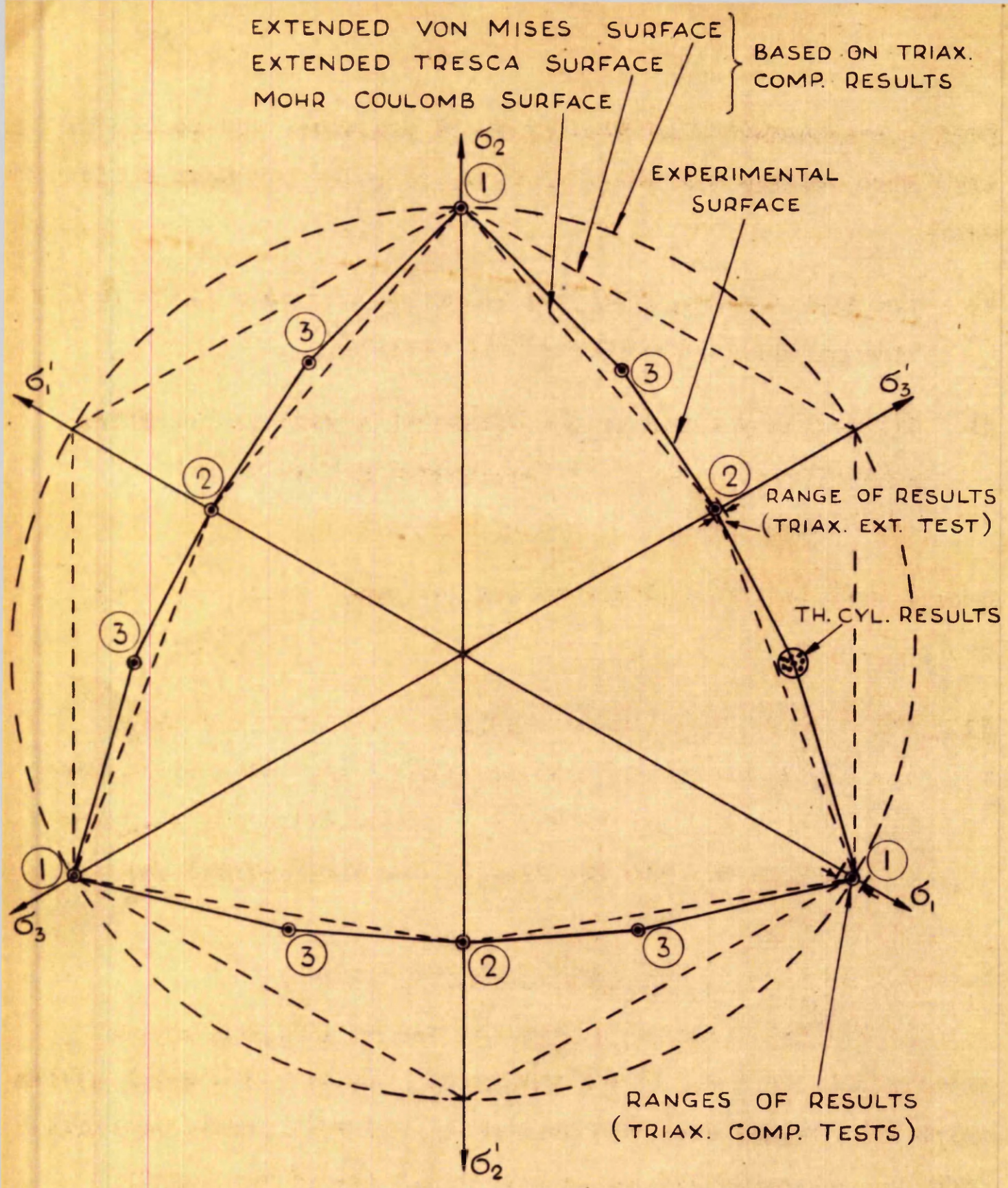

REDUCED RIGHT SECTION OF EXPERIMENTAL YIELD SURFACE
(AVERAGE STRESSES IN THICK CYLINDER TEST)
WITH RIGHT SECTIONS OF THEORETICAL SURFACES

FIG. 27

From a consideration of Figs.23 to 26 and Table III it can be said that, within the range of stresses used, for Loch Aline sand:

1) The Mohr Envelopes for all tests are straight and pass through the origin of the Mohr diagram.

2) The angles ϕ found in the compression test are in close agreement with those of the extension test at all porosities.

From a consideration of Fig.27 and 2) above, it can be said that:

3) The Mohr-Coulomb theory predicts accurately the yield condition for stress systems where $(\sigma_1 > \sigma_2 = \sigma_3)$ and $(\sigma_1 = \sigma_2 > \sigma_3)$ and that the extended Von Mises and Tresca theories do not fit the results for these stress systems.

6 c) <u>The Results of the Thick Cylinder Tests.</u>

In the Thick Cylinder Test the radial stresses at the outside and the bore of the sample are known. The axial stress which is constant over the section of the wall can be computed from the pressures acting on the closed end of the sample. The average tangential stress can be calculated from the equilibrium of the sample under the bore and outside pressures.

By assuming a distribution of radial stress across the

wall of the sample the average radial stress can be calculated. Using the average radial and tangential stresses and the axial stress, points on the surface of yield can be obtained to give an approximation to the true surface. It has already been shown that the Mohr-Coulomb theory predicts the yield condition for the sand where the stress systems are $(\sigma_1 > \sigma_2 = \sigma_3)$ and $(\sigma_1 = \sigma_2 > \sigma_3)$ and the suggested extended Von Mises and Tresca theories do not fit the experimental results (see Fig.27). It is likely therefore that the Mohr-Coulomb theory will predict the conditions of yield in the thick cylinder tests and that the distribution of radial stress across the wall of the sample will be practically linear (Section 4 a).

By assuming a linear distribution the average radial stress is calculated from

$$\sigma_{r_{av.}} = \sigma_1 = P_o + \frac{1}{2}(P_i - P_o)$$

The average tangential stress from the equilibrium of the sample is obtained from

$$\sigma_{t_{av.}} = \sigma_3 = \frac{P_o\, b - P_i\, a}{b - a}$$

(eqn.2% Section 4 a)

The axial stress is

$$\sigma_a = \sigma_2 = \frac{P_o b^2 - P_i a^2}{b^2 - a^2} \quad \text{(eqn.27 Section 4 a)}$$

The stresses at yield in the thick cylinder tests calculated in the above manner are shown in Table IV.

Table IV.

Average Yield Stresses in Thick Cylinder Tests

Test	P_o lb./in^2	P_i lb./in^2	$\sigma_{r_{av.}}$ lb./in^2	$\sigma_{t_{av}}$ lb./in^2	σ_a lb./in^2
1	14.40	21.21	17.81	3.36	10.50
2	18.70	27.18	22.94	4.84	13.30
3	30.60	44.08	37.34	8.08	22.30
4	38.50	55.68	47.09	9.75	27.95
5	45.80	65.75	55.78	10.55	32.30
6	47.92	68.63	58.28	10.95	34.05
7	50.30	72.88	61.59	13.32	35.90
8	54.02	77.16	65.59	13.67	38.90
9	54.80	78.43	66.62	12.95	38.20

6 d) The Experimental Surface of Yield.

To investigate the surface of yield for a material it is necessary to enquire into the shape of the surface in space and to investigate the shape of right sections of the surface.

The experimental results used in the investigation of the surface are obtained from the triaxial tests of series 4 and the thick cylinder tests.

The reduced right section of the surface of yield using the triaxial results and the average yield stresses in the thick cylinder tests is shown in Fig.27 . The position of the points representing the thick cylinder results is at 3 (Fig.27). The theoretical Mohr-Coulomb and the extended Von Mises and Tresca right sections are also shown. As was stated previously the experimental results for the triaxial compression and extension tests coincide with the Mohr-Coulomb theory. The experimental results of the thick cylinder tests indicate a slight increase in strength over that predicted by the Mohr-Coulomb theory. The experimental results are sufficiently removed from the extended Von Mises and Tresca theories to show that they do not predict yield for this material.

Use of the average stresses in the thick cylinder tests gives an approximation of the surface at points intermediate between those defined by the triaxial extension and compression tests. This approximation is sufficient to show that the Mohr-Coulomb theory gives a close indication of the yield conditions.

Assuming that the Mohr-Coulomb theory holds, the distribution of the tangential stress can be found, and the shape of the yield surface can be checked from the measured radial and axial stresses at the bore and outside of the sample. The tangential stress $\sigma_t = \lambda \sigma_r$ at any point in the wall of the sample. λ is calculated from eqn.(23) Section 4 a)

$$P_i = P_o \left(\frac{a}{b}\right)(\lambda - 1)$$

The states of stress sufficient to cause yield are then defined by $(\sigma_1 = P_i,\ \sigma_2 = \sigma_a,\ \sigma_3 = \lambda P_i)$ at the bore and by $(\sigma_1 = P_o,\ \sigma_2 = \sigma_a,\ \sigma_3 = \lambda P_o)$ at the outside.
The stresses calculated in the above manner are shown in Table V.

Table V.

Yield Stresses in Thick Cylinder Tests According to the Mohr-Coulomb Theory.

Test	λ	At Outside		At Bore		$\sigma_a = \sigma_2$
		$P_o = \sigma_1$ lb./in^2	$P_o = \sigma_3$ lb./in^2	$P_i = \sigma_1$ lb./in^2	$P_i = \sigma_3$ lb./in^2	
1	0.196	14.40	2.82	21.21	4.16	10.50
2	0.208	18.70	3.89	27.18	5.65	13.30
3	0.216	30.60	6.61	44.08	9.52	22.30
4	0.215	38.50	8.28	55.68	11.95	27.95
5	0.192	45.80	8.80	65.75	12.61	32.30
6	0.198	47.92	9.48	68.63	13.60	34.05
7	0.215	50.30	10.81	72.88	15.63	35.90
8	0.219	54.02	11.83	77.16	16.90	38.90
9	0.197	54.80	10.80	78.43	15.40	38.20

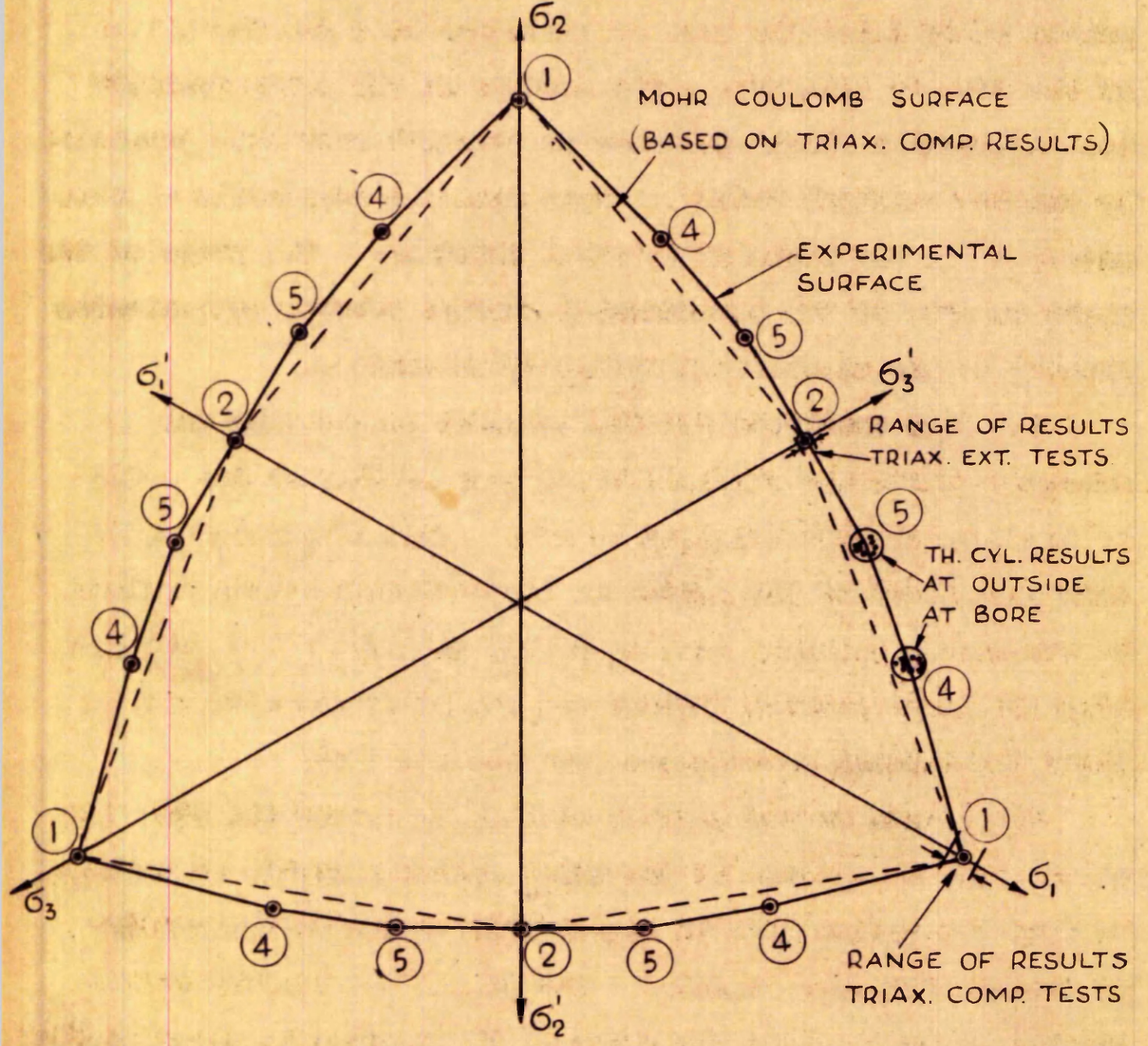

REDUCED RIGHT SECTION OF EXPERIMENTAL YIELD SURFACE
(STRESSES AT BORE AND OUTSIDE)

FIG. 28

The reduced right section of the yield surface obtained from these stresses is shown in Fig.28 . The position of the points is at 4 for the bore stresses and at 5 for the stress at the outside (Fig.28). The results of the thick cylinder test indicate a slight increase in strength over that predicted by the Mohr-Coulomb theory. This increase represents approximately 2^0 in the angle of internal friction. The shape of the right section of the experimental surface however approximates closely to the theoretical Mohr-Coulomb surface.

The Mohr envelopes for the triaxial compression and extension tests are straight lines passing through the origin of the Mohr diagram (Figs.23 to 26). This is sufficient to show that locii of the points on the surface in space defined by the stress systems $(\sigma_1 > \sigma_2 = \sigma_3)$ and $(\sigma_1 = \sigma_2 > \sigma_3)$ are straight lines passing through the origin of the system of three dimensional coordinates (see Section 3 b).

The points on the surface defined by either the stresses at the bore or outside of the thick cylinder sample do not lie on the same radius (O'P in Fig.AP.III.1.) due to the scatter of the results (see Fig.28). The points are however sufficiently close to allow the shape of the surface in space to be investigated along their directions. In Fig.29 the angles made by the lines joining the points on the surface, defined by the stresses at the bore and the outside of the sample, to the origin of the system of coordinates and the space diagonal (angle POO' in Fig.AP.III.2.) are plotted against the distance

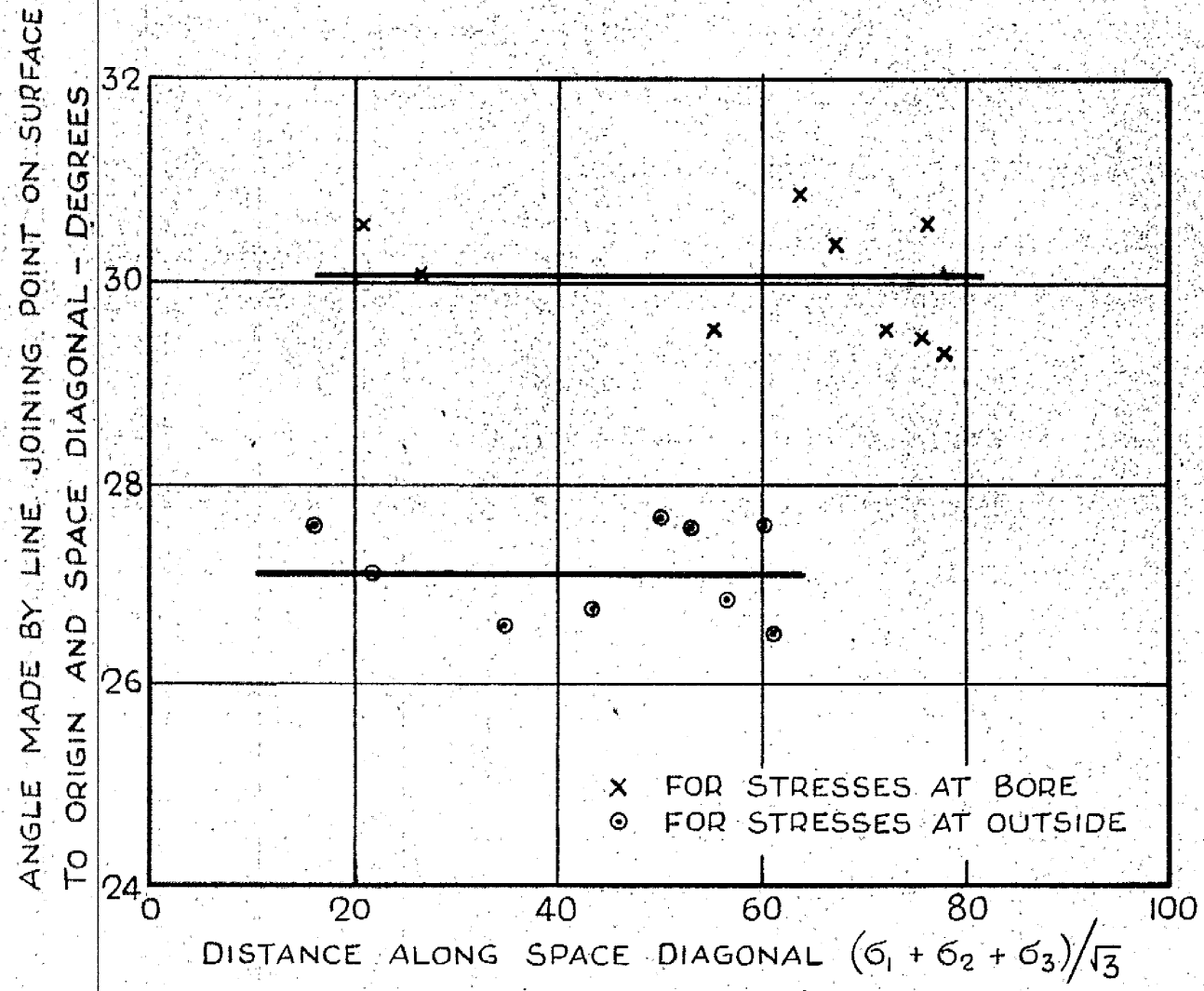

THICK CYLINDER RESULTS

FIG. 29

along the space diagonal. It is seen from Fig.29 that there is no variation of the angles with the distance along the space diagonal. The locii of the points defined by stresses in the thick cylinder test can therefore be considered to be straight lines which pass through the origin of the system of three dimensional coordinates.

From the above discussion it can be said that the surface in space is a pyramid with its apex at the origin of a system of three dimensional coordinates (σ_1, σ_2, σ_3) and that sections of the surface are similar in shape but increase with distance from the origin along the space diagonal.

SECTION 7.

Discussion of Experimental Results and Other Investigations.

It was noted in the Review (Section 1) that a considerable discrepancy exists between the findings of different investigators in drained triaxial compression and extension tests. The author's results show close agreement at all porosities in the angle of internal friction found in the two tests. This finding is in agreement with Bishop and Eldin[1] (Eldin[2]) for tests performed throughout the limits of porosity on a medium fine sand. The differences existing between the results of the author, Bishop and Eldin, and those of Habib[3][4] and Taylor[14] are difficult to explain but the close approximation of the results of the thick cylinder test with the Mohr-Coulomb theory suggests that the angle of internal friction exhibited in the triaxial compression and extension test should be the same.

The results of the torsion tests performed by Habib show a wide variation from the Mohr-Coulomb theory. These tests were performed on cylindrical samples confined in rubber membranes in the normal manner. Failure was induced by applying a torque to the end of the sample. Some doubt is cast on the accuracy of the torsion results due to the effect of the rubber membrane on the torsional resistance. The membrane is situated at the maximum radius of the sample where its influence on the measured

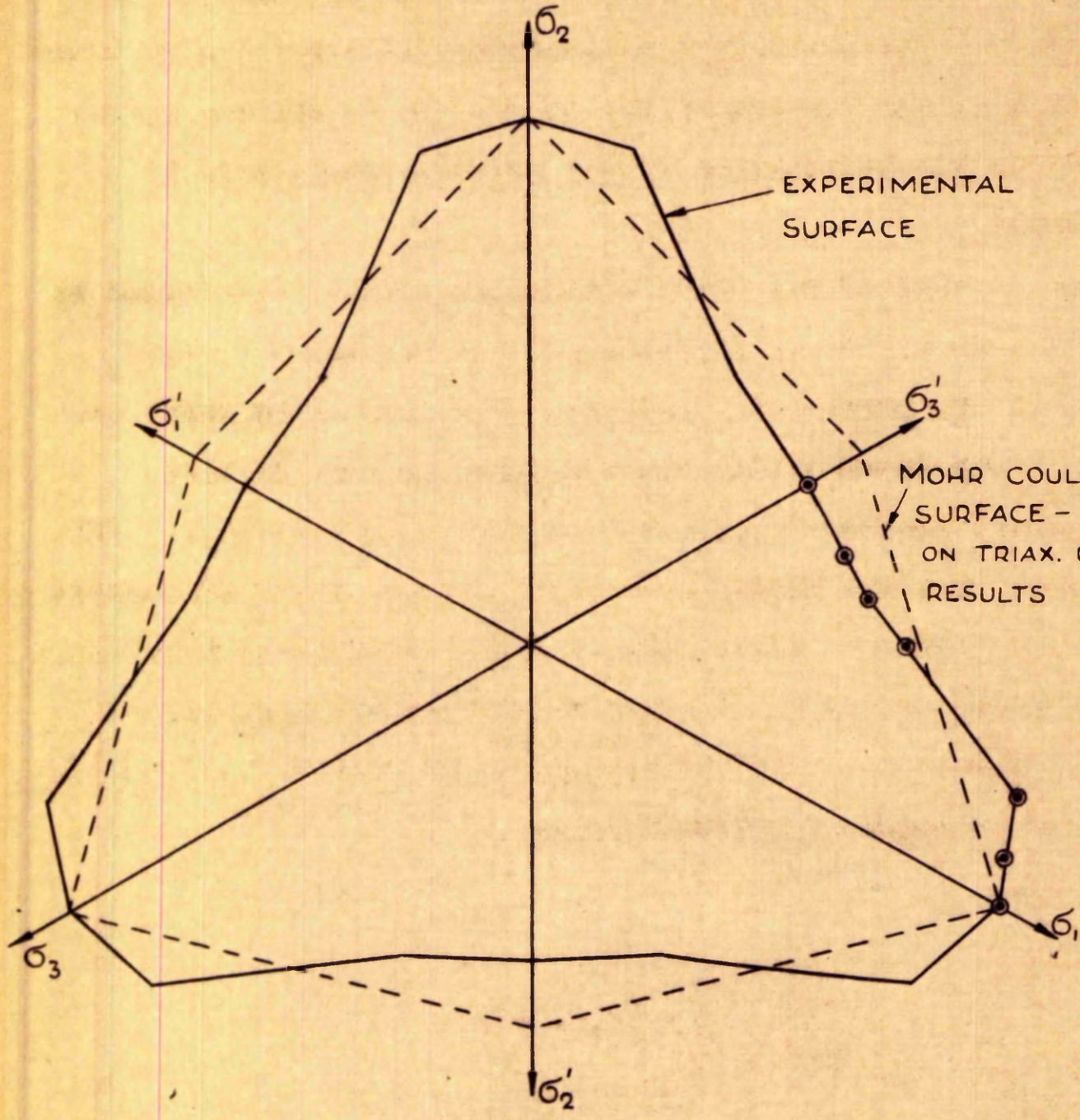

REDUCED RIGHT SECTION OF YIELD SURFACE FROM RESULTS OF HABIB

FIG. 30

torsional resistance is greatest. No satisfactory method of estimating the effect of the rubber membrane appeared to have been found. The assumption of a uniform distribution of shear stress across the section of the sample may be another source of error in the calculation of the shearing resistance in these tests.

The results of the Habib's tests have been transformed by the method described in Appendix III and the reduced right section of the surface of yield that they define is shown in Fig.30. The experimental right section is seen to vary widely about the theoretical Mohr-Coulomb right section. The difference from the theoretical right section along directions σ_1', σ_2', and σ_3' represents an angle of internal friction for the extension tests 7° lower than for the compression tests. The total variation represents a range of 11° in the measured angle of internal friction.

SECTION 8.

Summary and Conclusions to Part I.

The thick cylinder apparatus has proved satisfactory in its function and in its operation. The apparatus is suitable for investigations in other types of soils. The new method of presenting the results to illustrate the reduced right section of the experimental surface of yield can be adapted for use in other soils or for any isotropic material whose yield surface is pyramidal or conical in form.

The experimental results show that the Mohr-Coulomb theory accurately predicts yield for the sand for stress systems in which the intermediate principal stress has a value either equal to the minor or the major principal stresses, this condition being true at all porosities. For stress systems where the intermediate principal stress has a value $\sigma_2 \doteq \frac{\sigma_1 + \sigma_3}{2}$ the Mohr-Coulomb theory is found to underestimate the strength. The amount of the underestimation is slight and is considered to have no practical importance.

The close agreement between the experimental results and the theory in the triaxial compression and extension tests would lead to the conclusion that the assumption made in the Mohr-Coulomb theory, that the intermediate principal stress has no effect on the yield of sands, is correct. It is thought

that the condition of plane strain which approximately obtains in the thick cylinder test is in some way responsible for the increase in strength measured in those tests and that the general condition of yield in sands depends to some extent on strain.

Since the increase in strength, over that predicted by the Mohr-Coulomb theory, produced in the thick cylinder tests, is only slight a further investigation of the yield surface is considered unnecessary.

It is therefore concluded that the Mohr-Coulomb theory provides a reliable means of estimating the strength of sands under conditions of full drainage.

PART II

NOTES ON THE STRENGTH AND DEFORMATION OF SANDS

FIG. 31a. FRONT VIEW.

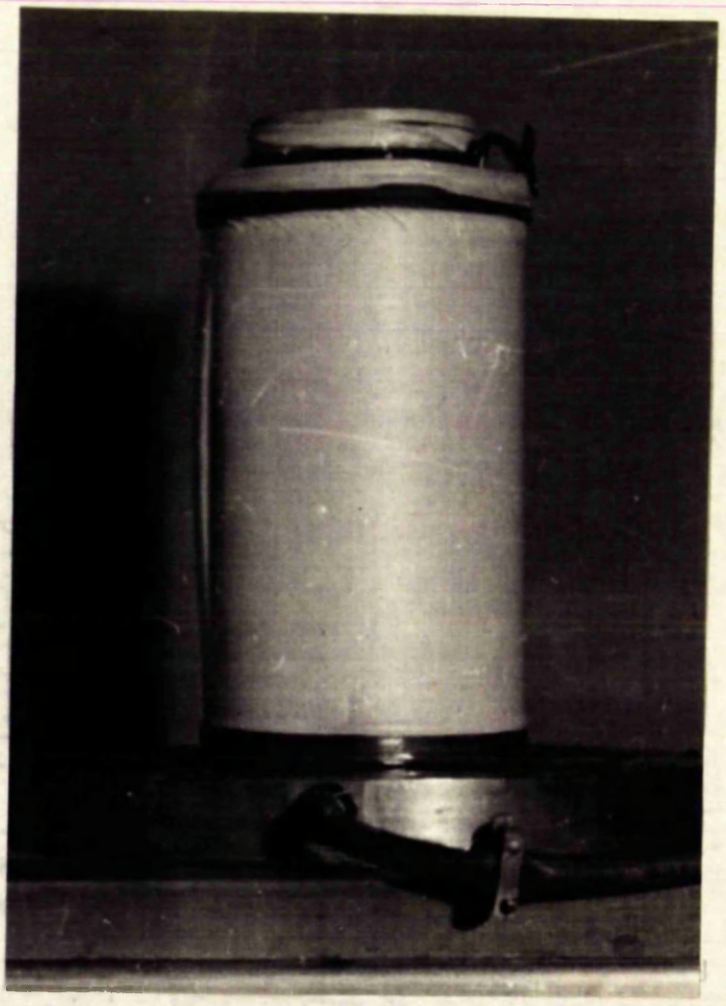

FIG. 31b. SIDE VIEW.

FIG. 31. THICK CYLINDER SAMPLE WITH 1 FAILURE CRACK.

PART II.

The data presented and discussed in Part II is that obtained from the tests performed for the purposes of Part I. The experimental work is described in Section 5 Part I and details of the sand used in the tests are given in Appendix I.

SECTION 9.

Presentation of Test Data.

9 a) Thick Cylinder Tests.

1) Mode of Failure of Thick Cylinder Samples.

Failure in the thick cylinder samples was due to the formation of vertical cracks in the wall of the sample. In all cases but one a single crack was produced such as shown in Fig.31 . A front view of the failure crack is shown in Fig.31a, Fig.31b shows a side view of the same sample looking from the right in Fig.31a. These photographs and measurements taken on failed samples indicate that part of the wall on one side of the crack has rotated outwards, about an axis remote from the crack, while the remainder of the sample has retained its cylindrical shape (see Fig.33). The increase in bore volume after the peak pressures were reached was due to the outward

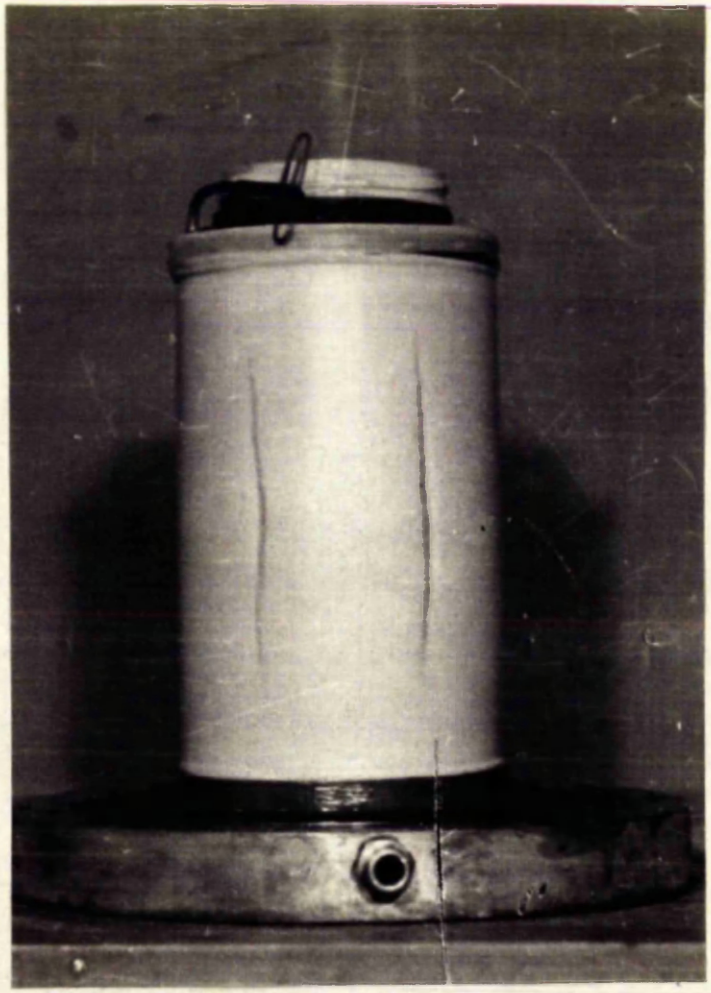

FIG. 32a. FRONT VIEW.

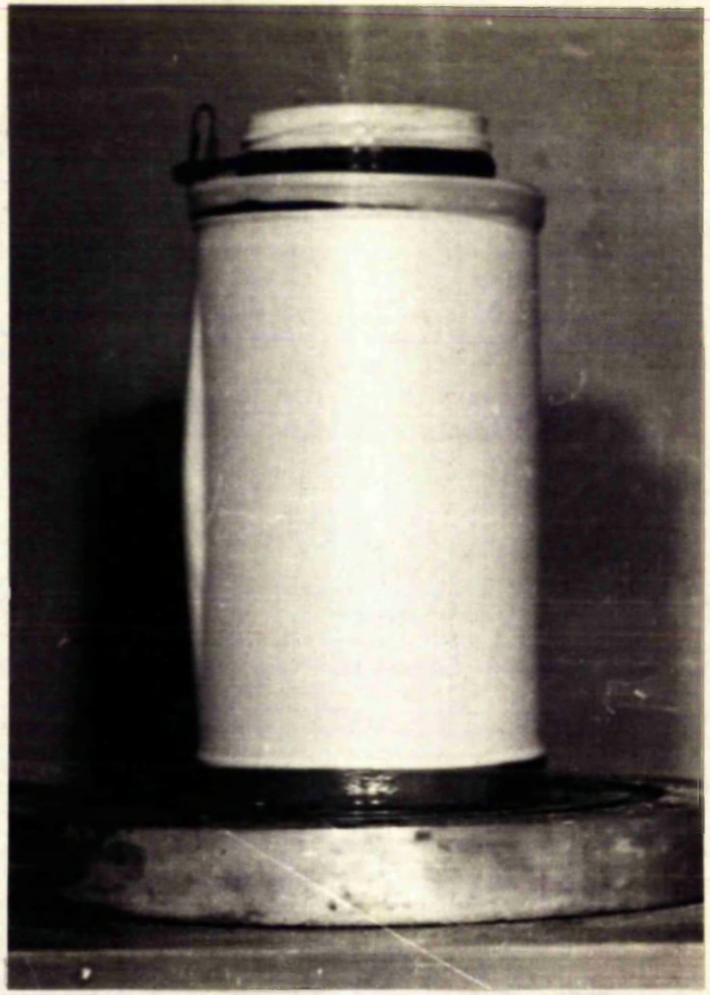

FIG. 32b. SIDE VIEW.

FIG. 32. THICK CYLINDER SAMPLE WITH 2 FAILURE CRACKS.

rotation of this part of the wall. Fig.32a and 32b show the front and side views of the sample which failed as the result of two cracks forming in the wall. In this sample the portion of the wall between the cracks has been forced outwards.

The Loch Aline sand used in the tests showed a slight cohesion when wet and it was possible to strip the membranes from some of the failed samples without the sample collapsing. A scale drawing of a section cut through the centre of such a sample is shown in Fig.33 . A visual inspection of the section showed that only a small wedge of material in the vicinity of the crack had been deformed. No sign of a single surface of rupture was noticed and slip had evidently occurred within the wedge of deformed material. The points where the boundaries of the wedge struck the surface of the wall were well defined (AA, and BB, in Fig.33) but it was not possible to trace their path through the wall.

It is thought that the lines AA and BB (Fig.33), forming the boundaries of the wedge, represent shear trajectories as defined by the Mohr-Coulomb theory of strength. The equation of the trajectories is derived in Appendix V (eqn.AP.V.4). In Fig.34 the theoretical trajectories for angles of internal friction $\phi = 40^{\circ}$ and $\phi = 26^{\circ}$ are shown. The trajectories for low values of ϕ are inclined less steeply to radial planes and sweep out longer paths through the wall than the trajectories for larger values of ϕ. The trajectory BB in Fig.33 is steeper

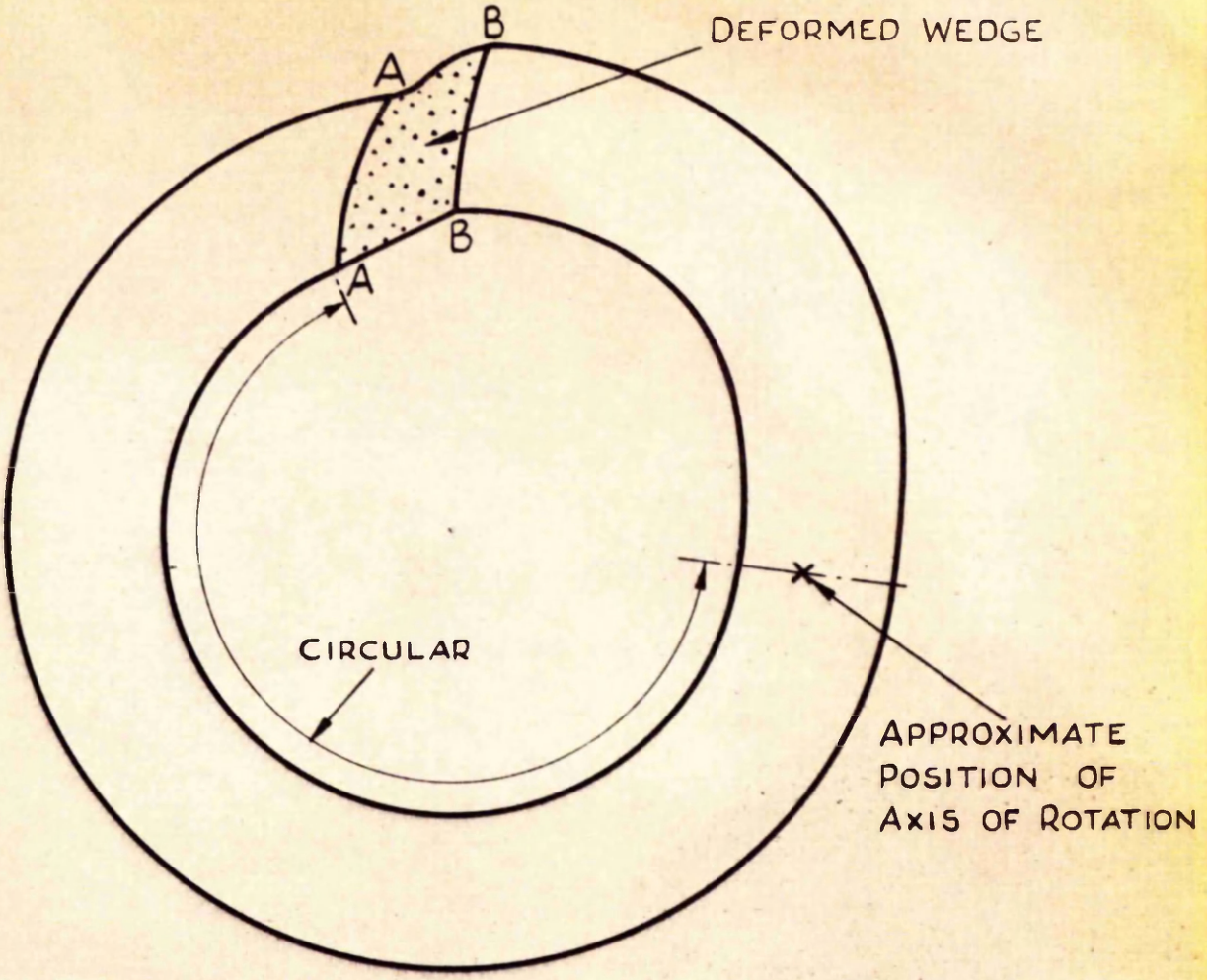

SECTION THROUGH FAILED THICK CYLINDER SAMPLE

FIG. 33.

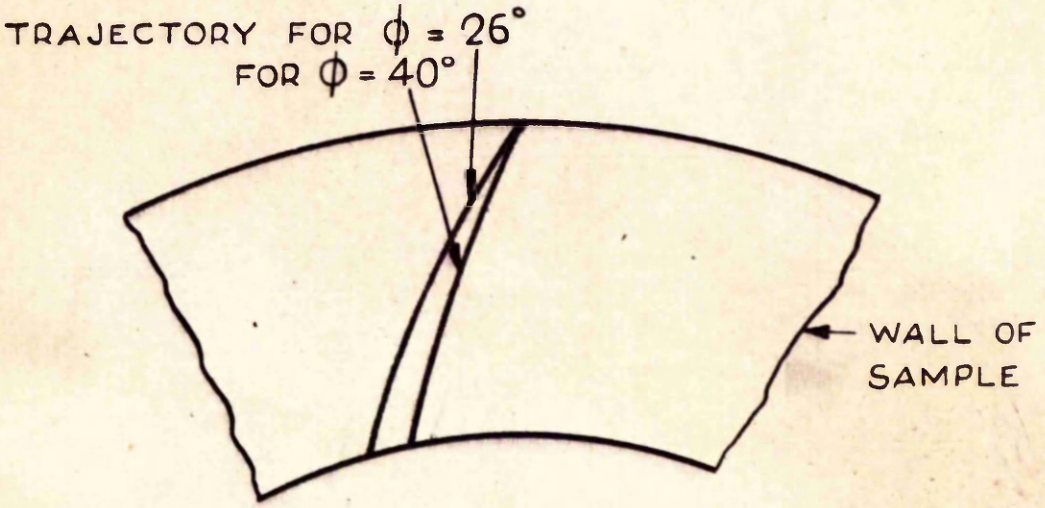

SHEAR TRAJECTORIES IN THICK CYLINDER SAMPLE

FIG. 34.

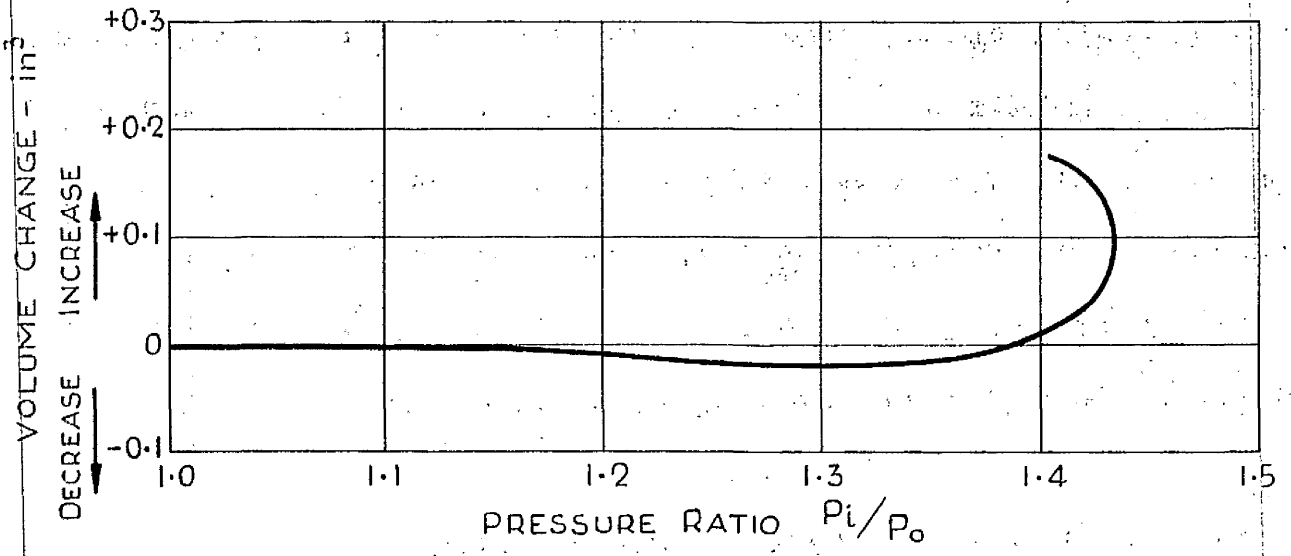

TYPICAL CURVE FOR SAMPLE WITH 1 FAILURE CRACK

FIG. 35a.

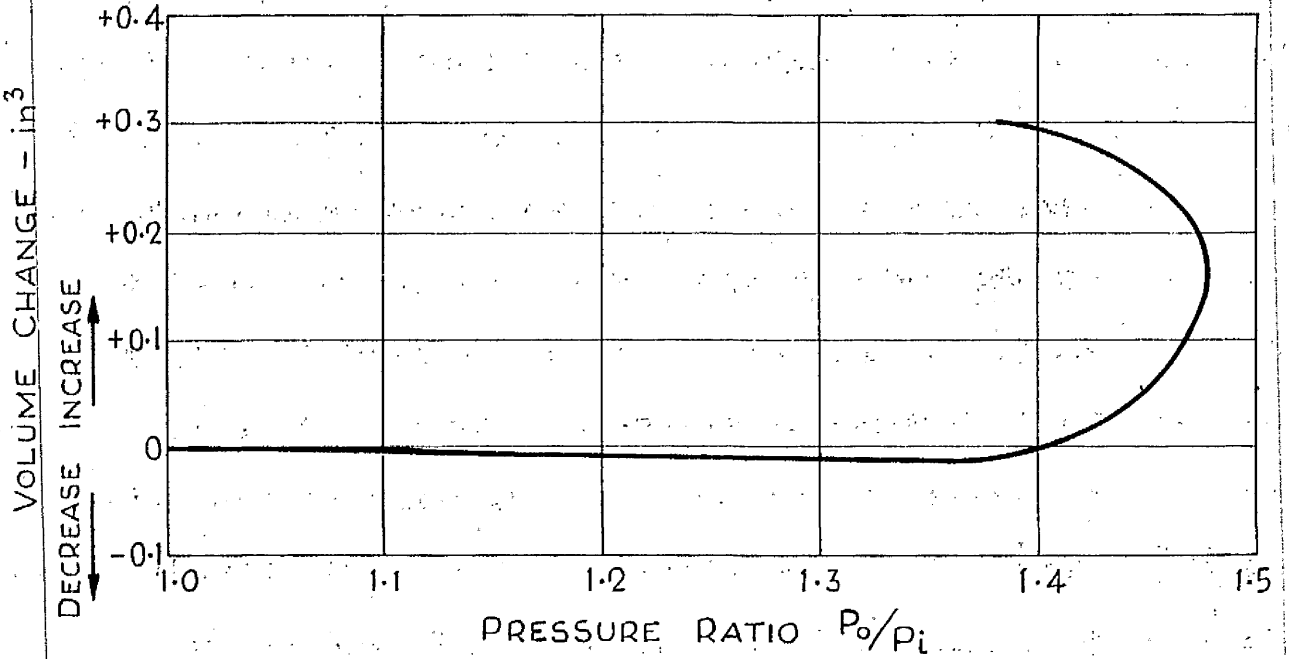

CURVE FOR SAMPLE WITH 2 FAILURE CRACKS

FIG. 35.b.

THICK CYLINDER TESTS

VOLUME CHANGE - PRESSURE RATIO CURVES

FIG. 35

than trajectory AA and would therefore represent a higher angle of internal friction. Although measurements could not be taken with sufficient accuracy to allow the ϕ values to be estimated it is thought that the trajectory through BB represents the peak angle of internal friction while that through AA represents the ultimate angle of internal friction.

2) Volume Changes in Thick Cylinder Tests.

A typical curve showing the volume change plotted against the ratio of the bore and outside pressures for a thick cylinder sample which failed as the result of a single failure crack is illustrated in Fig.35a. An initial volume decrease followed by a volume increase is noted. The pressure ratios at the point of volume increase is in the range of 1.32 to 1.38 for all tests. The rate of the volume increase is greatest at the peak pressures and reduces after the peak pressures have obtained. In tests continued beyond the peak pressures it was found that the volume never became constant. This was probably due to the extension of the crack in the wall of the sample.

The volume increases measured in the thick cylinder tests are very small. The average ultimate increase represents approximately 0.45% of the total volume of the sample and is considerably lower than the average of 7.5% obtained in the triaxial tests of series 4 which were conducted near the same porosity. The volume change-pressure ratio curve for the

sample which failed by two failure cracks is shown in Fig.35b . The volume increase produced in this sample is seen to be considerably greater than that produced in the sample which failed by a single crack.

The smallness of the volume increases measured in the thick cylinder test lends support to the observation made on failed samples that only a very small part of the sample has deformed during the test. The volume increases appear to be dependent on the total length of the cracks produced in the wall of the sample indicating that the deformed part of the sample lies in the neighbourhood of the crack as is shown in Fig.33 .

9 b) Triaxial Tests.

1) General Remarks.

The test data reviewed is that obtained from the triaxial tests described in Section 5 Part 1. The results of three additional compression tests are however included. These tests were performed at high porosities and are included in Series 1. A summary of the tests is given in Table VI. The initial porosity in Table VI is the porosity after consolidation under the confining pressure.

For the reasons described in Section 10 a) it was desired to compare the volume changes produced in compression samples which failed by bulging with those of compression samples which

failed by a plane of rupture. These two failure types were produced intentionally in the compression tests of series 4.

Table VI.

Summary of Triaxial Tests.

Series	Type of Test	Range of Initial Porosity %
1	Triaxial Compression	41.2 - 43.7
	Triaxial Extension	42.8 - 43.2
2	Triaxial Compression	38.1 - 38.9
	Triaxial Extension	
3	Triaxial Compression	36.3 - 36.9
	Triaxial Extension	
4	Triaxial Compression	34.7 - 35.5
	Triaxial Extension	

It was noted early in the performance of the tests on the dense samples of series 4 that bulging failures were always obtained. To obtain the required rupture-plane failures it was necessary to induce a slight eccentricity of loading to the sample. This was achieved by placing the sample slightly off centre on the base pedestal of the apparatus.

To illustrate the types of failures produced some of the samples of series 4 were placed in alternate layers of dyed and natural sand. The dyeing of the sand did not affect the shearing properties in any way.

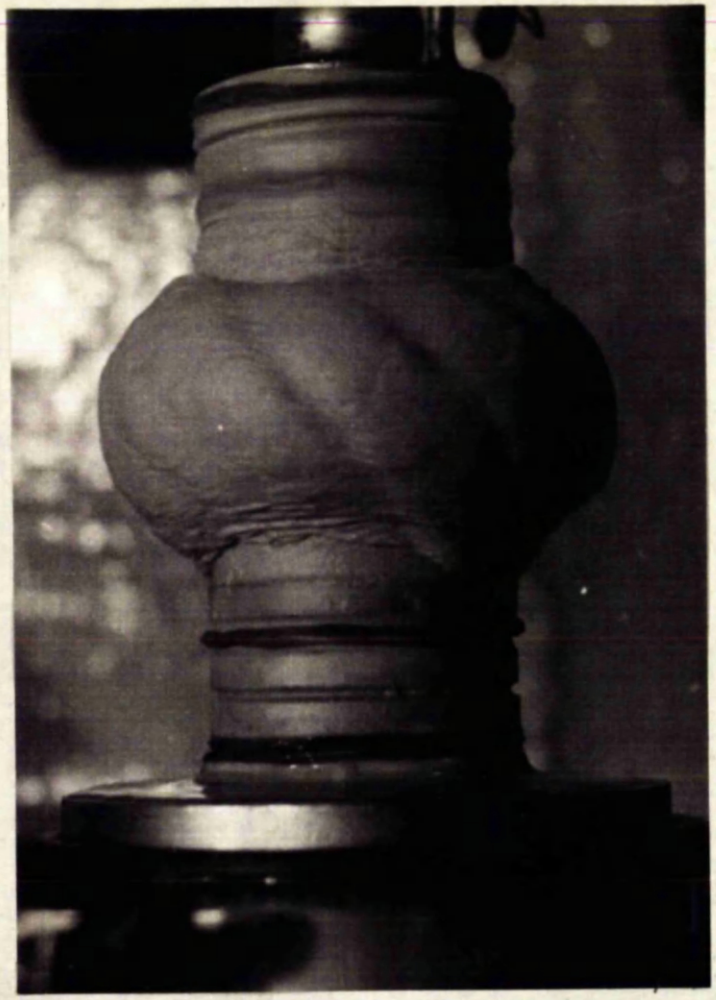

FIG. 36. BULGE FAILURE IN COMPRESSION TEST.

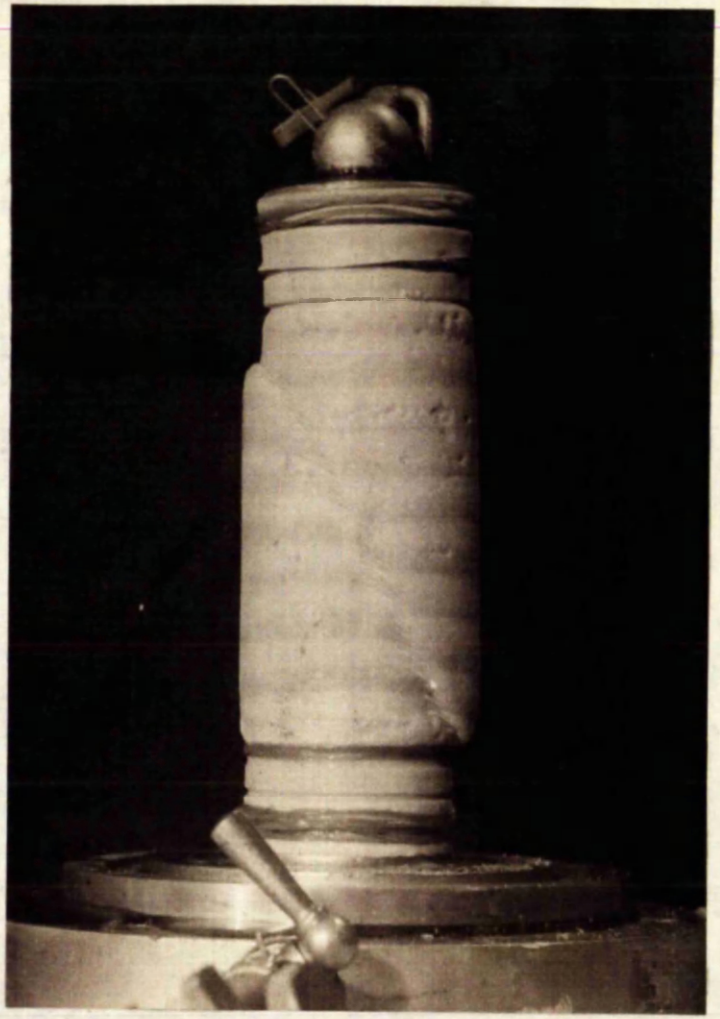

FIG. 37. RUPTURE PLANE FAILURE IN COMPRESSION TEST.

2) The Mode of Failure of Triaxial Samples.

a) Compression Samples.

The results of the compression tests indicate that all triaxial compression samples independent of their porosity should fail by symmetrical bulging rather than by a plane of rupture. In the compression tests performed on the samples at the lowest porosity (series 4) rupture plane failures could only be obtained by subjecting the sample to a slight eccentricity of axial load. If the sample was carefully centred in the apparatus, bulging failures were always produced. The only rupture plane failure other than those of series 4 was obtained in series 3. This was obtained without intention and it is assumed to have been caused by some eccentricity of loading.

A compression sample which has failed by "bulging" is shown in Photo.Fig.36 . The strain in this sample was carried well beyond the usual and the photograph shows that the "bulging" is caused by the development of numerous planes of slip.

A photograph of a compression sample which has failed by a plane of rupture is shown in Fig.37 .

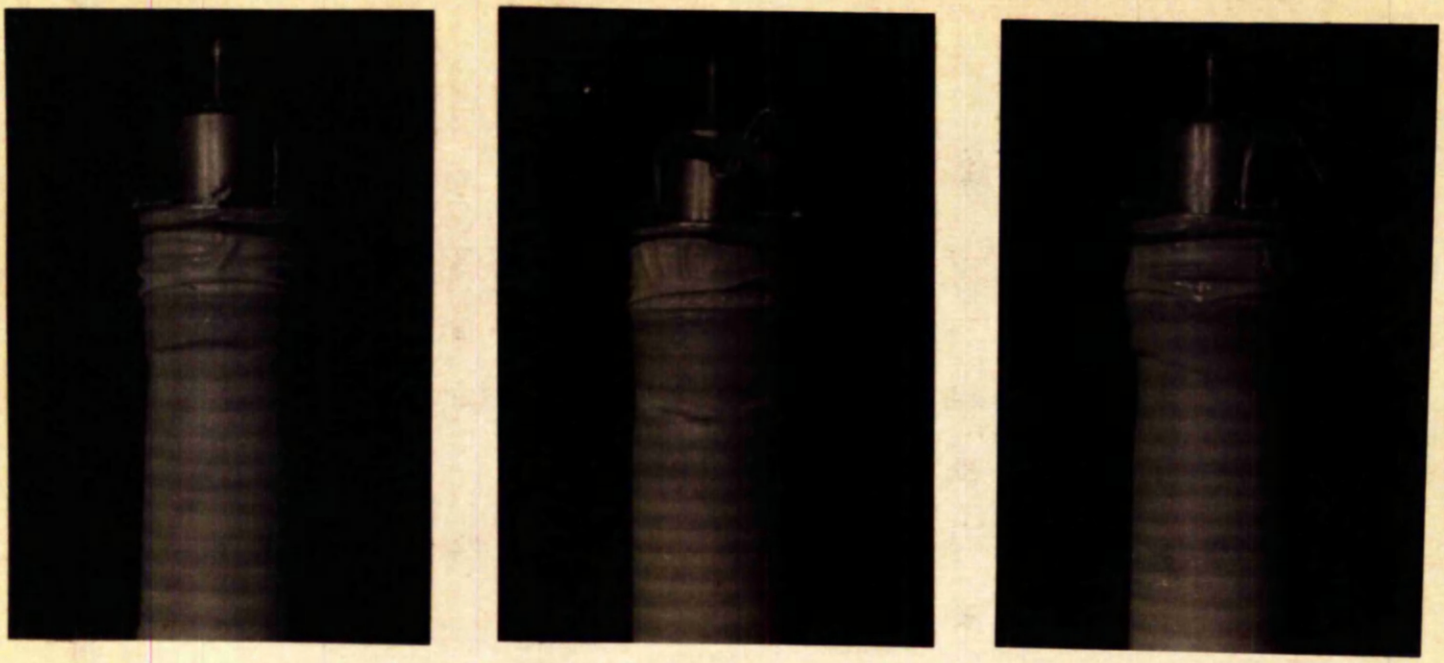

(a) FRONT VIEW (b) BACK VIEW (c) SIDE VIEW

EXTENSION SAMPLE WITH COMBINED SURFACE OF RUPTURE

FIG. 38.

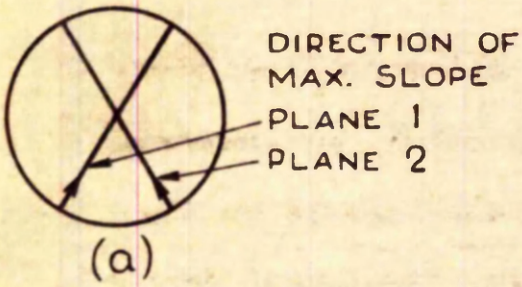

(a)

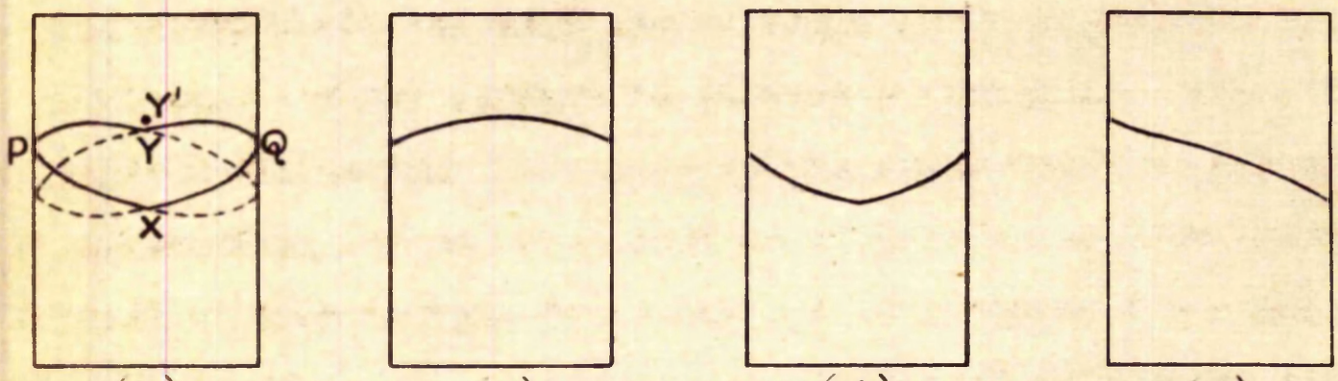

(b) (c) FRONT VIEW (d) BACK VIEW (e) SIDE VIEW

ILLUSTRATION OF COMBINED SURFACE OF RUPTURE

FIG. 39.

b) Extension Samples.

All extension samples tested at low porosities failed by a plane of rupture while in most samples at high porosities a local reduction in area resulted in necking.

It appeared from a close examination of the rupture failures of series 4 that some of these samples had not failed along a single rupture plane but that the surface along which slip had occurred was made up of a combination of more than one plane. The photographs in Fig.38 show the front, back and side views of such a sample. In the front view Fig.38a, the surface of rupture is seen to strike the outside of the sample in a smooth obtuse curve. The back view Fig.38b shows the surface as a much more acute V shaped curve.

An explanation of these shapes is given in Fig.39 where failure is assumed to be caused by slip down the combination of two planes. These planes are at the same levels in the sample but their directions of maximum slope are displaced Fig.39a. The planes intersect at points X and Y in the elevation shown in Fig.39b. A possible surface of rupture can be considered along XPY on plane 1 and XQY on plane 2. The shape of this combined surface is similar to that shown in the photographs of Fig.38a and b except that the small indentation at Y in Fig.39b is not evident in the photograph Fig.38a. It is likely however that this indentation will be eroded at larger strains until it is at position Y'. The surface would then pass through PXQY'.

TABLE VII Principal Data From Triaxial Compression Tests.

Series	Initial Porosity	Failure Type	Confining Pressure lb./in^2	ϕ peak	Initial Volume Decrease -in^3	σ_1/σ_3 at Pt. of Volume Incr.	Total Vol. Incr. at Peak -in^3.	σ_1/σ_3 at Ult.	Total Vol. Incr. at Ult. -in^3.
1	42.9	Bulge	20	30°34'	0.058	3.07	0	2.68	0.020
	43.7	"	40	28°54'	0.054	2.78	0.001	2.48	0.054
	43.0	"	60	29°20'	0.041	2.84	0.001	2.67	0.018
	41.8	"	20	31°00'	0.005	2.55	0.045	2.45	0.150
	41.2	"	40	31°30'	0.008	2.81	0.012	2.72	0.086 N.C.[1]
	41.3	"	60	30°34'	0.023	2.80	0.028	2.63	0.078 N.C.
2	RANGE								
	38.1-38.9	"	20	32°12'	0.011	2.74	0.075	2.50	0.290
	"	"	25	33°04'	0.013	2.96	0.065	-	N.C.
	"	"	30	31°48'	0.011	2.75	0.074	-	N.C.
	"	"	40	32°36'	0.009	2.71	0.065	-	N.C.
	"	"	50	31°54'	0.013	2.69	0.063	2.64	0.210
	"	"	60	32°10'	0.016	2.70	0.056	-	N.C.
	"	"	70	32°54'	0.021	2.84	0.053	2.79	0.200
3	RANGE								
	36.3-36.9	"	20	33°38'	0.006	2.56	0.120	-	N.C.
	"	"	30	35°08'	0.005	2.72	0.085	-	"
	"	"	40	34°08'	0.005	2.56	0.095	-	"
		R.P.[2]	50	34°02'	0.014	2.90	0.053	-	"
4	RANGE								
	34.7-35.5	Bulge	20	39°18'	0.005	3.08	0.135	-	N.C.
	"	"	20	39°32'	0.004	2.76	0.090	3.04	0.386 N.C.
	"	"	20	38°32'	0.005	2.91	0.104	2.67	0.430 N.C.
	"	"	40	39°02'	0.007	2.93	0.097	2.70	0.403 N.C.
	"	"	60	38°24'	0.008	2.60	0.070	2.60	0.397 N.C.
	"	"	67	38°48'	0.013	2.91	0.110	2.80	0.331
	"	R.P.	30	39°48'	0.007	3.16	0.096	3.03	0.298
	"	"	30	39°38'	0.010	2.62	0.075	2.98	0.278
	"	"	50	39°36'	0.001	2.80	0.068	3.05	0.180
	"	"	50	37°52'	0.007	2.87	0.056	2.69	0.140
	"	"	67	39°04'	0.012	3.08	0.088	2.85	0.279

1 N.C. = Volume Not Constant. 2 R.P. - Rupture Plane

Table VIII Principal Data From Triaxial Extension Tests.

Series	Initial Porosity %	Failure Type	Confining Pressure lb./in^2	ϕ peak	Initial Volume Decrease -in^3	σ_1/σ_3 at Pt. of Volume Increase	Total Vol. Incr. at Peak -in^3	σ_1/σ_3 at Ult.	Total Vol. Incr. at Ult. -in^3
1	RANGE 42.8-43.2	Neck[2]	20	30°00'	0.053	3.00	0	2.47	0.023
	"	R.P.[2]	40	30°18'	0.063	3.04	0	2.38	0.008
	"	Neck	60	29°14'	0.055	2.91	0	2.35	0.017
2	RANGE 38.1-38.9	R.P.	20	32°28'	0.013	2.56	0.016	2.57	0.016[1]
	"	Neck	30	32°02'	0.014	2.38	0.029	-	N.C.[1]
	"	"	40	33°12'	0.008	2.47	0.020	-	"
	"	"	50	33°12'	0.015	2.55	0.020	-	"
	"	"	60	33°30'	0.011	2.50	0.029	-	"
	"	"	70	32°24'	0.010	2.56	0.032	-	"
3	RANGE 36.3-36.9	R.P.	40	36°10'	0.003	2.74	0.008	2.65	0.063
	"	R.P.	50	33°46'	0.000	2.45	0.025	2.54	0.060
	"	R.P.	60	34°14'	0.000	2.45	0.028	2.82	0.053
	"	R.P.	67	35°52'	0.005	2.68	0.033	2.88	0.051
4	RANGE 34.7-35.5	R.P.	60	39°24'	0.006	2.78	0.059	2.44	0.071
	"	R.P.(at end)	100	38°12'	0.003	2.69	0.031	3.34	0.054
	"		120	39°20'	0.009	2.93	0.028	2.63	0.066
	"	R.P.	129	38°14'	0.000	2.62	0.047	2.54	0.107
	"	R.P.	138	38°34'	0.008	3.08	0.026	2.88	0.097

1 N.C. - Volume Not Constant 2 R.P. - Rupture Plane

The front back and side views of this surface Fig.39c,d and e, closely resemble the photographs of Fig.38a,b and c.

3) Angles of Internal Friction.

The principal data from the triaxial compression and extension tests is shown in Tables VII and VIII. Referring to these tables it is seen that for the range of confining pressures used the peak angle internal friction (ϕ peak) within each range of porosity can be considered constant. No variation is found in the compression tests between the peak angle of internal friction for samples which have failed by bulging and those which have failed by a plane of rupture. Close agreement is also found between the angle of internal friction for the compression and extension tests at each porosity.

The measured ultimate angle of internal friction, for those tests continued to the ultimate, is found to vary from test to test. It is however in the range expressed by the principal stress ratios (σ_1/σ_3) 2.34-3.05 and can be considered independent of the initial porosity. The variations in the ultimate angle of internal friction are probably due to the non-uniform conditions of the sample at large strains and to inaccuracies in the estimation of the sample dimensions at the ultimate stages of the tests.

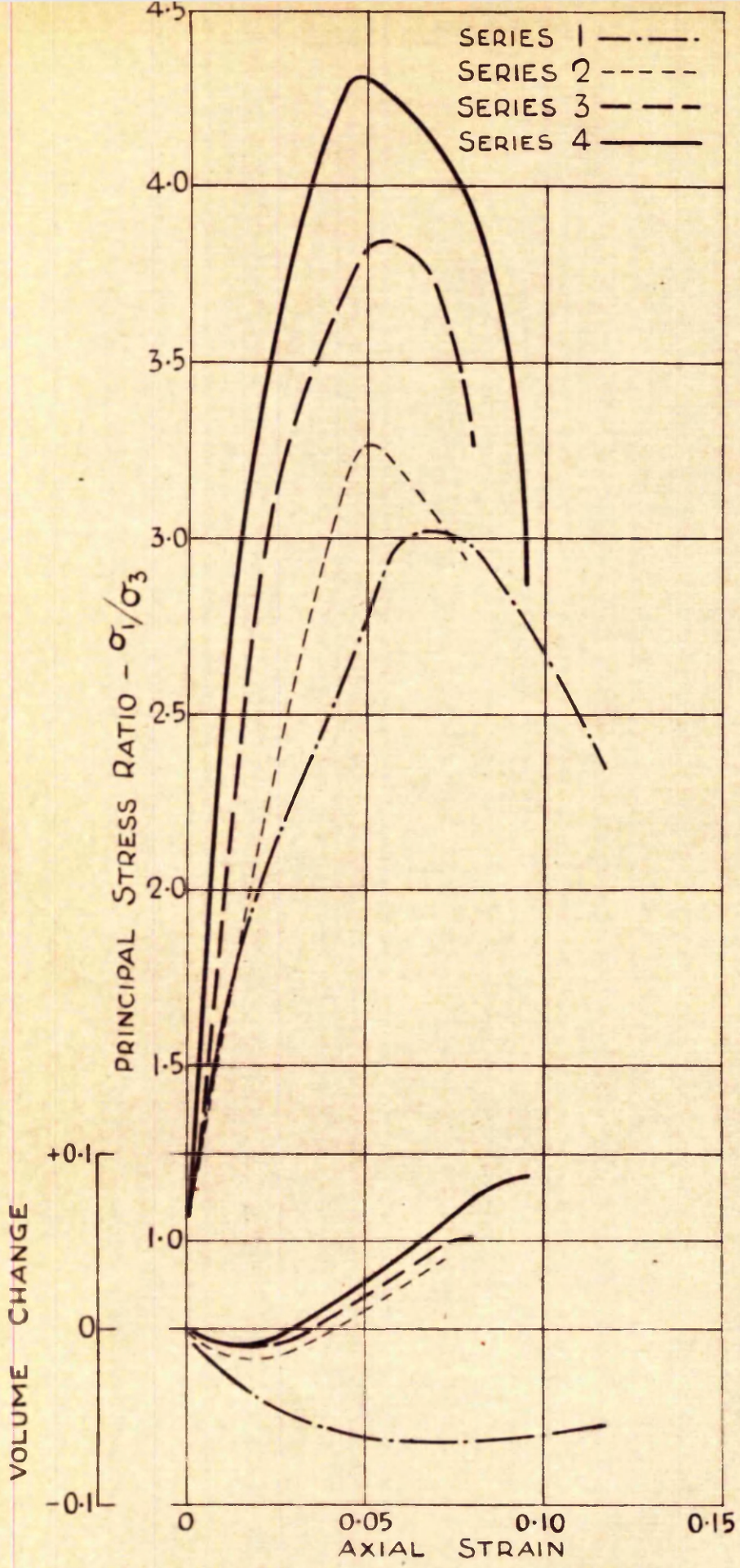

TYPICAL STRESS STRAIN VOLUME CHANGE CURVES FOR EXTENSION TESTS

FIG. 40.

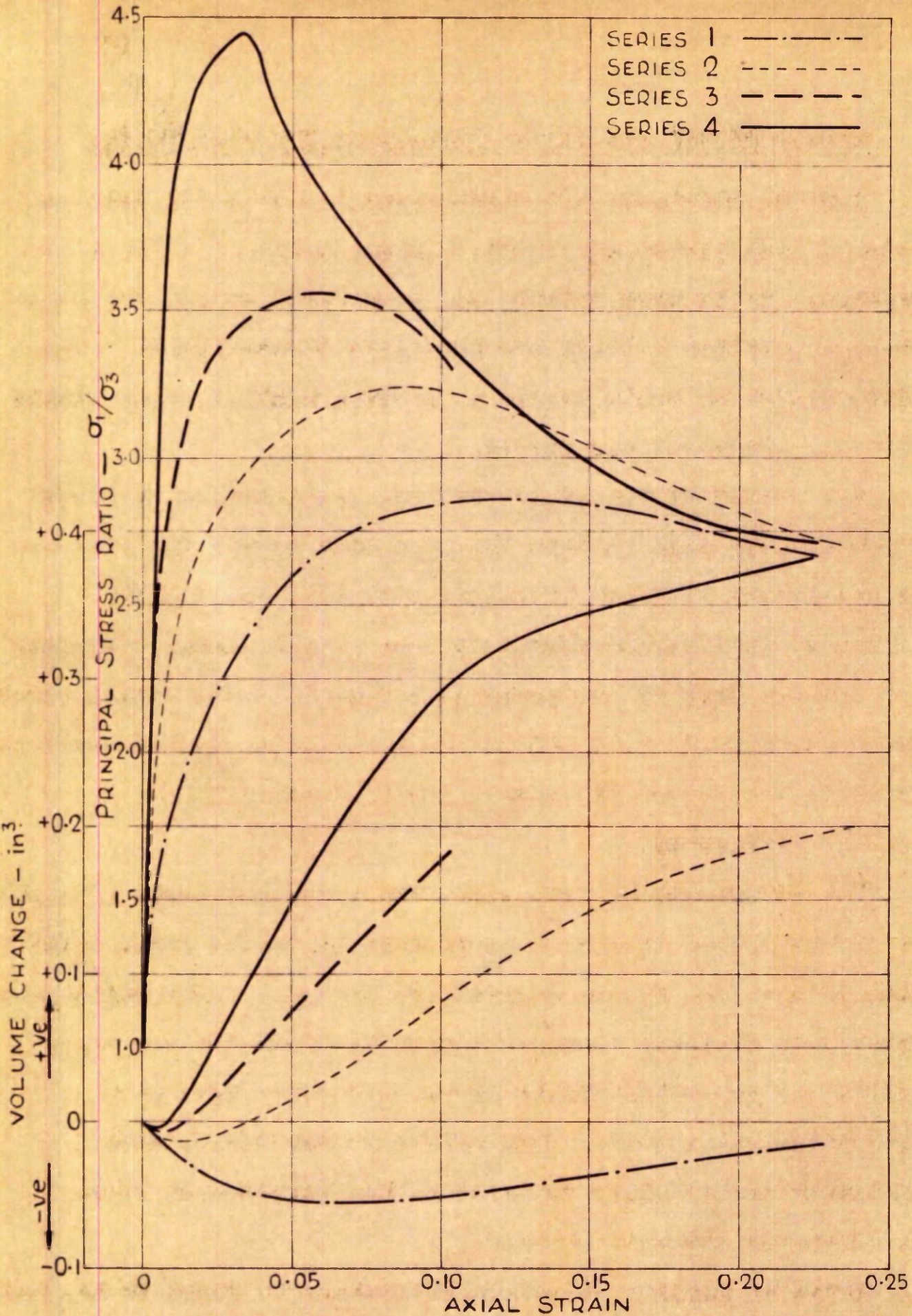

TYPICAL STRESS – STRAIN – VOLUME CHANGE CURVES
FOR COMPRESSION TESTS (BULGE FAILURES)

FIG. 41.

4) Stress Strain and Volume Changes in Triaxial Tests.

Typical stress-strain-volume change curves for triaxial tests of each series are shown in Figs.40 and 41. To allow comparison to be made between the individual curves the axial strain is plotted against the principal stress ratio. The volume change in cubic inches is plotted against axial strain below the stress strain curves.

The curves of Fig.41 are typical for compression tests on sands; the peak strains increase with increasing porosity and the volume increase increases with decreasing porosity. An initial decrease in volume is seen in all curves including that for the test at low porosity series 4. The stress-strain curves are seen to fall into a group contained by the envelope formed by the curves for high porosity (series 1) and low porosity (series 4).

The stress-strain curves for the extension tests (Fig.40) are characterised by a more rapid drop in stress ratio with axial strain than in the compression tests. These curves are however not directly comparable with those of the compression tests since the axial strain in the extension test is not the major principal strain. The volume change curves show similar characteristics to those of the compression tests but the increases are much smaller.

After an initial reduction the volume is found to increase in tests at all porosities. The stress ratio at the point of

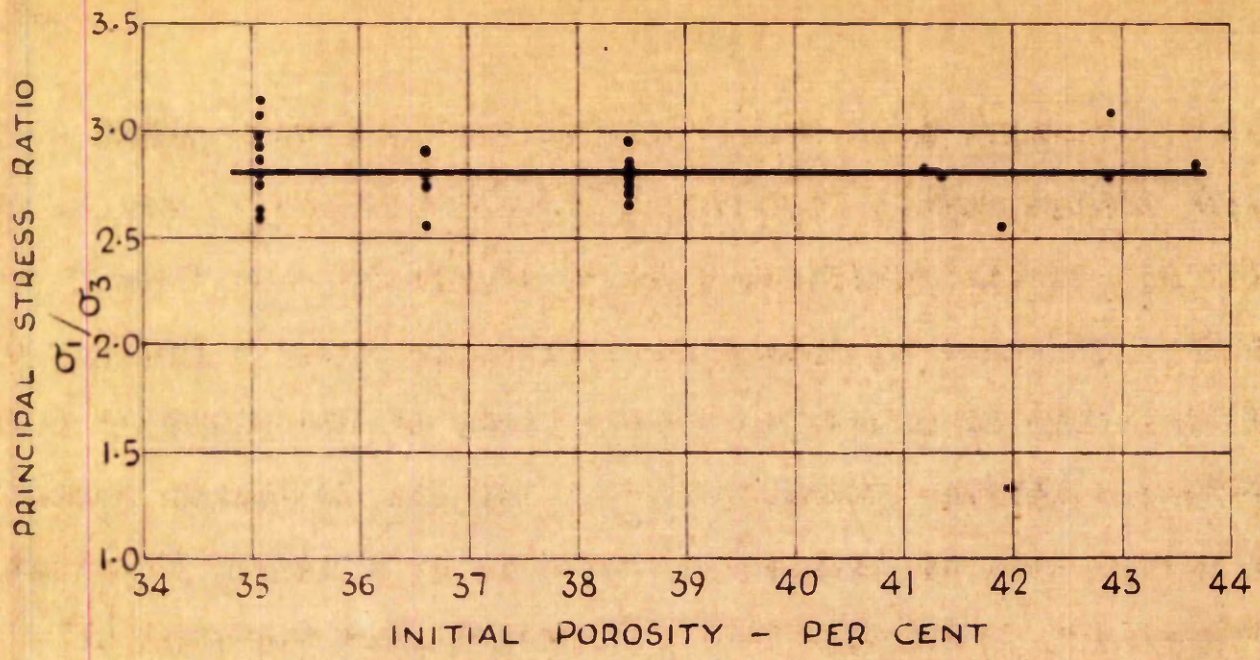

COMPRESSION TESTS

FIG. 42a.

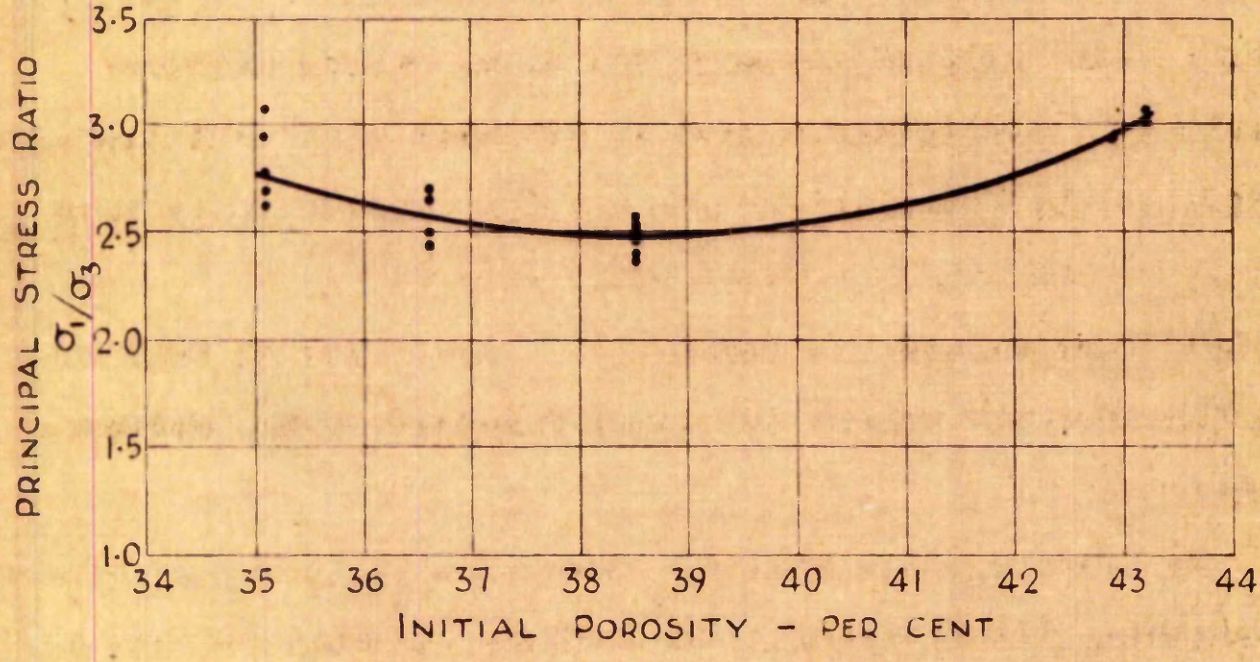

EXTENSION TESTS

FIG. 42b.

PRINCIPAL STRESS RATIO σ_1/σ_3 AT POINT OF VOLUME INCREASE

FIG. 42.

volume increase, i.e. corresponding to the lowest point on the volume change curve, is found to be independent of the initial porosity for the compression tests as can be seen from Fig.42a . The average value of this stress ratio is 2.80. Fig.42b shows the variation of principal stress ratio at the point of volume increase with the initial porosity for the extension tests. The curves show an unexpected trend to be slightly lower at intermediate porosities than at high and low porosities.

In Tables VII and VIII (pages 77 and 78) the total volume increase, that is the increase from the point of maximum decrease, is shown. It can be seen from these tables that within each range of porosity the total volume increase measured is noticeably higher at the peak point and markedly higher at the ultimate for compression samples which have failed by bulging than those which have failed by a plane of rupture (see values for Series 4). These are in turn much greater than the volume increases measured in the extension tests.

In rupture plane failures the volume is found to become constant at the ultimate. The volume in bulge failures in the compression tests however seldom becomes constant and in most cases continues to increase at a greatly reduced rate.

The amount of the ultimate volume increase measured in extension tests appears to be influenced by the position of the plane of rupture. This is most evident in the extension tests

of Series 4 (see Table VIII). In the tests in which the rupture plane has developed near the sample ends (samples tested at confining pressures of 100 and 120 lb./in^2) the measured volume increase is smaller than for those tests in which the plane has developed in the centre.

SECTION 10.

Discussion of Test Data.

10 a) The Reliability of Volume Change Measurements in the Triaxial Apparatus.

In the thick cylinder test failure took place as the result of slip within a deformed wedge shaped volume in the wall of the sample. The sand within the wedge appeared to be the only part of the sample which had expanded during the test. To study the possibility that this was characteristic of the failure of sands, and that failure in the triaxial samples also resulted in the expansion of wedge shaped volumes situated about the planes of slip, it was desired to compare the volume increases measured in the compression tests failing by bulging with those of the compression tests failing by a single plane of rupture and those of the extension tests failing by a single plane of rupture. It was for this reason that the rupture plane failures of the compression tests of series 4 were obtained. A method for predicting the stage by stage formation of the suspected wedges was developed assuming that the wedges were swept out by the planes of maximum obliquity at the stage reached in the test. Due to the complexity of the failure types met with in the tests no experimental proof of the method could be obtained.

Although it was not possible to prove that wedges similar to those developed in the thick cylinder tests are developed in the triaxial tests, the volume changes measured in the triaxial tests indicate that only part of the sample has undergone expansion during these tests. Large differences in the quantities of the volume increases were found in each series for compression samples which failed by bulging, for compression samples which failed by a plane of rupture and for the failures in the extension tests. These quantities in series 4 tests are approximately in the ratio of 5 to 3 to 1 at the ultimate. If the measured volume increases are caused by the expansion of the material of the whole sample it would be expected that the increases measured in all triaxial samples tested at the same porosity would be the same. This was not found to be so as the above figures indicate and it must be presumed that only part of the triaxial samples have undergone expansion during the tests. The nearest approach to the complete deformation of the sample is obtained in bulge failures in the compression tests. Volumes at the ends of these samples however are likely to remain undisturbed as is indicated by the photograph Fig.36.

The fact that large variations in the amounts of the volume increase can be produced by producing different types of failure illustrates the unreliable nature of the volume change measurements taken in the triaxial tests. For a critical investigation into the dilatancy properties of soils an

apparatus which constrains the whole sample to undergo a uniform deformation should be used. Of the apparatus available, that designed by Roscoe[11] for the application of simple shear may prove the most suitable.

10 b) Angle of Rubbing Friction.

The volume in all triaxial samples tended to increase after an initial reduction. The volume increase means that the grains are moving apart and coming out of their locking positions. This movement can only take place after the rubbing friction of the grains is mobilised. The stress ratio at which the volume starts to increase should therefore represent the angle of rubbing friction of the material.

The initial reduction in volume at low stresses is likely to be caused by the general compaction of the sample. This is probably due to local shear failures occurring in the lattice of the grains causing the particles to come into more intimate contact. Due to the non uniform conditions which exist in the triaxial sample the initial compaction will continue in parts of the sample after the point at which expansion starts in other parts. The stresses at the actual point of initial expansion will therefore not be obtained from triaxial data, and the stresses at the point of volume increase which are used to define the angle of rubbing friction will provide an over-estimation of the true angle.

The rubbing friction component of the shear strength is the part of the strength excluding other effects such as interlocking. It is to be expected therefore that this component is constant and independent of the porosity. The principal stress ratio at the point of volume increase in the triaxial compression tests was found to be independent of the initial porosity and had an average value of 2.80 (Fig.42a). In the extension tests a trend was found for this stress ratio to be slightly lower at intermediate porosities than at high and low porosities (Fig.42b). This trend is difficult to explain and the reason may lie in the inaccuracy of the estimation of the exact point at which the volume starts to increase.

The angle of rubbing friction estimated from the average value of the principal stress ratio at the point of volume increase in the compression tests has a value of 28° 16'. This overestimated angle is slightly higher than a value of 24° 30' found by Tschebotarioff and Welch[15] for submerged tests in which the friction between a rough quartz crystal surface and a polished quartz surface was directly measured. It is however smaller than the value of 33° found by Penman[10] for similar tests in which flat quartz surfaces were used. Although the author's results lie between those of the above investigators the exact significance is not clear but it may be that the condition of area contact for the aggregate grain material in the compression test is intermediate between those

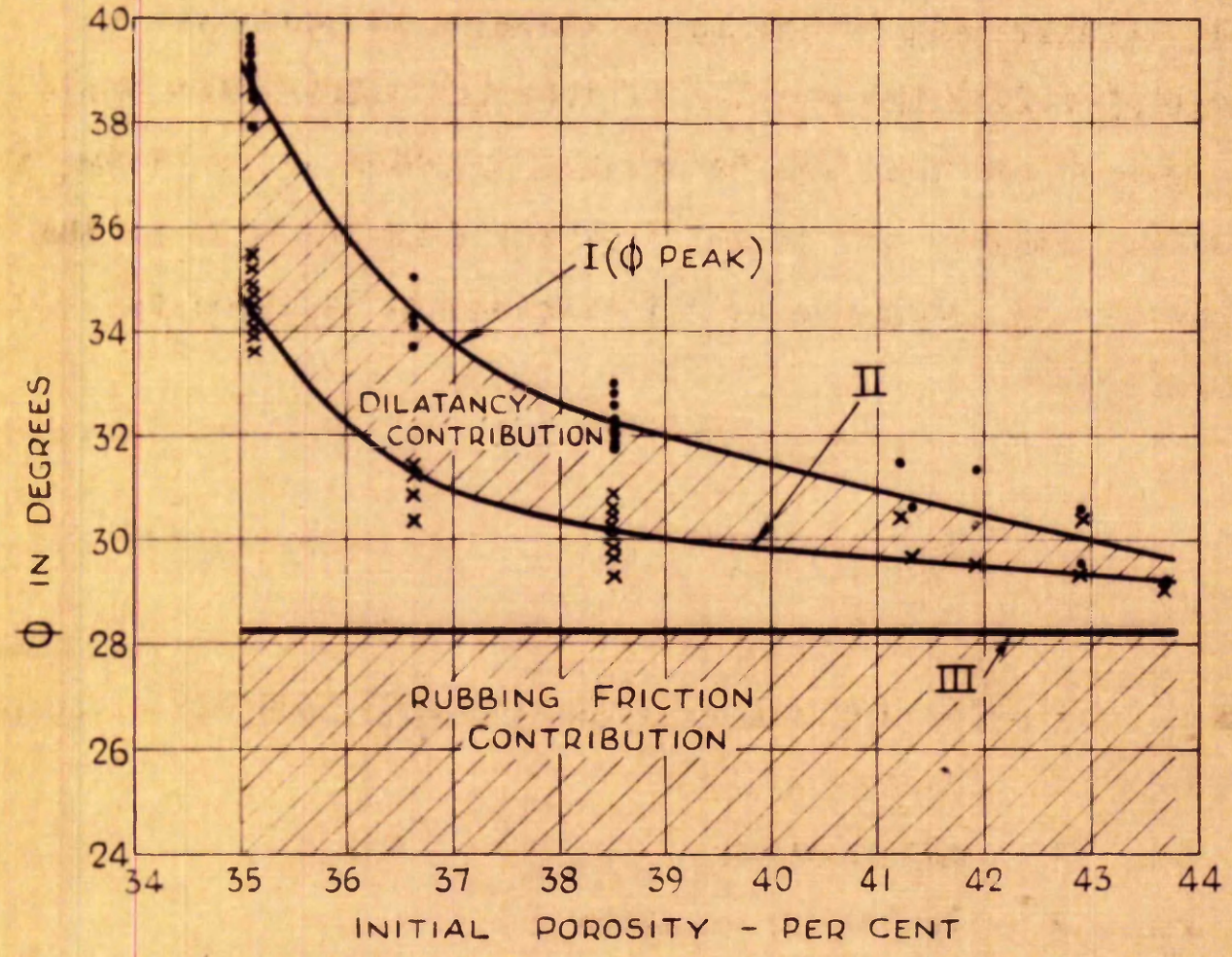

TRIAXIAL COMPRESSION RESULTS

FACTORS CONTRIBUTING TO SHEAR STRENGTH OF SANDS

FIG. 43

existing in the two direct friction tests.

If the stress ratio at which the volume starts to increase is considered to represent the angle of rubbing friction, two factors contributing to the shear strength of sands can be distinguished from the results of triaxial compression tests. These factors are that due to rubbing friction and that due to dilatancy. Bishop and Eldin[1] showed that the part of the strength due to dilatancy in the compression test can be expressed by

$$\sigma_D = \frac{dV}{dE}\sigma_3 \quad \text{.....(29)}$$

where σ_D denotes contribution to the strength made by dilatancy

V " volume strain

E " axial strain

σ_3 " confining pressure

Fig.43 shows the variation with porosity of, the peak angle of internal friction (curve I), the peak angle of internal friction corrected for dilatancy (curve II) and the angle of rubbing friction (III) as obtained from the compression tests. The contributions made by dilatancy and by the rubbing friction are shaded. Fig.43 shows that there is an additional factor contributing to the shear strength which is not accounted

for by the dilatancy as calculated from equation (29), or by the rubbing friction found from the compression tests. This factor increases with decreasing porosity.

In the extension tests the value of ϕ after being corrected for dilatancy was found to decrease with decreasing porosity instead of increasing as in the compression tests. This difference was also noted by Bishop and Eldin[1].

SECTION 11.

Conclusions to Part II.

1) The action of failure in sands is not yet fully understood. It is probable that the complete mass under stress does not deform and that failure is due to the development and subsequent deformation of a number of wedges or zones of material within the mass.

2) The variation of porosity during shear tests on sands cannot be estimated from the volume change measurements taken in standard apparatuses due to the non-uniform conditions which exist within the samples.

APPENDIX I

DESCRIPTION OF LOCH ALINE SAND

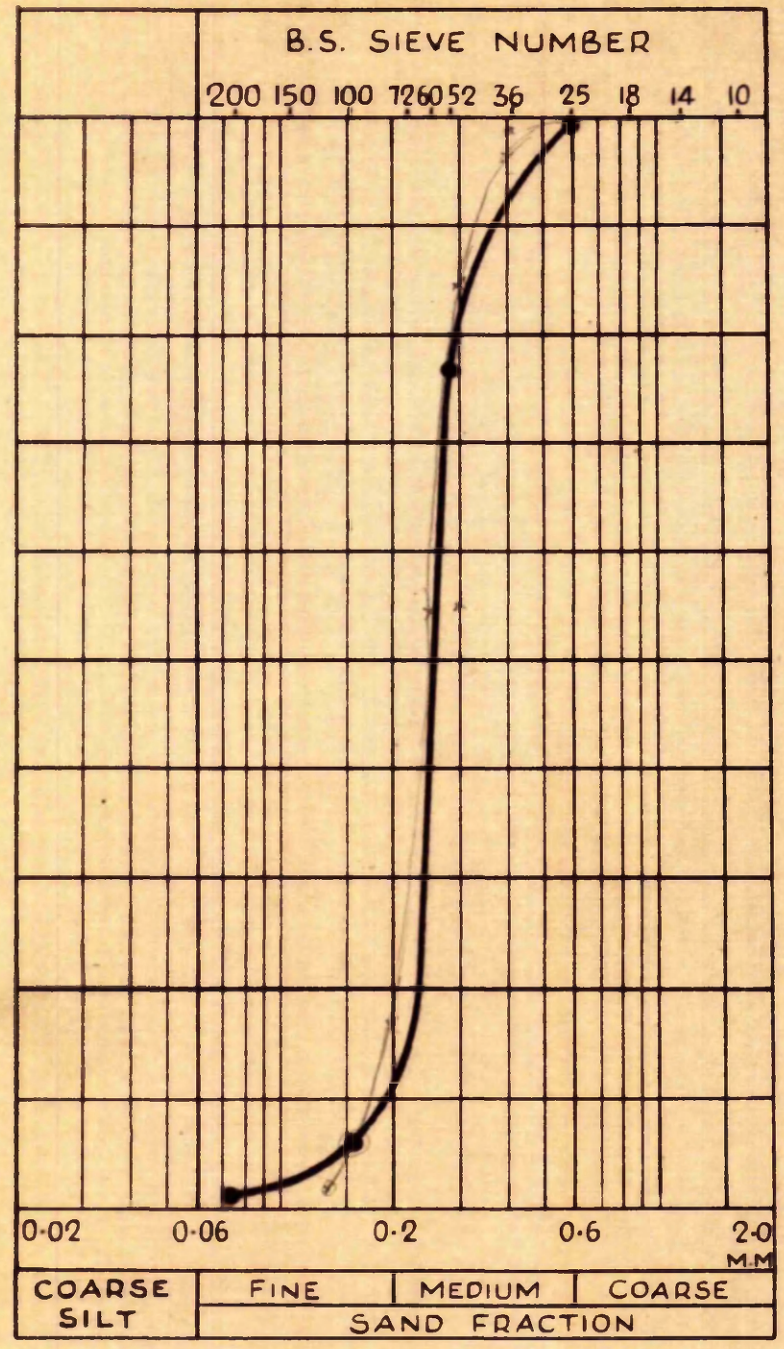

LOCH ALINE SAND
PARTICLE SIZE DISTRIBUTION

FIG. AP I.1.

FIG. Ap. 1. 2. X 30 ENLARGEMENT OF LOCH ALINE GRAINS.

In all experimental work described in this thesis the material tested was Loch Aline sand. The sand is white and the grains are almost entirely of pure quartz.

Particles finer than B.S.Sieve No.200 were removed from the natural sand to prevent these finer grains from penetrating the piping systems of the apparatuses. The particle size distribution of the sand as used is shown in Fig.AP.1.1. The curve illustrates a poorly graded medium sand.

A 30 times enlargement of the grains of the sand is shown in Fig.AP.1.2. The aggregate is seen to be a mixture of rounded and angular grains.

The limiting porosities found by the method suggested by Kolbuszewski[7] are 34.7% and 45.4%

APPENDIX II

COORDINATES OF POINTS ON A RIGHT SECTION OF A SURFACE OF YIELD

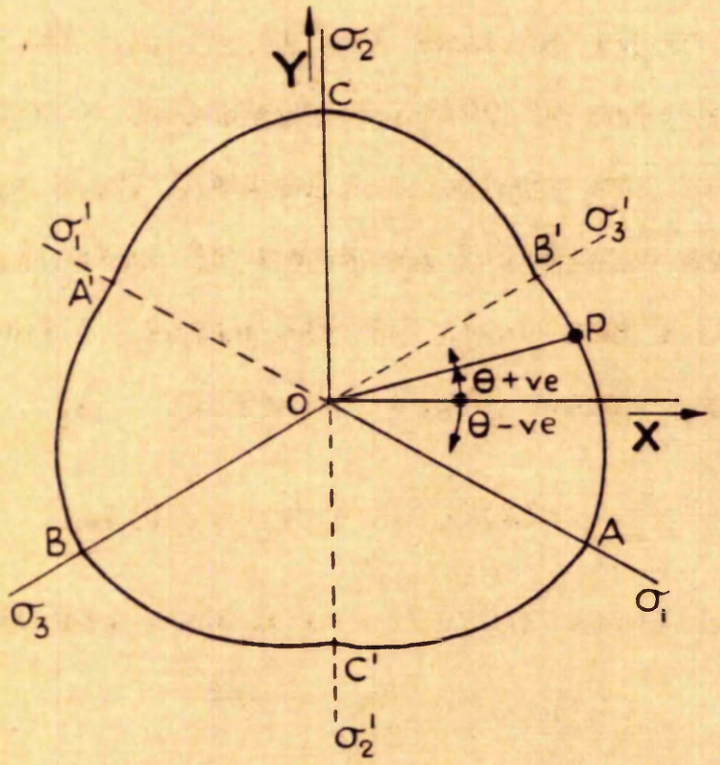

RIGHT SECTION OF A YIELD SURFACE FOR AN ISOTRORIC MATERIAL

FIG. AP. II 1.

A state of stress can be represented as a point in space by its three principal stresses (σ_1, σ_2, σ_3) with reference to a system of three dimensional coordinates (σ_1, σ_2, σ_3). The locus of all the points describing the stresses at yield represents a surface in space known as the surface of yield.

A view of a right section of a surface of yield is seen in Fig.AP.II.1. The right section can be at any distance from the origin of the system of three-dimensional coordinates but it lies on the plane of the paper. A point P (σ_1, σ_2, σ_3) on the right section can be expressed in terms of cartesian coordinates X and Y, which act in the plane of the paper. The cartesian coordinates of P in segment B' O A (where $\sigma_1 \geqslant \sigma_2 \geqslant \sigma_3$) are:

$$X = \sigma_1 \cos(X,\sigma_1) + \sigma_2 \cos(X,\sigma_2) + \sigma_3 \cos(X,\sigma_3)$$

where (X,σ_1) is the angle between the X axis and the σ_1 axis, etc.

$$X = \frac{\sigma_1}{\sqrt{2}} - \frac{\sigma_3}{\sqrt{2}} \quad **$$

and $$Y = \sigma_1 \cos(Y,\sigma_1) + \sigma_2 \cos(Y,\sigma_2) + \sigma_3 \cos(Y,\sigma_3)$$

$$Y = -\sigma_1 \frac{1}{\sqrt{6}} + \sigma_2 \sqrt{\frac{2}{3}} - \sigma_3 \frac{1}{\sqrt{6}}$$

$$Y = \frac{2\sigma_2 - \sigma_3 - \sigma_1}{\sqrt{6}} \quad **$$

** Stated by Hill in ref.(6).

The angle θ between vector OP and the X axis is obtained from

$$\text{Tan } \theta = \frac{Y}{X} = \frac{2\sigma_2 - \sigma_3 - \sigma_1}{\sqrt{3}(\sigma_1 - \sigma_3)}$$

Lode's[8] parameter

$$U = \frac{2\sigma_2 - \sigma_3 - \sigma_1}{\sigma_3 - \sigma_1} = -\sqrt{3} \tan \theta$$

θ can have any value ranging from

$$\tan^{-1} \frac{1}{\sqrt{3}} \quad (+30^\circ)$$

for point P at B' to

$$-\tan^{-1} \frac{1}{\sqrt{3}} \quad (-30^\circ)$$

for point P at A.

APPENDIX III

THE METHOD OF PRESENTING EXPERIMENTAL RESULTS

ON THE REDUCED RIGHT SECTION

In Appendix II it was shown that right sections of the surface of yield can be plotted in the plane of the paper using the cartesian coordinates X and Y which are functions of the three principal stresses. The yield surface for sands is expected to be either pyramidal or conical so that right sections of the surface will vary in extent with the distance along the space diagonal. In plotting right sections of the experimental surface of yield it is therefore necessary that the different experimental results can be considered to define points on the same right section.

Fig.AP.III.1. shows a right section of a yield surface. The section is in the plane of the paper and is obtained by looking down the space diagonal O'O. Let P any point on the surface at this section have coordinates (σ_1, σ_2, σ_3). On this section point P can be defined by its cylindrical coordinates O'P and θ. θ can have a value between $+30^\circ$ and -30° (see Appendix II) in any of the six sectors marked by the major stress directions. θ has the value obtained from the expression

$$\theta = -\tan^{-1} \frac{1}{\sqrt{3}} \left(\frac{2\sigma_2 - \sigma_3 - \sigma_1}{\sigma_3 - \sigma_1} \right)$$

for segment shown where:

σ_1 is the major principal stress

σ_2 is the intermediate principal stress

σ_3 is the minor principal stress

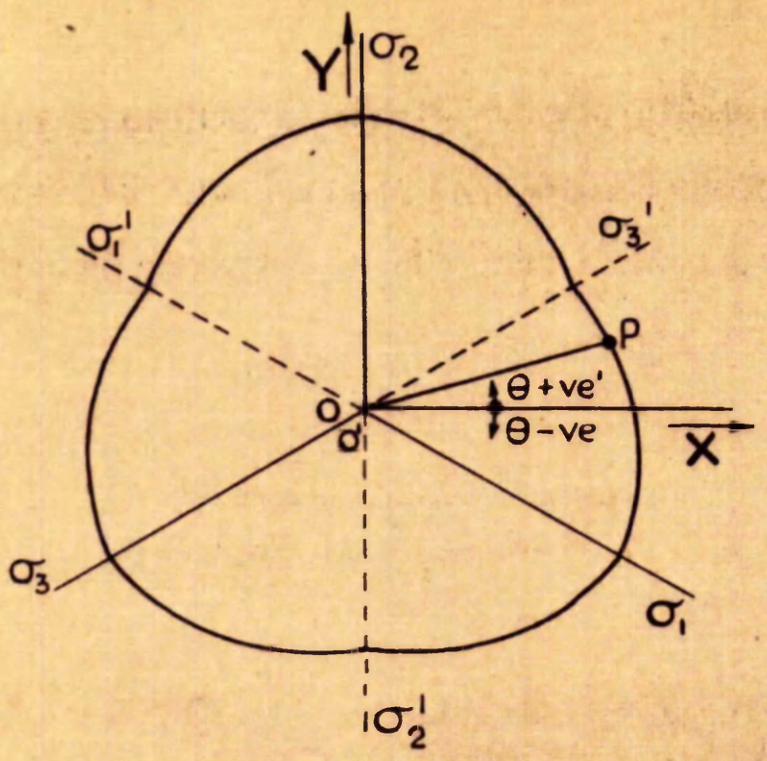

FIG. AP. III 1.

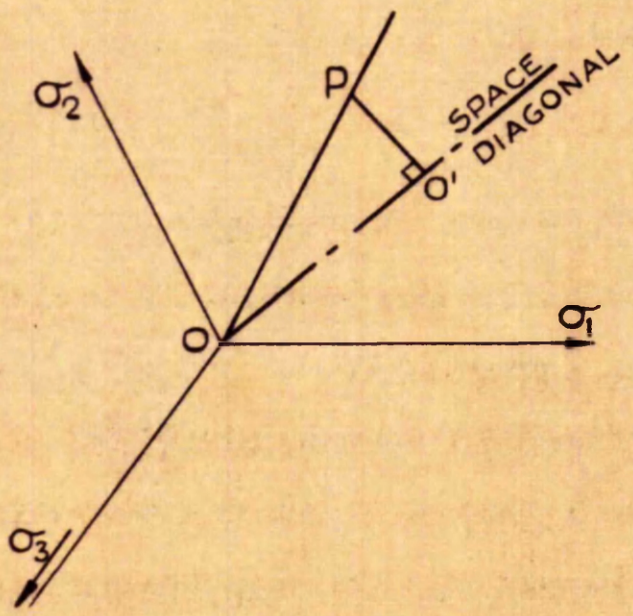

FIG. AP. III. 2.

The radius vector O'P can be found by taking a section of the yield surface along the space diagonal and through point P as shown in Fig.AP.III.2. The space diagonal is defined by the conditions $\sigma_1 = \sigma_2 = \sigma_3$.

$$\text{Distance PO} = \sqrt{\sigma_1^2 + \sigma_2^2 + \sigma_3^2}$$

$$\text{and } OO' = \frac{(\sigma_1 + \sigma_2 + \sigma_3)}{\sqrt{3}}$$

$$\therefore \text{ Angle } POO' = \cos^{-1} \frac{\sigma_1 + \sigma_2 + \sigma_3}{\sqrt{3}\sqrt{\sigma_1^2 + \sigma_2^2 + \sigma_3^2}}$$

$$\text{and } PO' = OO' \tan\left(\cos^{-1} \frac{\sigma_1 + \sigma_2 + \sigma_3}{\sqrt{3}\sqrt{\sigma_1^2 + \sigma_2^2 + \sigma_3^2}}\right)$$

The condition for the results to define points on the same right section of the surface of yield is that the sum of their principal stresses $(\sigma_1 + \sigma_2 + \sigma_3) = \text{constant}$. Difficulty is found in representing the experimental results on a diagrem to illustrate the right sections since it is impracticable to arrange the experiments so that the above condition is obtained. However if the lines bounding the surface are straight the difficulty can be overcome by plotting

the tangent of the angle made by the line joining the point on the surface to the origin and the space diagonal (i.e. ∠ P O O' Fig.AP.III.2) instead of the true vector distance (O'P). The equivalent right section obtained in this way will be known as the reduced right section. By making OO' = 1, vector O'P is expressed by

$$O'P = \tan\left(\cos^{-1}\frac{\sigma_1 + \sigma_2 + \sigma_3}{\sqrt{3}\sqrt{\sigma_1^2 + \sigma_2^2 + \sigma_3^2}}\right)$$

The point P on the reduced right section of the surface of yield Fig.AP.III.2 is then defined by:-

$$\text{Vector } O'P = \tan\left(\cos^{-1}\frac{\sigma_1 + \sigma_2 + \sigma_3}{\sqrt{3}\sqrt{\sigma_1^2 + \sigma_2^2 + \sigma_3^2}}\right)$$

$$\text{and } \angle\theta = -\tan^{-1}\frac{1}{\sqrt{3}}\,\frac{2\sigma_2 - \sigma_3 - \sigma_1}{\sigma_3 - \sigma_1}$$

Since the locus of the points causing yield must be symmetrical about $\sigma_1\sigma_1'$, $\sigma_2\sigma_2'$, $\sigma_3\sigma_3'$ the position of point P in the other 5 sectors can be found in a similar manner.

APPENDIX IV.

EFFECT OF SMALL ERRORS OF MEASUREMENT

ON THE RESULTS OF THE THICK CYLINDER TEST

By assuming that the Mohr-Coulomb theory is applicable for estimating the yield stresses in the thick cylinder test the effect of small errors in measurement on the angle of internal friction ϕ can be studied from the equation

$$P_i = P_o \left(\frac{b}{a}\right)^{(1-\lambda)} \quad \text{.....(AP.IV.1)}$$

(eqn.23 Sect.4 a)

1. Errors in Measurement of Pressure.

Bore Pressure (P_i)

Assuming no error in P_o, a or b (AP.IV.1.) on differentiat- becomes

$$\frac{dP_i}{P_i} = -\, d\lambda \,(\log b - \log a) \quad \text{.....(AP.IV.2)}$$

$$\lambda = \left(\frac{1 - \sin\phi}{1 + \sin\phi}\right) \quad \text{.....(AP.IV.3)(from 17b Sect.2d)}$$

$$\therefore \quad d\lambda = -\left[\frac{2\cos\phi}{(1 + \sin\phi)^2}\right] d\phi \quad \text{.....(AP.IV.4)}$$

Substituting for $d\lambda$

$$\frac{dP_i}{P_i} = 2\left[\frac{\log b - \log a}{(1 + \sin\phi)^2}\right] \cos\phi \,.\, d\phi \quad \text{...(AP.IV.5)}$$

Assuming ϕ, in the middle of the range expected, as 36° the allowable error in P_i for 1° error in estimation ϕ is obtained from (AP.IV.5)

$$\left(\frac{dP_i}{P_i}\right)100 = \pm 2\left[\frac{\log 2 - \log 1.25}{(1 + \sin 36^{\circ})^2}\right] \cos 36^{\circ} \cdot \frac{\pi}{180} \cdot 100$$

for $a = 1.25"$ and $b = 2"$

$\therefore$ the allowable error in $P_i = \pm 0.525\%$.

Outside Pressure (P_o)

Similarly the allowable error in $P_o = \pm 0.525\%$ for an error of 1° in ϕ.

2) Errors in Estimation of Sample Dimensions.

Bore Radius (a)

Assuming no error in P_i, P_o and b (AP.IV.1) on differentiating becomes

$$\frac{da}{a} = \left(\frac{\log a - \log b}{1 - \lambda}\right) d\lambda \ldots\ldots\ldots\ldots\ldots (AP.IV.6)$$

Substituting for λ and $d\lambda$ from (AP.IV.3) and (AP.IV.4),

(AP.IV.6) becomes

$$\frac{da}{a} = -(\log a - \log b)\frac{\cos\phi}{\sin\phi(1+\sin\phi)}\,d\phi \quad \ldots\ldots(AP.IV.7)$$

For 1° error in ϕ with $\phi = 36^\circ$, a = 1.25" and b = 2" the allowable error in measuring a is obtained from (AP.IV.7)

$$\left(\frac{da}{a}\right)100 = -(\log 1.25 - \log 2)\frac{\cos 36^\circ}{\sin 36^\circ(1+\sin 36^\circ)}\cdot\frac{\pi}{180}\cdot 100$$

$\therefore$ allowable error in a = $\pm$ 0.71%

Outside radius (b).

Similarly the allowable error in measuring the outside radius (b) = $\mp$ 0.71% for an error of 1° in ϕ.

APPENDIX V

SHEAR TRAJECTORIES IN THICK CYLINDER SAMPLE

(ACCORDING TO MOHR-COULOMB THEORY)

According to the Mohr-Coulomb Theory the limiting condition of yielding for sands is expressed by eqn.(17a Section 2d) and restated here as

$$(\sigma_1 - \sigma_3) = \pm (\sigma_1 + \sigma_3) \sin \phi$$

where $\sigma_1 \geqslant \sigma_2 \geqslant \sigma_3$

The equation represents the Mohr envelope for the material and is the common tangent of the major principal stress circles on the Mohr diagram. The slope of the envelope is determined by quantity ϕ which is a material constant Fig.(AP.V.1). The points of tangency on the stress circles P,P' etc. represent the planes in the material where yield or slip takes place. The orientation of these planes with respect to the principal planes can be found from the Fig.(AP.V.1). It can easily be proved that the planes of slip are inclined at

$$(45^\circ + \phi/2) \quad \ldots\ldots\ldots\ldots\ldots\ldots (AP.V.1)$$

to the direction of the major principal planes and at

$$(45^\circ - \phi/2) \quad \ldots\ldots\ldots\ldots\ldots\ldots (AP.V.2)$$

to the direction of the minor principal planes. Point P

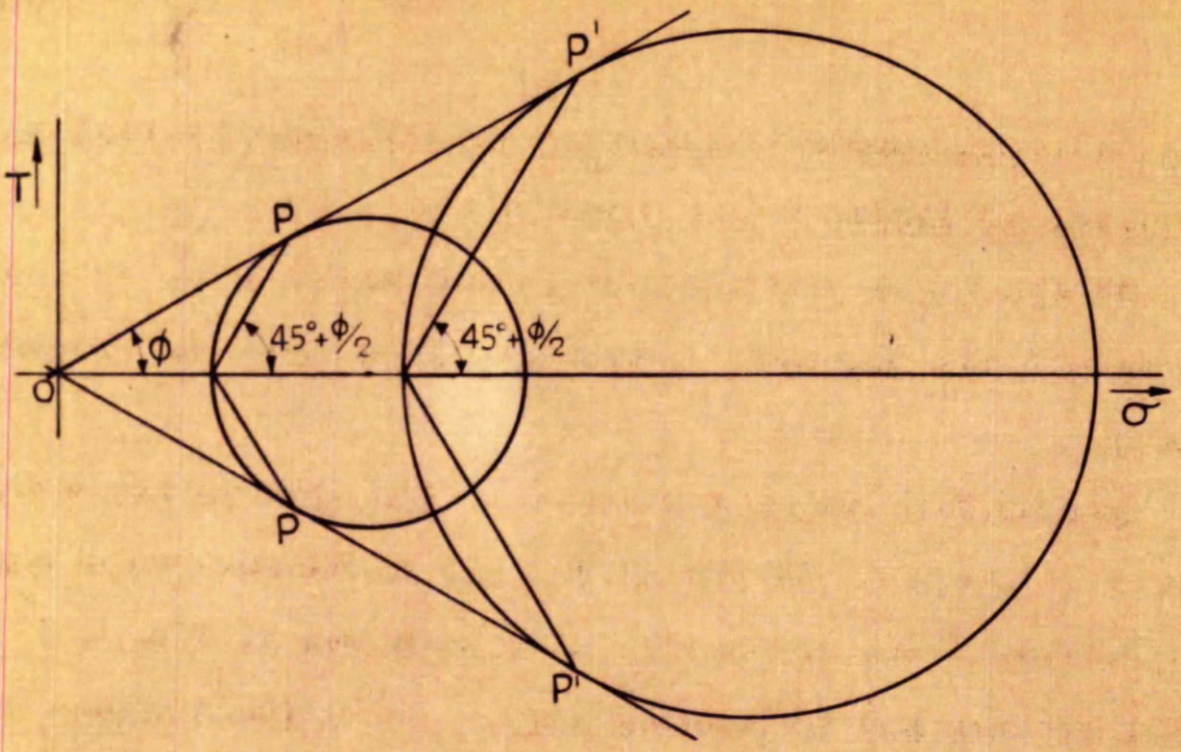

ORIENTATION OF PLANES OF SLIP
ACCORDING TO MOHR COULOMB THEORY
FIG. AP. V1

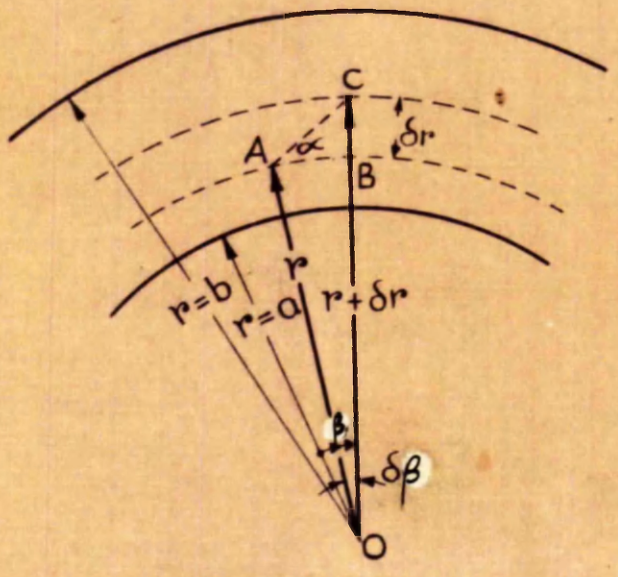

SHEAR TRAJECTORIES IN
THICK CYLINDER SAMPLE
FIG. AP. V2

therefore represents a system of slip planes inclined as indicated by (AP.V.1) and (AP.V.2).

In the thick cylinder sample the major principal planes are radial and the minor principal planes are the tangential planes.

Fig.AP.V.2 shows a section of the wall of the thick cylinder sample. In Fig.AP.V.2 let AC be part of a shear trajectory. Let the radius at A be r and at C be $r + \delta r$. ($BC = \delta r$) and let AC subtend angle $\delta\beta$ at the centre.

For small values of δr and $\delta\beta$ AC can be considered a straight line making a constant angle α with the radial plane AB.

Therefore $$\frac{\delta r}{AB} = \tan\alpha$$

or $$\frac{\delta r}{r\delta\beta} = \tan\alpha$$

$$\lim_{\beta \to 0} \frac{\delta r}{\delta\beta} = \frac{dr}{d\beta} = r \tan\alpha$$

and $$\int \frac{dr}{r} = \int d\beta \tan\alpha$$

which on integrating becomes

$$\log r = \beta \tan\alpha + \log C$$ (where C is a constant of integration)

At bore radius $r = a$, let $\beta = 0$

therefore constant $C = a$

The equation of the trajectory then becomes

$$\frac{r}{a} = e^{\beta \tan \alpha} \qquad \text{.....(AP.V.3)}$$

and is in the form of a logarithmic spiral.

α is the inclination of the trajectory to the radial, major principal planes, and has the value $(45^{\circ} + \frac{\phi}{2})$ according to the Mohr-Coulomb theory (AP.V.1). The equation of the trajectory according to the theory is therefore

$$\frac{r}{a} = e^{\beta \tan(45^{\circ} + \frac{\phi}{2})} \qquad \text{.....(AP.V.4)}$$

where a denotes the bore radius

and r denotes the radius at angle β from the point where the trajectory strikes the bore surface of the sample (i.e. $\beta = 0$ at $r = a$).

APPENDIX VI

BIBLIOGRAPHY

N.B. Indirect reference is made to the works of certain celebrated authors. These works are considered to be well known and the reference number found in the text indicates the publication in which the information was obtained.

1) Bishop, A.W. and Eldin, A.K.Gamal. (1953): "The effect of stress history on the relation between ϕ and porosity in sand." Proc.3rd.Int.Conf.Soil Mech. and Found.Eng., Vol.I, p.100.

2) Eldin, A.K.Gamal. (1951): "Fundamental factors controlling shear properties of sands." Ph.D.Thesis, University of London.

3) Habib, P. (1953): "Influence de la variation de la contrainte principale moyenne sur la résistance au cisaillement des sols." Proc.3rd.Int.Conf.Soil Mech. and Found.Eng., Vol.I. p.131.

4) Habib, P. (1952): "La résistance au cisaillement des sols." Doctor's Thesis, University of Paris.

5) Henkel, D.J. and Gilbert, G.D.(1952): "The effect of the rubber membrane on the measured triaxial strength of clay samples." Geotechnique Vol.III, 1, p.20.

6) Hill, R. (1950): "The Mathematical Theory of Plasticity." The Clarendon Press, Oxford. Chap.II.

7) Kolbuszewski, J.J. (1948): "An experimental study of the maximum and minimum porosities of sands." Proc.2nd. Int.Conf.Soil Mech. and Found.Eng., Vol.I, p.158.

8) Lode, W. (1926): "Versuche über den Einflus der Mittleren Hauptspannung auf das Fliesen der Metalle Eisen, Kupfer und Nickel." Zeits.fur Physik, Vol.36, p.913.

9) Nadai, A. (1950): "Theory of Flow and Fracture of Solids." McGraw-Hill, New York. Vol.I, Chap.15.

10) Penman, A.D.M. (1953): "Shear characteristics of a saturated silt, measured in triaxial compression." Géotechnique Vol.III, 8, p.312.

11) Roscoe, K.H. (1953): "An apparatus for the application of simple shear to soil samples." Proc.3rd.Int.Conf.Soil Mech. and Found.Eng. Vol.I, p.186.

12) Schleicher, F. (1925): "Die Energiegrenze der Elastizität (Plastizitatsbedingung)." Zeits.fur ang.Math.Mech. Vol.5 p.478.

13) Skempton, A.W. and Bishop, A.W. (1950): "The measurement of the shear strength of soils." Géoteohnique Vol.II, 2, p.90.

14) Taylor, D.W. (1941): Shear Research - 7th Progress Report. Soil Mechanics lab. M.I.T.

15) Tschebotarioff, G.P. and Welch, J.D. (1948): "Lateral earth pressures and friction between soil minerals." Proc.2nd.int.Conf.Soil Mech.and Found.Eng. Vol.VII, p.135.

General References

16) Taylor, D.W. (1948): "The Fundamentals of Soil Mechanics." J.Wiley and Sons, New York.

17) Terzaghi, K. (1943): "Theoretical Soil Mechanics." J.Wiley and Sons, New York.

Also including 6), 9) and 13) above.

§§§§§§§§§§